

THESIS FOR THE DEGREE OF DOCTOR OF PHILOSOPHY

Slurry Hydrotreatment of Biomass Materials over Metal Sulfide-based
Supported and Unsupported Catalysts

YOU WAYNE CHEAH

Department of Chemistry and Chemical Engineering
CHALMERS UNIVERSITY OF TECHNOLOGY
Gothenburg, Sweden 2023

Slurry Hydrotreatment of Biomass Materials over Metal Sulfide-based Supported and Unsupported Catalysts

YOU WAYNE CHEAH
ISBN 978-91-7905-867-8

© YOU WAYNE CHEAH, 2023.

Doktorsavhandlingar vid Chalmers tekniska högskola
Chalmers Tekniska Högskola.
Ny serie nr 5333
ISSN 0346-718X

Department of Chemistry and Chemical Engineering
Chalmers University of Technology
SE-412 96 Gothenburg
Sweden
Telephone + 46 (0)31-772 1000

Cover:

Graphical illustration of the catalytic hydroconversion of a lignin polymer over an unsupported NiMo sulfide to renewable transportation fuels.

Back cover:

Photograph by Jieling Shao

Printed by Chalmers Digitaltryck
Gothenburg, Sweden 2023

Slurry Hydrotreatment of Biomass Materials over Metal Sulfide-based Supported and Unsupported Catalysts

You Wayne Cheah

Department of Chemistry and Chemical Engineering
Chalmers University of Technology, Gothenburg 2023

Abstract

The scarcity of fossil feedstocks and the deterioration of the current global climate condition have prompted the search for reliable alternatives for fossil fuel replacement. Biomass feedstocks are abundant, carbon-rich, and renewable bioresources that can be used to produce renewable bio-oils that can fill the gap left by fossil-derived oils. Such bio-oils require an upgrading process, such as catalytic hydrodeoxygenation (HDO), to improve their quality for use as advanced biofuels and chemicals. Transition metal sulfides (TMS) are typically used in the traditional petroleum refining industry. In this thesis, we have explored the use of unsupported and supported metal sulfides in the hydrotreatment of Propylguaiacol (PG), a bio-oil model compound, Kraft lignin (KL), and pyrolysis bio-oil. In the recent work, the co-processing of the Kraft lignin and pyrolysis oil over the unsupported NiMoS was also performed.

Firstly, MoS₂ supported on γ -Al₂O₃ catalysts and promoted by transition metals, such as Nickel (Ni), Copper (Cu), Zinc (Zn), and Iron (Fe) were evaluated for the HDO of PG in a batch reactor setup. The catalyst screening results showed that the sulfided Ni-promoted catalyst gave a 94% yield of deoxygenated cycloalkanes, however, 42% of the phenolics remained in the reaction medium after 5 h for the sulfided Cu-promoted catalyst. A pseudo-first kinetic model that took into consideration the main side reactions was developed to elucidate the deoxygenation routes for the HDO of PG using sulfided catalysts. It was demonstrated that the activity of the transition metal promoters for the HDO of PG correlated to the yield of deoxygenated products from the hydrotreatment of KL. Further, the effect of the annealing treatment of a hydrothermally synthesized unsupported MoS₂ dispersed catalyst was studied and evaluated for the HDO of PG. The annealing treatment of the as-synthesized catalyst under N₂ flow at 400 °C for 2 h was found to enhance the HDO activity of PG. The annealed unsupported MoS₂ demonstrated a high capacity for deoxygenation with a selectivity of 78.6% and 20.1% for cycloalkanes and aromatics from KL hydrotreatment, respectively. The results also indicate that a catalyst with high activity for deoxygenation and hydrogenation reactions can suppress char formation and favor a high lignin bio-oil yield.

The main hurdle during Kraft lignin liquefaction was the occurrence of repolymerization reactions during depolymerization that lead to the production of undesired solid char residues and subsequently cause low bio-oil yield. In this regard, the combination of NiMo sulfides with various ultra-stable Y zeolites (USY) for the KL hydrotreatment was studied. The use of the physical mixture of the unsupported NiMoS and the USY support was also studied to better understand the role of the catalyst components, and their interactions during lignin depolymerization, HDO, and also repolymerization of the reactive lignin intermediates. Further work was then extended to the co-hydrotreatment of KL and pyrolysis oil over the unsupported NiMo Sulfides. The synergistic effect between the complex feedstocks (KL and pyrolysis oil) was further explored by investigating the effect of supplementing various bio-oil monomers during KL liquefaction. It was found that the strategy of co-feeding bio-derived monomers and pyrolysis oil in the KL hydrotreatment presented an insight for co-processing and also the role of second co-feed was able to facilitate efficient lignin depolymerization increasing the desired bio-liquid yield and limiting lignin condensation. Further, a two-stage fast pyrolysis bio-oils (FPBO) processing concept that involves first a stabilization step in the slurry hydrocracker over an unsupported NiMoS and then followed by downstream fixed-bed hydrotreating producing renewable hydrocarbon was studied. The liquid products were thoroughly analyzed to understand their chemical and physical properties.

Keywords: Advanced biofuels, Pyrolysis oil, Propylguaiacol, Kraft lignin, Hydrotreatment, Transition metals, MoS₂, Unsupported TMS, Reaction network, Slurry hydrocracking

Preface

This dissertation is submitted as partial fulfillment of the degree of Doctor of Philosophy. The work was conducted mainly at the Division of Chemical Engineering in the Department of Chemistry and Chemical Engineering of Chalmers University of Technology in Gothenburg, Sweden, between October 2018 and June 2023. The work was supervised by Professor Louise Olsson and Professor Derek Creaser. The work was also co-supervised by Dr. Olov Öhrman from Preem AB. This project is a collaboration between the Competence Centre for Catalysis, Chemical Engineering Division at Chalmers, Preem AB, and RISE Energy Technology Centre (ETC). The project was funded by the Swedish Energy Agency (grant no. 2017-010890 and 2018-012459), Formas (grant number: FR-2021/0005), and Preem AB.

List of publications

This thesis is based on the following appended papers, which are referred to in the text by their Roman numerals:

Paper I: Role of transition metals on MoS₂-based supported catalysts for hydrodeoxygenation (HDO) of Propylguaiacol.

You Wayne Cheah, Muhammad Abdus Salam, Prakhar Arora, Olov Öhrman, Derek Creaser, and Louise Olsson
Sustainable Energy & Fuels, (2021), 5, 2097-2113

Paper II: Thermal annealing effects on hydrothermally synthesized unsupported MoS₂ for enhanced deoxygenation of Propylguaiacol and Kraft lignin.

You Wayne Cheah, Muhammad Abdus Salam, Joby Sebastian, Sreetama Ghosh, Olov Öhrman, Derek Creaser, and Louise Olsson

Sustainable Energy & Fuels, (2021), 5, 5270-5286

Paper III: Elucidating the role of NiMoS-USY during the hydrotreatment of Kraft lignin.

Muhammad Abdus Salam, You Wayne Cheah, Phuoc Hoang Ho, Diana Bernin, Abdenour Achour, Elham Nejadmoghadam, Olov Öhrman, Prakhar Arora, Louise Olsson, and Derek Creaser

Chemical Engineering Journal, (2022), 442, 136216

Paper IV: Slurry Co-hydroprocessing of Kraft lignin and pyrolysis oil over unsupported NiMoS catalyst: a strategy for char suppression.

You Wayne Cheah, Rawipa Intakul, Muhammad Abdus Salam, Joby Sebastian, Phuoc Hoang Ho, Prakhar Arora, Olov Öhrman, Louise Olsson, and Derek Creaser

Manuscript under review

Paper V: Upgrading of Fast Pyrolysis Bio-Oils to Renewable Hydrocarbons using Slurry- and Fixed Bed Hydroprocessing.

Niklas Bergvall, You Wayne Cheah, Christian Bernlind, Alexandra Bernlind, Linda Sandström, Louise Olsson, Derek Creaser, and Olov Öhrman

Manuscript

Paper VI: Upgrading of triglycerides, pyrolysis oil, and lignin over metal sulfide catalysts: A review on the reaction mechanism, kinetics, and catalyst deactivation.

You Wayne Cheah, Muhammad Abdus Salam, Joby Sebastian, Sreetama Ghosh, Prakhar Arora, Olov Öhrman, Louise Olsson, and Derek Creaser

Journal of Environmental Chemical Engineering, 2023, 109614

Statement of the Authors' Contributions

Paper I: Role of transition metals on MoS₂-based supported catalysts for hydrodeoxygenation (HDO) of Propylguaiacol

Y.W.C. planned and defined the scope of the study with co-authors. **Y.W.C.** performed all the catalytic reactor experiments, catalyst characterizations, and liquid product analysis with the help of **M.A.S.** and **P.A.** in this work. **D.C.** constructed the first simplified kinetic model for HDO of PG and **Y.W.C.** developed the model further. **Y.W.C.** analyzed the results with co-authors and wrote the first draft of the manuscript. **Y.W.C.** revised the manuscript with feedback from co-authors. The final version of the paper was reviewed and written with contributions from all the authors.

Paper II: Thermal annealing effects on hydrothermally synthesized unsupported MoS₂ for enhanced deoxygenation of Propylguaiacol and Kraft lignin

Y.W.C. planned and defined the scope of the study with co-authors. **Y.W.C.** performed all the catalytic reactor experiments, catalyst characterizations, and liquid product analysis with the help of **M.A.S.**, **J.S.**, and **S.G.** in this work. **Y.W.C.** analyzed the results with co-authors and wrote the first draft of the manuscript. **Y.W.C.** revised the manuscript with feedback from co-authors. The final version of the paper was reviewed and written with contributions from all the authors.

Paper III: Elucidating the role of NiMoS-USY during the hydrotreatment of Kraft lignin

Y.W.C. discussed, planned, and performed some of the catalytic reactor experiments, catalyst characterizations, and liquid product analysis with **M.A.S.** **Y.W.C.** synthesized the unsupported NiMoS catalyst and also performed its characterizations. **Y.W.C.** analyzed the results with co-authors and revised the first draft and also the final version of the manuscript.

Paper IV: Slurry Co-hydroprocessing of Kraft lignin and pyrolysis oil over unsupported NiMoS catalyst: a strategy for char suppression

Y.W.C. planned and defined the scope of the study with co-authors. **Y.W.C.** and **J.S.** discussed the initial workflow of this work. **Y.W.C.** and **R.I.** performed all the catalytic reactor experiments, catalyst characterizations, and liquid product analysis with the help of **M.A.S.** **Y.W.C.** supervised **R.I.** in her Master's thesis related to this work. **Y.W.C.** performed the FTIR analysis with the help of **P.H.H.** **Y.W.C.** analyzed the results with co-authors and wrote the first draft of the manuscript. **Y.W.C.** revised the manuscript with feedback from all the co-authors. The final version of the paper was reviewed and written with contributions from all the authors.

Paper V: Upgrading of Fast Pyrolysis Bio-Oils to Renewable Hydrocarbons using Slurry- and Fixed Bed Hydroprocessing

N.B. designed the experimental campaign. **Y.W.C.** joined the experimental campaign, operating the slurry hydrocracker pilot plant in Piteå (SHC) with **N.B.** in the summer of 2022. **Y.W.C.** synthesized the unsupported NiMoS catalyst used in the stabilization of FPBO. **Y.W.C.** analyzed the stabilized FPBO and hydrotreated bio-oil products using 2D GC × GC-MS FID. **Y.W.C.** analyzed and discussed the results and wrote the manuscript draft with co-authors.

Paper VI: Upgrading of triglycerides, pyrolysis oil, and lignin over metal sulfide catalysts: A review on the reaction mechanism, kinetics, and catalyst deactivation

Y.W.C., **M.A.S.**, and **P.A.** planned and defined the scope of this work that started in 2019. **Y.W.C.** and **M.A.S.** shared the first authorship of this work. **Y.W.C.** directed and coordinated the work between authors. **Y.W.C.** collected and distributed all related articles for the past decade to co-authors. **Y.W.C.** contributed to Chapters 1, 3, 4, 5, 6, 7, and 8 of the paper. **P.A.** and **M.A.S.** contributed to Chapter 2 of the paper. **M.A.S.** contributed to Chapters 1, 2, 3, 4, 6, and 8 of the paper. **J.S.** contributed to Chapter 4 of the paper. **S.G.** contributed to Chapter 5 of the paper. **Y.W.C.** and **M.A.S.** answered all reviewer's comments and performed the revision. All authors reviewed and polished the final version of the manuscript.

Results related to this work have also been presented at the following conferences

1. Hydrodeoxygenation of Dihydroeugenol over NiMo, CuMo, and FeMo Alumina supported catalysts: A Bio-oils Model Compounds study

You Wayne Cheah

Summer school, Catalysis: Fundamentals and Practice, Department of Chemistry, University of Liverpool, 15-19 July 2019 (Poster)

2. Natural bauxite: a cheaper alternative catalyst for lignin hydrotreatment?

You Wayne Cheah

Lignin Conference 2022 hosted by LignoCOST, Wageningen, The Netherlands, 31 May-3 June 2022 (Poster)

3. Natural bauxite: a cheaper alternative catalyst for lignin hydrotreatment?

You Wayne Cheah

Science and Technology Day, Chalmers University of Technology, Gothenburg, Sweden, 12 May 2022 (Poster)

4. Natural bauxite: a cheaper alternative catalyst for lignin hydrotreatment?

You Wayne Cheah

The 9th Tokyo Conference on Advanced Catalytic Science and Technology (TOCAT9), Fukuoka, Japan, 24-29 July 2022 (Oral presentation)

Publications not included in this thesis

1. NiMoS on alumina-USY zeolite for hydrotreating lignin dimers: Effect of support acidity and cleavage of C-C bond
Muhammad Abdus Salam, Prakhar Arora, Houman Ojagh, You Wayne Cheah, Louise Olsson, and Derek Creaser
Sustainable Energy & Fuels, (2020), 4, 149-163
2. The role of catalyst poisons during hydrodeoxygenation of renewable oils
Prakhar Arora, Hoda Abdolahi, You Wayne Cheah, Muhammad Abdus Salam, Eva Lind Grennfelt, Henrik Rådberg, Derek Creaser, and Louise Olsson
Catalysis Today, (2020), 11 (1), 28-42
3. Hydrotreatment of lignin dimers over NiMoS-USY: effect of silica/alumina ratio
Muhammad Abdus Salam, You Wayne Cheah, Hoang Phuoc Ho, Louise Olsson, and Derek Creaser
Sustainable Energy & Fuels, (2021), 5, 3445-3457
4. The promoter and poison effects of the inorganic elements of kraft lignin during hydrotreatment over NiMoS catalyst
Joby Sebastian, You Wayne Cheah, Diana Bernin, Derek Creaser, and Louise Olsson
Catalysts, (2021), 11(8), 874
5. Slurry Hydroconversion of Solid Kraft Lignin to Liquid Products Using Molybdenum- and Iron-based Catalysts
Niklas Bergvall, Linda Sandström, You Wayne Cheah, and Olov Öhrman
Energy and Fuels, (2022), 36, 17, 10226-10242

List of abbreviations

AC	Activated carbon
BJH	Barret Joyner Halenda
BET	Brunauer Emmett Teller
BDE	Bond dissociation energy
DME	Demethylation
DDO	Direct-deoxygenation
DMO	Demethoxylation
DMDS	Dimethyl disulfide
EDX	Energy dispersive x-ray
FID	Flame ionization detector
FB	Fixed-bed
GC	Gas chromatography
GHG	Greenhouse gas
HAADF	High-angle annular dark field
HDO	Hydrodeoxygenation
HDS	Hydrodesulfurization
HDN	Hydrodenitrogenation
HDM	Hydrodemetallization
HYD	Hydrogenation-dehydration
HRTEM	High-resolution transmission electron microscopy
ICP-SFMS	Inductively coupled plasma sector field mass spectrometry
kDa	Kilodaltons
MS	Mass spectroscopy
MTOE	Million tons of oil equivalent
ODE	Ordinary differential equations
RPM	Revolutions per minute
SSR	Residual sum of squares
SEM	Scanning electron microscopy
STEM	Scanning transmission electron microscopy
SHC	Slurry hydrocracking
TMS	Transition metal sulfides
TIA	TEM Imaging and Analysis
XRD	X-ray diffraction
XPS	X-ray photoelectron spectroscopy

Contents

1	Introduction	1
1.1	Greenhouse gas (GHG) emissions, the transportation sector in Europe, and biofuels	1
1.2	Objectives, scope, and outline of the thesis	3
2	Background	9
2.1	Transition metal sulfides (TMS) as hydrotreating catalysts	9
2.2	Lignin, bio-oil properties, and catalytic hydrodeoxygenation (HDO)	10
2.3	HDO of bio-oil model compounds over supported sulfided catalysts	13
2.4	HDO of bio-oil model compounds over unsupported sulfided catalysts	18
2.5	Hydrotreatment of real bio-oils and lignin over sulfided catalysts	21
2.6	Slurry hydrotreatment of pyrolysis oil over sulfided catalysts	23
2.7	Strategy to suppress char formation reactions – use of co-solvent, co-reactant, or capping agent	25
3	Experimental	27
3.1	Catalyst synthesis	27
3.1.1	Supported sulfided catalysts	27
3.1.2	Unsupported sulfided catalysts	27
3.2	Kinetics measurements	28
3.3	Product analysis	31
3.4	Catalyst characterizations	34
3.4.1	Nitrogen (N ₂) physisorption	34
3.4.2	X-ray powder diffraction (XRD)	34
3.4.3	X-ray photoelectron spectroscopy (XPS)	34
3.4.4	Raman spectroscopy	34
3.4.5	Electron microscopy (SEM & TEM)	34
3.4.6	Temperature Programmed desorption (TPD) and reduction (TPR)	35
3.5	Solid lignin and lignin-derived solid char characterization	36
4	Results and discussion	37
4.1	Role of transition metals on MoS ₂ -based supported catalysts for hydrodeoxygenation (HDO) of Propylguaiacol	38
4.1.1	HDO of PG over supported Mo sulfided catalysts	38
4.1.2	Catalyst characterization	42
4.1.3	Modeling the reaction network for HDO of PG over sulfided catalysts	45

4.2	Annealing treatment of unsupported MoS ₂ for hydrodeoxygenation of propylguaiacol and hydrotreatment of Kraft lignin.....	50
4.2.1	Hydrothermal synthesis of unsupported MoS ₂ for HDO of PG.....	50
4.2.2	Catalyst characterization	52
4.3	Elucidating the role of ultra-stable Y (USY) supported and unsupported NiMoS catalysts during the hydrotreatment of Kraft lignin.....	58
4.3.1	Kraft lignin hydrotreatment using sulfided NiMo-impregnated USY zeolites.....	58
4.3.2	The role of NiMoS and Y30 in Kraft lignin hydrotreatment.....	59
4.3.3	Catalyst characterizations.....	61
4.4	Slurry Co-hydrotreatment of Kraft lignin and pyrolysis oil over unsupported NiMoS catalyst: a char suppression strategy.....	66
4.4.1	Pyrolysis-oil-assisted Kraft lignin hydrotreatment.....	66
4.4.2	Investigating the effect of model pyrolysis oil compounds as co-reactants in Kraft lignin hydrotreatment	68
4.4.3	Influence of mass ratio of Kraft lignin versus 4-propylguaiacol during co-processing.....	70
4.4.4	Effect of reaction time on co-hydrotreatment of Kraft lignin with 4-propylguaiacol.....	72
4.4.5	Reaction network for pyrolysis oil-assisted Kraft lignin hydrotreatment.....	77
4.5	Pilot slurry hydrocracking and fixed-bed hydrotreating of fast pyrolysis bio-oils (FPBO).....	79
4.5.1	Properties of FPBO	80
4.5.2	Liquid products properties.....	80
4.5.3	Process material flow	86
5	Conclusions	89
6	Future outlook	93
7	Acknowledgments	95
8	References	97

1 Introduction

1.1 Greenhouse gas (GHG) emissions, the transportation sector in Europe, and biofuels

Depleting fossil resources, increasing greenhouse gas (GHG) emissions, and deteriorating global climate conditions have prompted efforts to speed up the deployment of a sustainable society. Several aspiring goals have been set by governmental agencies to tackle these issues and environmental-related issues. One of these is the ambitious target to reduce greenhouse gas (GHG) emissions by 40% in 2030 and achieve climate neutrality by 2050, as drafted in the roadmap of the European Green Deal illustrated in **Figure 1**¹. 32% lower emissions of GHGs were achieved in 2020 than in 1990 levels, indicating that the EU remained on track with its goal of a 20% reduction in GHG emissions by 2020 (**Figure 1**)¹. The reduction in GHG emissions in 2020 can also be attributed to the pandemic even though the emissions levels in 2018 and 2019 were already below the 2020 target. There is no doubt that substantial emission reductions are still needed in the coming years to meet the emission targets and ultimately achieve climate neutrality. To achieve the target of a 55% reduction in net emissions by 2030 as compared to the 1990 levels, a reduction of 134 Mt CO₂e per year on average for the period between 2021-2030 is needed (**Figure 1**). The projected emission cut is more than twice the average emission reduction achieved between 1990 and 2020, hence, it is clear that extensive efforts are still needed to halt GHG emissions and gain carbon neutrality.

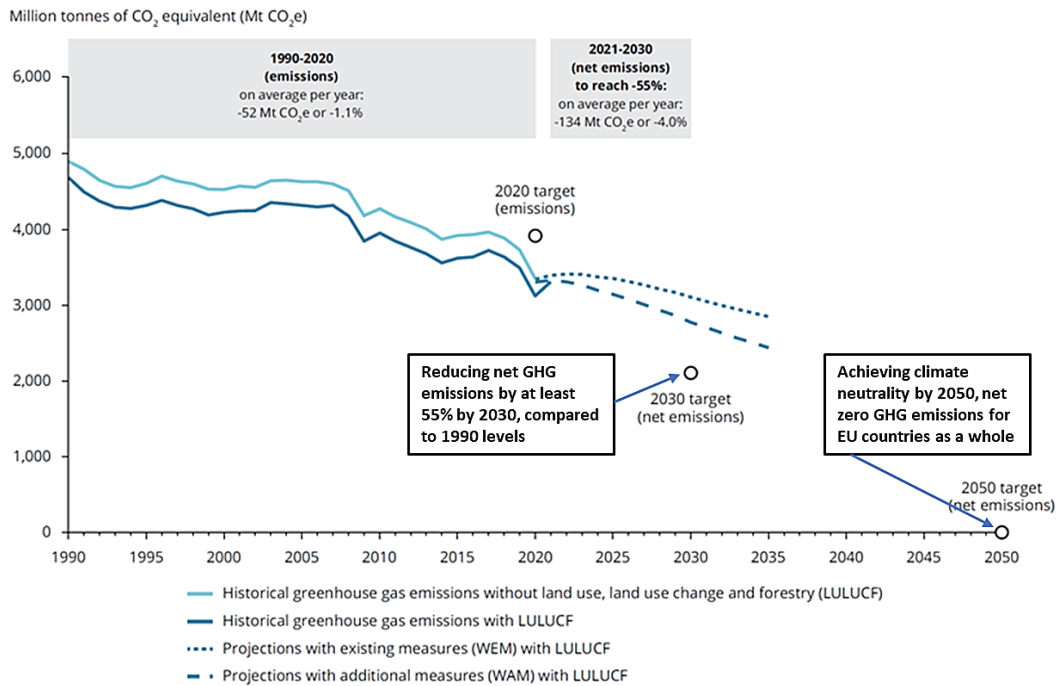


Figure 1. GHG emission trends, projections, and targets in EU¹.

Of all the economic sectors, transportation (including international aviation) accounts for almost a quarter of the GHG emissions in Europe and remains the second largest emissions source in the EU member states (EU-27), and at the same time, also causes air pollution in major cities (**Figure 2**)². The transport sector also remains one of the major economic sectors with an upward trend for GHG emissions with a steady increase between 2013 and 2019 (**Figure 3**). This increase can be mainly attributed to the ever-growing population and demand for passenger and

freight transport in emerging economies. The decrease in emissions between 2019 and 2020 can be reasoned by the pandemic which caused a substantial reduction in transport activities. However, according to the projection in **Figure 3**, an increase in emissions within the transportation sector until 2025 is expected with the scenario of not implementing any additional measures. The current billion-vehicle fleet in the transport sector is still largely dependent on fossil-derived liquid hydrocarbon fuels, e.g., diesel, gasoline, and kerosene with growing demand, especially in aviation and marine transport. Consequently, sustainable biofuels play a significant role in decarbonizing the transport sector and shifting towards a fossil-free society.

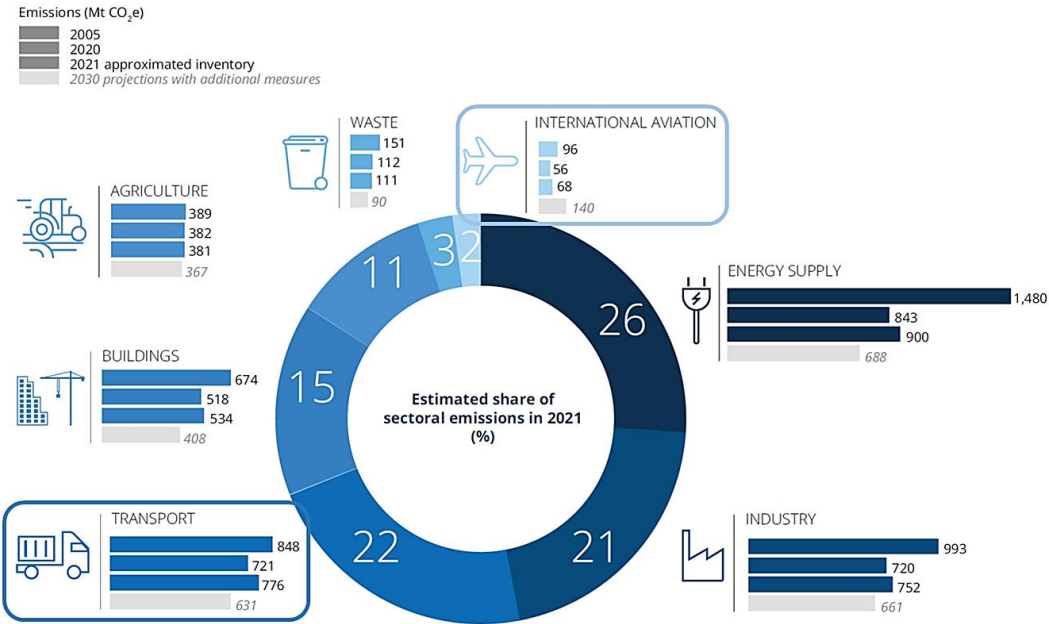


Figure 2. An overview of the historical and projected emissions development (Mt CO₂e) for the years 2005, 2020, 2021, and 2030 in various sectors (Agriculture, buildings, transport, industry, energy supply, international aviation, and waste), adapted from the Trends and projection report, 2022, European Environment Agency (EEA)³.

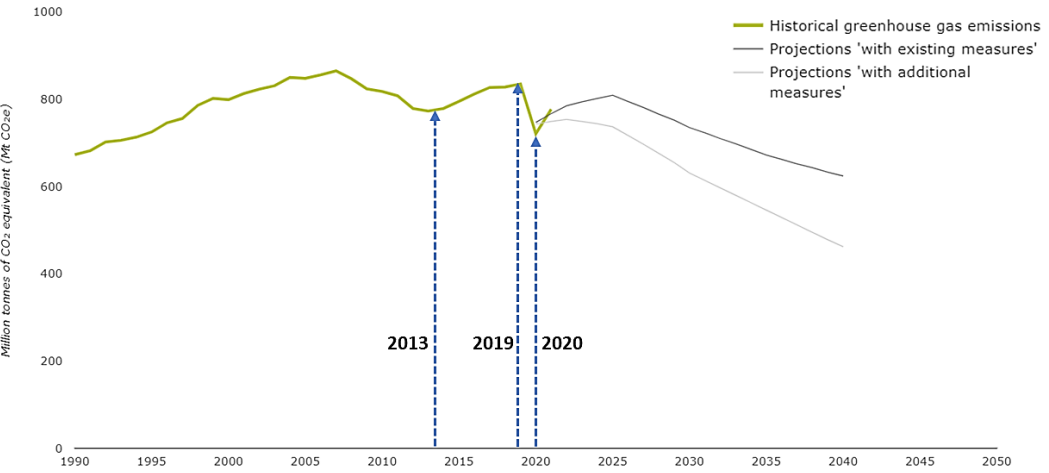


Figure 3. Greenhouse gas emissions (GHG) resulted from transportation in Europe (European Environment Agency). <https://www.eea.europa.eu/en>

Biofuels are renewable energy sources derived from biomass and their utilization is increasing owing to the legislation incentives aimed at the production of renewable transportation fuels. There are typically three types of biofuels: the first, second, and third-generation biofuels are characterized based on the biomass feedstocks used in their production process and their limitations as an energy source⁴ (**Figure 4**). The first-generation biofuels are derived from food crops such as sugar beets, corn starch, or vegetable oils. They are produced through well-understood processes such as fermentation, distillation, and transesterification. However, these feedstocks are criticized for competing with food crops, which impacts biodiversity and the competition for water. The production of second-generation biofuels was initiated to address the various disadvantages and limitations of first-generation biofuels. The second-generation biofuels use non-edible feedstocks from waste streams, e.g., food waste, residues from vegetable oil processing, and agricultural waste. These feedstocks can undergo different processes, such as thermochemical conversion (pyrolysis, gasification, liquefaction, and direct combustion), biochemical conversion, and hydroprocessing to yield renewable fuels. The production of renewable diesel from the hydroprocessing of vegetable oils and esters and fatty acids are great examples that fall under this category. The third-generation biofuels include solid bio-waste, mixed plastic waste, and engineered crops, such as algae biomass, which have a different growth yield in comparison to the typical lignocellulosic biomass.

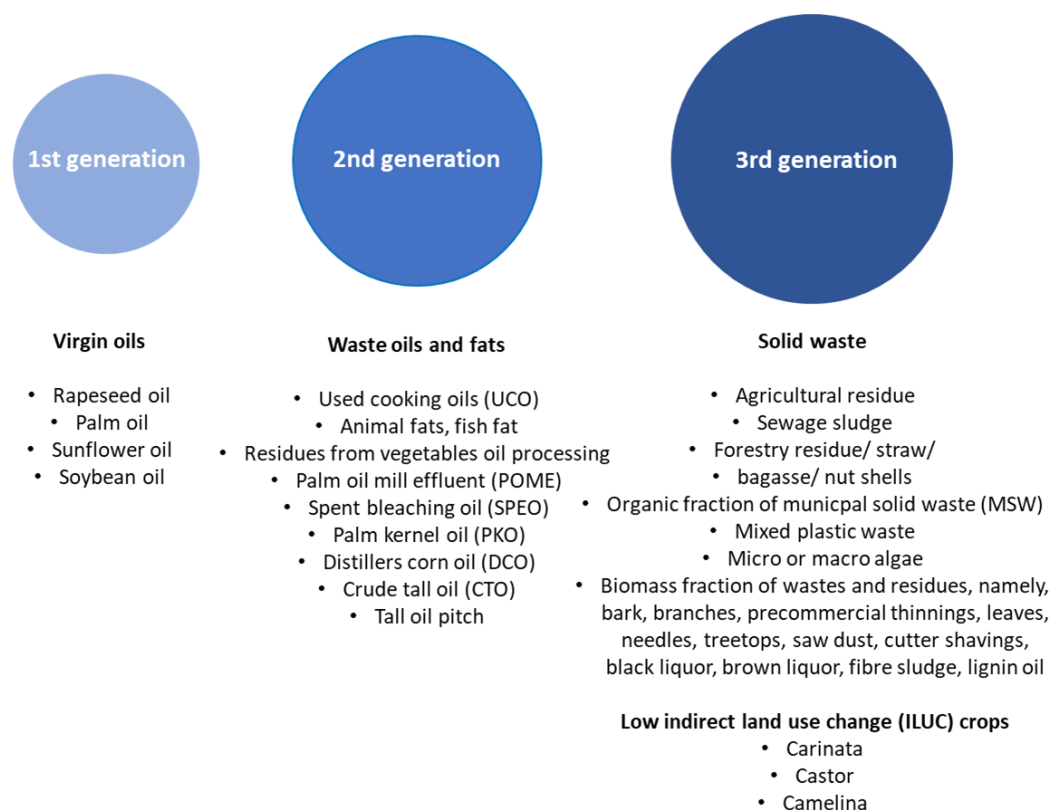


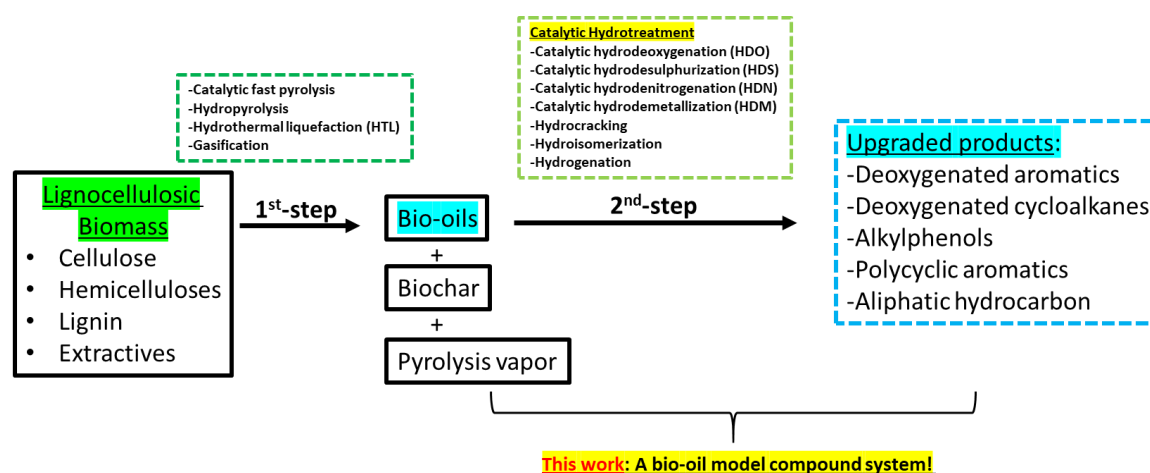
Figure 4. List of potential renewable feedstocks for biofuel production.

1.2 Objectives, scope, and outline of the thesis

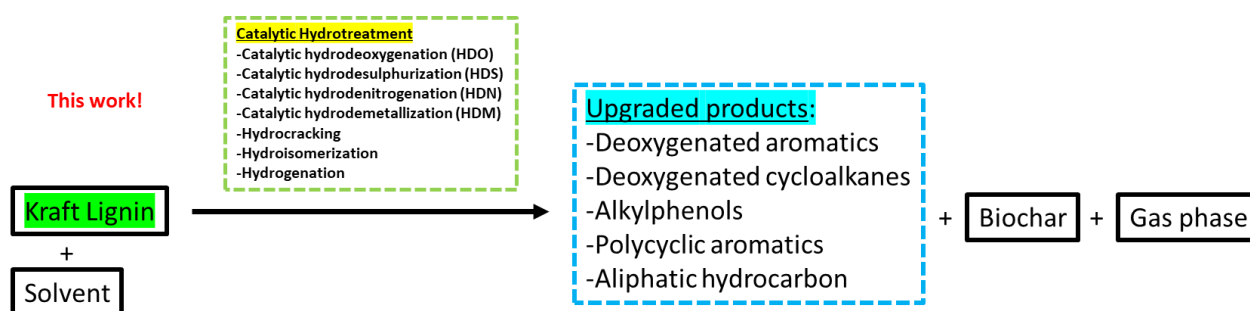
Lignocellulosic biomass-derived bio-oils produced via the thermochemical conversion of solid biomass and further upgrading through catalytic hydrotreatment have gained tremendous attention as a substitute for fossil-derived fuels in recent years. This two-stage process was drawn and is shown in **Scheme 1**. These biomass-derived oils from for example fast pyrolysis are also known as pyrolysis oil. Pyrolysis oil has a water content of 15-30 wt%

and a high oxygen content which contributes to its poor quality and also makes its utilization as fuel in internal combustion engines difficult. Hence, catalytic hydrotreatment, the second stage as shown in **Scheme 1** is required to refine the biomass-derived bio-oils so that they can be used as liquid transportation fuels.

Of the different biomass conversion technologies and upgrading processes, catalytic HDO remains an interesting subject to study for the improvement of the quality of biomass-derived bio-oils for direct use as transportation fuels. The main challenges of the complex HDO reaction of biomass-derived bio-oils are catalyst development, catalyst stability and poisoning, reaction network and mechanistic elucidation. Therefore, in this work, the focus has been placed on the main upgrading process, catalytic hydrodeoxygenation of a bio-oil model compound as illustrated in the 2nd-step in **Scheme 1** to produce deoxygenated aromatics, cycloalkanes, and alkylphenols. Moreover, biorefinery waste such as Kraft lignin provides an alternative to fossil feedstocks for the production of renewable chemicals and fuels. Thus, the simultaneous depolymerization, liquefaction, and hydrodeoxygenation of Kraft lignin in the presence of a solvent in one step were also investigated, as shown in **Scheme 2**. The current work provides a potential strategy for an efficient one-step valorization of the waste stream into high-value chemicals, platform chemicals, and liquid fuels.



Scheme 1. Two-stage process in the transformation of raw biomass to valuable products such as chemicals and transportation fuels.



Scheme 2. One-step hydrotreatment of Kraft lignin in the presence of a solvent for the production of high-value chemical and fuel components.

The main effort has been placed on investigating different transition metal sulfides (TMS), with and without catalyst support in the HDO of a bio-oil model compound, propylguaiaicol (PG). The activity and selectivity of the

sulfided catalysts for different desired products, such as deoxygenated aromatics, cycloalkanes, and alkylphenols, were studied. A series of screening experiments were conducted in **Paper I** to examine the influence of Ni, Fe, Zn, and Cu on the Mo-based sulfided catalysts for the HDO of PG. The effect of these transition metals was studied and compared with the traditional NiMo sulfided catalysts. All catalysts were subjected to different characterization techniques, such as X-ray diffraction (XRD), inductively coupled plasma (ICP)-sector field mass spectroscopy, nitrogen physisorption (BET), X-ray photoelectron spectroscopy (XPS), and transmission electron microscopy (TEM). A simplistic pseudo-first-order kinetic model that took into consideration side reactions was developed based on the proposed reaction network for HDO of PG over sulfided catalysts. Sulfided ZnMo, FeMo, and NiMo catalysts were also examined in the hydrotreatment of Kraft lignin, and the product selectivities were correlated with the results obtained from the HDO of PG.

The synthesis of unsupported MoS₂ catalysts using a facile hydrothermal synthesis method was examined in **Paper II**. The effect of an annealing treatment on the unsupported catalysts was studied in the HDO of PG. The combined effect of hydrothermal synthesis time and pH adjustment during the synthesis with the annealing treatment was investigated. Our in-house synthesized unsupported MoS₂ was compared with a sample of bulk MoS₂ in the model reaction and hydrotreatment of Kraft lignin. With the experience of working with Kraft lignin as a renewable feedstock in **Paper I** and **Paper II**, one of the major hurdles that we observed was the formation of undesired repolymerized/condensed solid residues and char fractions during hydrotreatment which leads to low monomer yield. In **Paper III**, to address the challenges when depolymerizing and upgrading lignin fragments, a series of NiMo sulfides and ultra-stable Y (USY) zeolites with the unsupported NiMoS catalyst were screened for the reductive liquefaction and further deoxygenation of Kraft lignin. The work also provided insight into the roles of NiMo sulfides and USY zeolites as a support, and their interactions during the depolymerization and deoxygenation of Kraft lignin, and repolymerization of lignin fragments forming char residues. In the further work, in **Paper IV**, we further explored the efforts in limiting and inhibiting the undesired secondary reactions during lignin depolymerization to ensure efficient depolymerization. On this subject, we worked on the co-hydrotreatment of Kraft lignin and pyrolysis oil over the unsupported NiMoS catalyst as a strategy to suppress solids formation. We further explored co-hydroprocessing with oxygenated monomers to understand the role of the co-reactant in suppressing char-induced reactions. The effect of several reaction parameters such as reaction time, temperature, catalysts loading, and co-feed reactant on the lignin hydrotreatment in terms of char and global bio-crude yield was studied. In **Paper V**, a two-stages hydrotreatment of fast pyrolysis-derived bio-oils that first involved the stabilization over an unsupported NiMoS catalyst in a continuous slurry hydrocracker and further upgraded in a fixed-bed reactor. The work aimed to demonstrate hydroprocessing a bio-feed at pilot-scale without any fossil co-feed producing a deoxygenated bio-hydrocarbon. Various analytical techniques were employed to better understand the composition and properties of the upgraded products. In **Paper VI**, a collective effort was gathered resulting in a review work that covered the upgrading of various renewable feeds (triglycerides, lignin model compounds, waste lignin, and pyrolysis oil) over metal sulfide catalysts. Special focus was placed on discussing aspects such as metal sulfide deactivation, reaction routes, and kinetics. Future research needs were also discussed in this review work. **Figure 5** presented the workflow and also topics included in each study.



Figure 5. Workflow and topics included in this thesis.

The outline of this thesis is as follows:

Chapter 2 introduces the use of transition metal sulfides in hydrotreating, the background of lignin, biomass-derived bio-oils, and catalytic hydrodeoxygenation (HDO). The same chapter also presents an extensive literature review on the HDO of phenolic monomers and real biomass feedstocks using supported and unsupported sulfided catalysts. The motivation for conducting studies using supported and unsupported sulfided catalysts is discussed. Slurry hydrotreatment of pyrolysis oil and approaches to suppress and limit the repolymerization of reactive lignin intermediates are also discussed.

Chapter 3 presents the experimental techniques used in catalyst synthesis, catalyst testing experiments, and the catalyst characterizations involved in appended papers.

Chapter 4 presents the main findings and discussions from the appended papers.

Chapter 5 provides the conclusion and summary of the thesis.

Chapter 6 discusses future work.

2 Background

2.1 Transition metal sulfides (TMS) as hydrotreating catalysts

In 1924, Krauch and Pier discovered the transition metal sulfides (TMS) as sulfur-resistant coal hydrogenation catalysts at the former Badische Anilin and Sodafabrik in Ludwigshafen⁵⁻⁷. TMS especially MoS₂ and WS₂ were found to be active in hydrogenation reactions. The application of TMS catalysts was further explored and employed in hydrodesulfurization (HDS), hydrodenitrogenation (HDN), and hydrodemetallization (HDM). These hydrotreating reactions aim to remove impurities such as sulfur, nitrogen, and metals that are present in the refractory fossil feedstocks. The modern hydrotreating catalyst systems used are the typical molybdenum (Mo) or tungsten (W) sulfide systems supported on alumina promoted by metals such as nickel (Ni) or cobalt (Co). TMS catalysts must be kept in sulfide form, and sulfiding agents, such as dimethyl disulfide (DMDS) or carbon disulfide (CS₂) are commonly co-fed in the hydrotreating on a lab scale to maintain the sulfidation degree of the catalysts. Industrially, the catalysts in the oxidized form are sulfided at the refinery site by passing sulfur-containing petroleum feed like gas oil through the catalyst bed⁸. Owing to the increase in interest in hydrotreating renewable feedstocks such as lignocellulosic biomass, pyrolysis bio-crudes, and triglyceride-derived feeds, which has a relatively high oxygen content of 10-40 wt%, hydrodeoxygenation (HDO) has gained tremendous attention in academia and also in the renewables business. TMS also plays a key role in HDO because of the similarity between the sulfur and oxygen atoms. The catalytic performance and progression of different reactions during HDO depend largely on the catalyst types, the catalyst support used, and HDO reaction conditions (reactor type, temperature, reaction time, solvent system, and pressure).

There are many reports related to the use of alumina as a support for hydrotreating catalysts because of its good textural and mechanical properties, and the fact that it is relatively inexpensive^{9,10}. The acidic properties of alumina are known to be beneficial in breaking the C-O bond in anisole which can be found in lignin oil⁹. The effect of different supports such as silica, activated carbon, and alumina on the activity of NiMo hydrotreating catalyst was also studied in vacuum residue hydrotreating reactions¹⁰. They concluded that the effectiveness of a hydrotreating catalyst depends largely on the size of the pore diameter, pore volume, and also the dispersion of the active metals that can contribute to a better hydroconversion¹⁰. This indeed highlights the importance of using support materials for the synthesis of hydrotreating catalysts. Mukundan et al. also studied the use of a carbon support for MoS₂-based catalysts and found promising results for HDO reactions^{11,12}. Carbon as a catalyst support attracts interest in HDO reactions because of its high surface area, inert nature, high thermal stability, stability in water, and low cost¹³.

Other than supported TMS catalysts widely reported in literature studies, many works have also been dedicated to the exploration of the potential of using unsupported (“bulk”) TMS catalysts for hydroprocessing. The exploration and development are also mainly driven by the increasing demand for the production of cleaner and greener fuel while shifting towards the utilization of heavy oils and vacuum residues and their conversion into lower boiling point fuel products. Apart from the heavy fossil-derived feedstocks, challenging renewable feedstocks (the so-called ‘unconventional’ feed) such as pyrolysis oil, forest residues, and waste bio-polymers like lignin also possess advantages when being processed with active bulk catalysts. The use of unsupported TMS catalysts allows for the

direct contact of the main active phase of the catalyst with the reactants/feedstocks and eliminates any possible interference with the support material during the hydroprocessing. By omitting the effect of mass transfer, diffusion limitations, and issues like pore-plugging, dispersed bulk catalysts can be effective in reactions such as slurry phase hydrotreating. One excellent example of the use of an unsupported catalyst system is the NEBULA technology that has been jointly established by ExxonMobil and Albemarle Catalysts^{14,15}. This commercialized and patented technology has been able to show the superior activity of the unsupported catalysts as compared to the conventional hydroprocessing catalysts¹⁵. Another application of the unsupported hydroprocessing catalysts was the Eni Slurry Technology (EST) process¹⁶. The EST process uses highly dispersed MoS₂ nanoparticles formed by the oleo-soluble molybdenum precursor co-fed with heavy oil feedstocks under reaction conditions of 400-450 °C and 150 bar with a continuous hydrogen flow resulting in high hydrogenation activity¹⁶. Furthermore, the promising results were demonstrated in a recent study using unsupported Mo precursors for the co-processing of fast pyrolysis bio-oil (FPBO) with heavy fossil feedstocks in a slurry hydrocracking unit¹⁷.

In this work, Kraft lignin was used as a renewable feedstock in the hydrotreatment process. Kraft lignin has a high molecular weight of typically around 16.7 kDa¹⁸. Hence, there is a significant obstacle to the diffusion of such large lignin polymer molecules or even their fragments into the porous support of the catalytic materials to access active sites. Besides, depolymerized lignin fragments produced from non-catalytic reactions can repolymerize and form char^{19,20}. Therefore, the transport limitations caused by the catalyst supports can hinder the stabilization of these radicals through hydrogenation reactions and promote char production. In this context, the use of highly active unsupported catalysts becomes attractive when dealing with lignin hydrotreatment. Moreover, Kraft lignin contains 1-2 wt% sulfur due to the pulping process and the sulfur content may act as a poison to noble metal catalyst systems²¹. Therefore, the use of sulfur tolerant catalysts like TMS can be of advantage when applied to the Kraft lignin hydrotreatment.

Besides, various hurdles such as the low solubility of solid lignin in the solvent, repolymerization, and condensation reactions of the depolymerized lignin fragments during hydrotreating resulting in the production of insoluble and intransigent solid char residues, lead to low bio-oil yield. The production of undesired char residues hampers the implementation of such solid bio-feedstocks in current facilities²². The necessity to limit and avoid the condensation and repolymerization reactions that occur under the liquefaction of lignin feed incentivizes the search for efficient lignin depolymerization methods for the production of lignin-derived monomers.

Sections 2.2, 2.3, 2.4, 2.5, 2.6, and 2.7 discuss lignin as a renewable feedstock, bio-crude properties, upgrading methods such as hydrodeoxygenation, the application of traditional supported and unsupported HDS catalysts in the upgrading of bio-oil monomer phenolics, co-processing of biomass feedstocks with emphasis on reaction mechanisms and networks, slurry hydrotreatment of pyrolysis oil, and approaches to suppress char residues, respectively.

2.2 Lignin, bio-oil properties, and catalytic hydrodeoxygenation (HDO)

Lignocellulosic biomass, one of the most abundant renewable on Earth has gained great interest in replacing fossil feedstocks as a major source of carbon, which is also renewable. It can play a vital role in the production of renewable carbon-based chemicals, materials, and fuels. The major mass of lignocellulosic biomass is found in the wood/plant cell wall which mainly consists of three biopolymers: cellulose (40-50%), hemicellulose (25-40%),

and lignin (20-30%), and also extractives. The composition of biomass largely depends on the biomass species. The fibers in the middle lamella and the bundled fibrils are bounded together by hemicellulose and lignin that give the tree and the wood its mechanical strength. Lignin is essentially comprised of phenylpropane units, such as coniferyl, sinapyl, and p-coumaryl alcohol (**Figure 6 b**) which are randomly interlinked by recalcitrant C-C and C-O bonds, as shown in **Figure 6 a**)²³. In the pulp and paper industry, lignin is a byproduct that has been often used as a renewable energy source by its combustion to produce heat and power for the paper mill and also to recover the inorganics. However, modern paper mills are increasingly energy-efficient, which has resulted in the energy from lignin combustion becoming unnecessary for the operation of the mill²⁴. Due to the increasing demand for a renewable carbon source in the production of biofuels and green chemicals, much research attention has been given to the efficient valorization of waste lignin into valuable chemicals and fuel components.

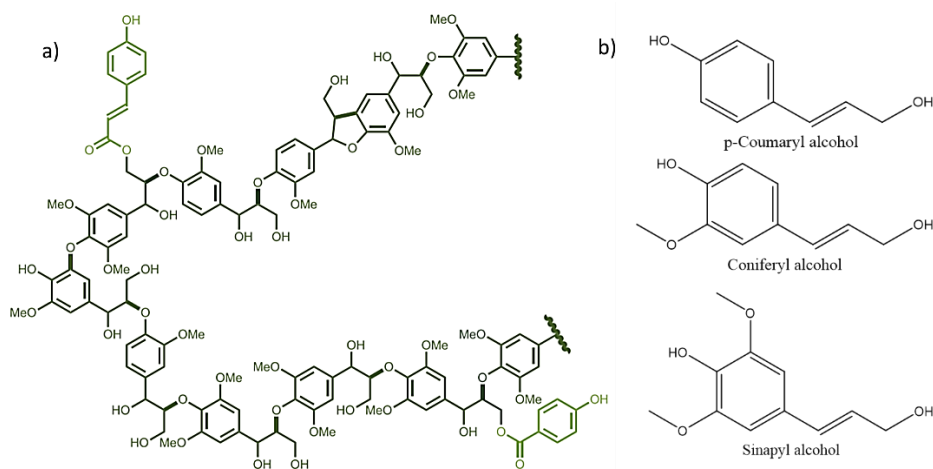


Figure 6. a) Model lignin chemical structure and b) building blocks of lignin.

Bio-oils can be produced via various processes and one of which is fast pyrolysis or thermal liquefaction of biomass²⁵. Fast pyrolysis is a thermochemical process where biomass is decomposed into bio-oils, bio-char, and volatile species at temperatures between 300-600 °C in the absence of oxygen with a short residence time of less than 2 s²⁶. The chemical composition of bio-oils can vary depending on the difference in the biomass feedstock used and the pyrolysis conditions. Different compound groups, such as acids, alcohols, aldehydes, ketones, phenolics, and sugars, can be found in the bio-oil constituents²⁶. This pool of compounds is derived from the depolymerized cellulose, hemicellulose, and lignin fraction of the lignocellulosic biomass. This liquid product also has a high-water content (15-30 wt%), which comes from the initial moisture of the biomass and it is acidic (pH 2-4) in nature due to the presence of carboxylic acids²⁶. The oxygen content of this product is also high at up to 40 wt% oxygen, giving it a high viscosity and a low heating value in comparison to fossil-derived hydrocarbon fuels²⁶.

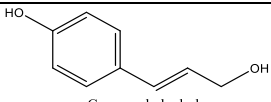
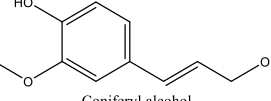
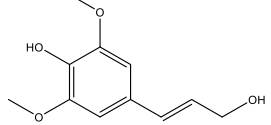
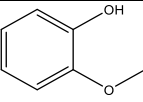
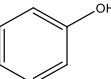
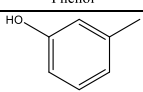
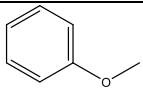
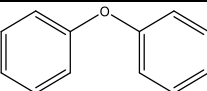
Biomass-derived bio-oils have various undesirable properties, leading to difficulties for their direct use as transportation fuels. Hence, bio-oils require a refining process to produce deoxygenated products that are compatible with existing fuel grades. Catalytic hydrotreating is a conventional hydroprocessing technology employed by refineries to improve the quality of fuels. This technology removes heteroatoms, such as sulfur, nitrogen, oxygen, and metals from the fossil feedstock through hydrodesulfurization (HDS), hydrodenitrogenation (HDN), hydrodeoxygenation (HDO), and hydrodemetallization (HDM). Bio-oils are different from petroleum oil,

because they typically have a negligible content of sulfur and nitrogen, whereas bio-oils have a high oxygen content. Hence, catalytic hydrodeoxygenation (HDO) has been adopted to remove excess oxygen from the bio-feedstocks in the form of water while using hydrogen as a co-reactant with the aid of a selective hydrotreating catalyst²⁷. Different reactions, such as demethoxylation (C-OCH₃ cleavage), dehydroxylation (C-OH cleavage), hydrogenation (C=O and aromatic ring saturation), hydrogenolysis, hydrocracking, transalkylation, and isomerization can occur to varying degrees during HDO, depending on the composition of the bio-oil, the reaction conditions and the catalyst used.

There has been great interest in studying the reaction networks and kinetics of the HDO of bio-oils over the past decades due to the increased utilization of such feedstocks for renewable fuel production. However, due to the complexity of the nature of bio-oils, several reactions can occur simultaneously during the upgrading process. Therefore, much research has been dedicated to the study of bio-oil model compounds in a lab-scale reactor to understand the reaction network and reaction mechanisms for HDO. The use of model compounds allows a quick assessment of the catalyst's activity and selectivity for compound groups, such as alkylphenols, deoxygenated cycloalkanes, and aromatics, before diving into complex feedstocks like lignin and pyrolysis oils. Different functional groups in the model compounds also facilitate the understanding of the relative activities and selectivity of the catalysts in cleaving different bonds and linkages. **Table 1** provides the bond dissociation energies (BDE) for different types of C-O bonds in bio-oil-derived model compounds²⁸. There are typically three types of C-O bonds: the bond between C_{aromatic}-OH (Ph-OH), C_{aromatic}-OCH₃ (Ph-Ome), and C_{aromatic}-O-CH₃ (Ph-O-Me) or C_{aromatic}-O-C_{aromatic} (Ph-O-Ph). The BDE analysis shows that the C-O bond energies decreased in the order: Ph-OH > Ph-Ome > Ph-O-Ph > Ph-O-Me. The etheric C-O bond is also weaker than the phenolic C-O bond.

In this thesis, the focus is on the HDO of the bio-oil model compound, 4-propylguaiacol (PG), and the hydrotreatment of Kraft lignin (KL). The selection of PG as a model bio-oil compound is because PG has a similar structure to coniferyl alcohol present in the lignin structure. The application of traditional transition metal sulfides (TMS) with and without catalyst support on the model reaction was investigated to understand the reaction network and kinetics of the HDO of PG. Furthermore, the role of the catalyst components was elucidated by comparing the supported and unsupported sulfided catalysts in the Kraft lignin hydrotreatment, and their interaction was studied giving insight into the depolymerization, and repolymerization routes forming char residues. In addition, the co-hydroprocessing of Kraft lignin with various bio-derived oxygenates over unsupported NiMoS catalysts was studied. The effect of the addition of a second reactant as a co-reactant during hydrotreatment was studied as a strategy for suppressing the undesired secondary reactions. The subsequent work also presented a strategy of valorizing fast-pyrolysis derived bio-oils in a slurry hydrocracker at pilot-scale using the unsupported NiMoS. The stabilized slurry feed was then hydrotreated in a fixed bed reactor over a commercial NiMo sulfide catalyst.

Table 1. The calculated homolytic bond dissociation energies (BDE) for different bio-oil model compounds calculated with B3lyp/6-311 G(d,p) level theory at 320 °C in the gas phase adapted from reference²⁸. The unit for BDE is given in kJ/mol.

Bond	Ph-OH	Ph-Ome	Ph-O-Me	Ph-O-OH
 p-Coumaryl alcohol	446.4	-	-	-
 Coniferyl alcohol	440.2	379.5	226.8	-
 Sinapyl alcohol	453.5	384.5	214.2	-
 Guaiacol	456.8	397.0	205.0	-
 Phenol	443.9	-	-	-
 m-cresol	443.5	-	-	-
 Anisole	-	384.0	238.0	-
 Diphenyl Ether	-	-	-	291.6

2.3 HDO of bio-oil model compounds over supported sulfided catalysts

Table 2 presents the state of the art of supported sulfided catalysts for the hydrotreating of phenolic monomers. Various catalytic systems employing mixed oxide supports in sulfided catalysts have been reported for the HDO of phenolics. Garcia-Mendoza et al. have studied the activities of NiWS supported on TiO₂, ZrO₂, and the mixed oxide TiO₂-ZrO₂ for the HDO of Guaiacol at 320 °C²⁹. Their results show that the support was responsible for the HDO reaction producing phenol, catechol, and methylated compounds with NiWS supported on TiO₂ showing an 80% HDO product selectivity at full guaiacol conversion²⁹. In a similar catalyst system, Hong et al. have shown that a 2 wt% Ni loading and 12 wt% W loading on such mixed oxide sulfided catalysts can give full guaiacol conversion and a 16% cyclohexane yield under different reaction conditions³⁰. The study also mentions that nickel (Ni) performs better than cobalt (Co) as a promoter in catalyzing the HDO of guaiacol³⁰. Another study using CoMoS supported on the mixed oxide Al₂O₃-TiO₂ for the HDO of phenol has also shown that the mixed oxide improved the HDO activity with a better metal-support interaction than the conventional CoMoS supported on Al₂O₃³¹. The use of activated carbon as catalyst support has also been reported in the literature³²⁻³⁴. Mukundan et

al. have prepared a single-layered amorphous MoS₂ on activated carbon for the HDO of guaiacol and found that a single-layer MoS₂ deposition promotes deoxygenation and hydrogenation better than multi-layered MoS₂ in the production of phenol³⁴.

The traditional NiMo on γ -Al₂O₃ in sulfided and reduced form was studied for phenol HDO³⁵. **Figure 7** shows the general reaction network for the HDO of phenol using a sulfided NiMo catalyst³⁵. The catalyst in sulfided form exhibited a higher than 90% cyclohexane selectivity, and the deoxygenation routes for the phenol HDO occurred in parallel, involving direct deoxygenation (DDO) of the hydroxyl group of phenol and the hydrogenation-dehydration (HYD) of the phenyl ring³⁵. The promoters play a role in conventional hydroprocessing catalysts. Badawi et al. have demonstrated that cobalt promotes both DDO and HYD pathways in the HDO of phenol to different extents³⁶. They have performed DFT calculations showing that both DDO and HYD pathways occur on sulfur vacancy sites (CUS)³⁶. Romero et al. have also reported the same findings³⁷. Using 2-ethylphenol as a model compound³⁸, they have found that both Ni and Co improve the deoxygenation rate, while Ni only facilitates the HYD pathway. The reaction mechanism for DDO and HYD is illustrated in **Figure 8** and **Figure 9**, respectively³⁷.

In addition to Ni and Co, a study conducted by Yang et al. has demonstrated that phosphorus (P) was able to promote the phenol HDO activity over a CoMoS-supported MgO catalyst, and they proved that DDO is the major pathway in phenol deoxygenation³⁹. A non-conventional hydrotreating catalyst like supported ReS₂ has been reported in several studies⁴⁰⁻⁴⁴. For instance, ReS₂ supported on SiO₂ or γ -Al₂O₃ catalyst was applied in the coprocessing of dimethyl dibenzothiophene and guaiacol⁴⁴. Both Re-based catalysts showed high HDS and HDO activities; ReS₂ supported on SiO₂ showed high HDO rates giving 40% HDO products⁴⁴. In addition to the cheap transition metals used as promoters, research has examined the use of noble metals as promoters for a metal sulfide catalyst in phenolics HDO^{41,45}. For instance, Ir and Pt have been incorporated into RuS₂/SBA-15 and used in the HDO of phenol⁴⁵. The results have demonstrated a higher conversion rate of phenol (37-41%) and better cyclohexane selectivity (62-63%) than the non-promoted RuS₂/SBA-15⁴⁵. It is important to note that the use of noble metals involves high costs for catalyst production, which limits their industrial application. The sulfur content in some bio-feedstocks, such as Kraft lignin, may act as a poison to such noble catalyst systems, nevertheless, studying such a system facilitates better insight into the reaction pathways of the HDO of phenolics.

Jongerius et al. have studied a pool of lignin model compounds using CoMoS supported on Al₂O₃ under the same reaction parameters (300 °C, 50 bar H₂, 4 h, and batch system) for comparison⁴⁶. Their main findings suggest that the mono-aromatic oxygenates underwent three distinct pathways that included HDO, demethylation, and methylation. This resulted in valuable products like phenol, benzene, cresols, and toluene⁴⁶. Less than 5% of hydrogenated products were detected in the reaction medium, indicating that hydrogenation is the least preferred reaction network for this catalyst system⁴⁶.

It is commonly found in the considerable number of studies on the HDO of phenolic compounds that sulfiding agents, such as dimethyl disulfide (DMDS) or carbon disulfide (CS₂), were co-fed during an experiment to create H₂S to maintain the sulfidation degree of the sulfided catalyst. Results show that adding a sulfiding agent during the HDO process had a negative effect on the HDO activity of phenolics but promoted the HDO of aliphatic oxygenates such as vegetable oils and animal fats⁴⁷. However, one should notice the addition of a sulfiding agent also plays a role in affecting the effectiveness of the catalyst other than the type of reactant being used. Ferrari et al. have studied the effect of H₂S partial pressure and sulfidation temperature on the conversion and selectivities

of phenolics³². It was found that the increase in H₂S partial pressure reduced the formation of deoxygenated products from the HDO of guaiacol over CoMoS supported on carbon³².

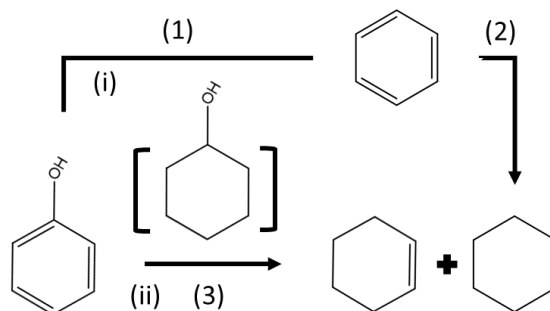


Figure 7. Reaction scheme for phenol HDO over sulfide supported NiMo catalyst³⁵. Reprinted (adapted) with permission from Templis, C. C, Revelas, C. J, Papastilianou, A. A, Papayannakos, N. G., *Ind. Eng. Chem. Res.*, 2019, 58 (16), 6278-6287. Copyright (2019) American Chemical Society.

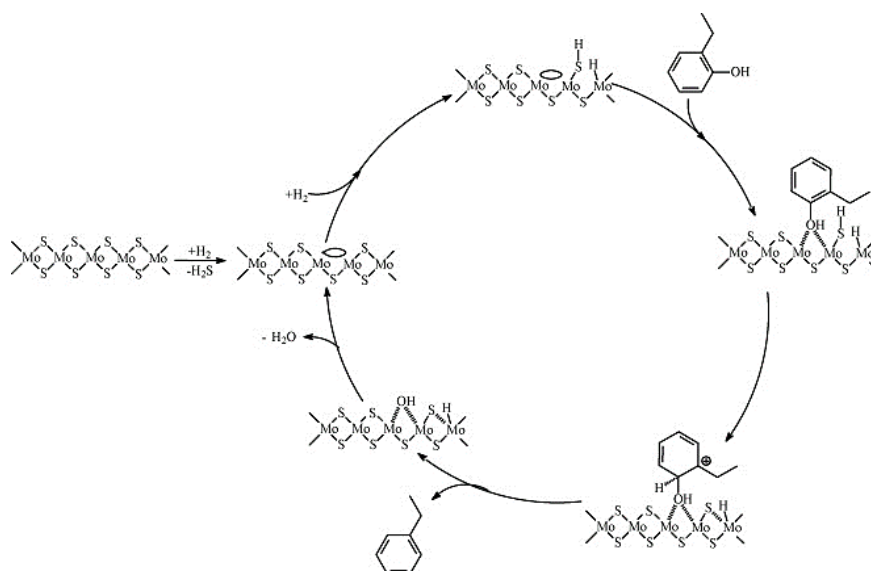


Figure 8. DDO reaction pathway for HDO of 2-ethylphenol over supported MoS₂ catalysts³⁷. This article was published in *Applied Catalysis B: Environmental*, Y. Romero, F. Richard, and S. Brunet, Hydrodeoxygenation of 2-Ethylphenol as a Model Compound of Bio-Crude over Sulfided Mo-Based Catalysts: Promoting Effect and Reaction Mechanism, *Appl. Catal. B Environ.*, 2010, 98 (3-4), 213–223, Copyright Elsevier (2010).

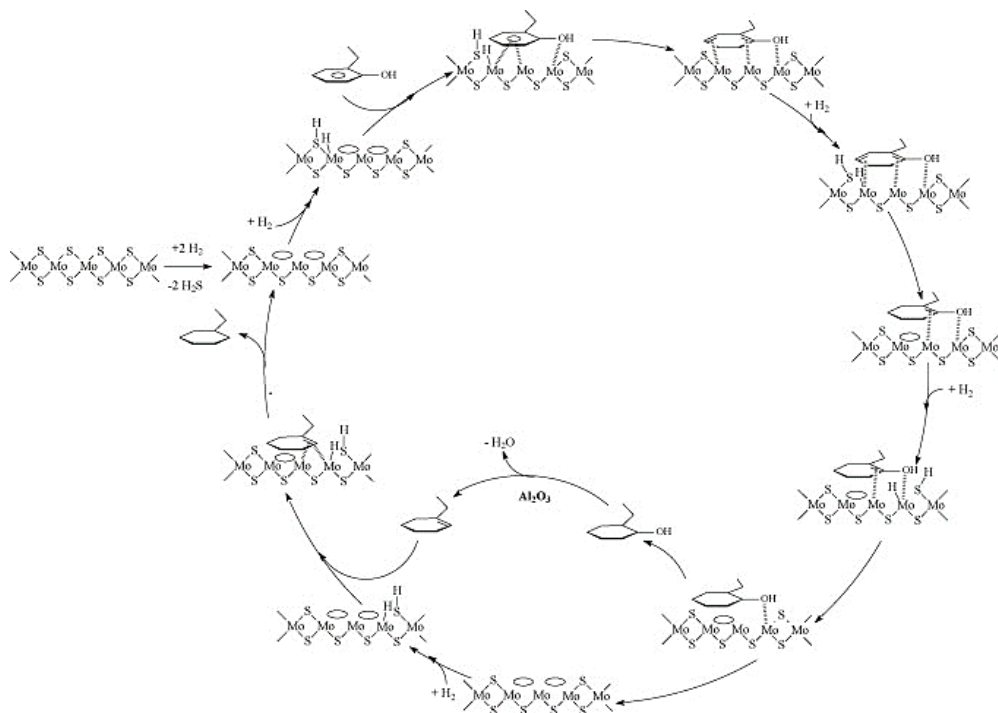


Figure 9. HYD reaction pathway for HDO of 2-ethylphenol over supported MoS₂ catalysts³⁷. This article was published in *Applied Catalysis B: Environmental*, Y. Romero, F. Richard, and S. Brunet, Hydrodeoxygenation of 2-Ethylphenol as a Model Compound of Bio-Crude over Sulfided Mo-Based Catalysts: Promoting Effect and Reaction Mechanism, *Appl. Catal. B Environ.*, 2010, 98(3-4), 213–223, Copyright Elsevier (2010).

Table 2. State-of-the-art sulfided supported catalysts for HDO of phenolic oxygenates.

Entry	Sulfided catalyst	Model compound	Solvent	Conversion (%)	Reaction conditions	HDO product selectivity (%)	Ref.
1	NiWS supported on TiO ₂ , ZrO ₂ , and TiO ₂ -ZrO ₂	Guaiacol	Hexadecane	100	Batch, 320 °C, 55 bar H ₂ and 1000 rpm	80% cycloalkanes (NiWS-TiO ₂)	29
2	CoMoS supported on Al ₂ O ₃ -TiO ₂	Phenol	Dodecane	93	Batch, 300 °C, 54 bar H ₂ and 1000 rpm	Benzene (65%), Cyclohexane (25%) and Cyclohexene (3%)	31
3	NiWS supported on TiO ₂	Guaiacol	n-decane	100	Batch, 2.5 h, 300 °C and, 70 bar	Phenol (37%), Cyclohexane (16%), Benzene (1%), Cresol (3%) and others (43%)	30
4	NiMoS supported on γ -Al ₂ O ₃	Phenol	Dodecane	-	Continuous, WHSV = 29/ 36 h ⁻¹ , 200/ 220/ 250 °C and 30 bar	Cyclohexene (traces), Cyclohexane (93.4%) and benzene (6.5%) for 200 °C and 29 h ⁻¹	35
5	CoMoS supported on Al ₂ O ₃	Phenol/2-ethylphenol	Toluene	-	Continuous, 400 °C, 70 bar	HDO activity (29.1 mmol.h ⁻¹ .g ⁻¹) for phenol and (22 mmol.h ⁻¹ .g ⁻¹) for 2-ethylphenol	36
6	NiMoS/CoMoS supported on γ -Al ₂ O ₃	Guaiacol/Phenol	m-xylene/n-hexadecane	30-100	Continuous/batch, 200-350 °C, 75-80 bar	Cycloalkanes (55% for NiMo and 45% for CoMo) at 300 °C	48

Table 2 (continued). State-of-the-art sulfided supported catalysts for HDO of phenolic oxygenates.

7	CoMoS supported on Al ₂ O ₃	Phenol, o-cresol, anisole, 4-methylanisole, catechol, guaiacol, 4-methylguaiacol, 1,3-dimethoxybenzene, syringol, and vanillin.	Dodecane	25-90	Batch, 4 h, 300 °C and, 50 bar	See ref ⁴⁶	46
8	NiMoS supported on γ -Al ₂ O ₃	Phenol and methyl heptanoate	Dodecane	100	Batch, 200/250 °C, and 75 bar	Cyclohexane (85%), cyclohexyl cyclohexane (14%), and others (1%)	49
9	MoS ₂ /NiMoS/CoMoS supported on Al ₂ O ₃	2-ethylphenol	Toluene	22-24	Continuous, 340 °C, and 70 bar	Oxygenated compounds (19.1%) and deoxygenated compounds (80.9%) for NiMoS	38
10	CoMoP/MgO	Phenol	Supercritical hexane	17-90	Batch, 350-450 °C, 1 h and 50 bar	Benzene (65%) and other (26%) at 450 °C	39
11	NiMoS/CoMoS supported on γ -Al ₂ O ₃	Phenol and methyl heptanoate	m-xylene	5-28	Batch/continuous, 250 °C, 1 h and 15 bar	See ref ⁴⁷	47
12	CoMoS supported on Al ₂ O ₃	Methyl-substituted phenols	n-heptane/n-decane	10-50	Continuous, 300 °C and 28.5 bar	See ref ⁵⁰	50
13	CoMoS on activated carbon	Guaiacol, ethyldecanoate, and 4-methylacetophenone	-	17-19	Continuous, 270 °C and 75 bar	See ref ³²	32
14	MoS ₂ on activated carbon	Guaiacol	Decalin	10-30	Batch, 300 °C, 50 bar, and 1000 rpm	See ref ³³	33
15	MoS ₂ on activated carbon	Guaiacol	Dodecane	55	Batch, 300 °C, 50 bar, 5 h, and 1000 rpm	Phenol (52%), Cycloalkanes (12.2%), cyclohexanol (5%), anisole (0.3%), benzene (0.4%), catechol (1.8%), veratrole (0.8%), methanol (0.04%) and gases.	34
16	(Ir or Pt) RuS ₂ /SBA-15	Phenol	Decalin	37-41	Continuous, WHSV = 1.28 h ⁻¹ , 310 °C, 30 bar, and TOS = 4 h	For Ir-RuS ₂ /SBA-15, cyclohexane (63%), cyclohexene (11%), benzene (7%), and cyclohexanol (19%)	45
17	ReS ₂ /SiO ₂	Guaiacol and phenol	Hexadecane and dodecane	15-20	Batch, 250 °C, 50 bar, and 4 h	For guaiacol, phenol (13%), catechol (1%), and cyclohexanol (0.5%)	41
27	ReS ₂ /SiO ₂	Guaiacol	Dodecane	80	Batch, 300 °C, 50 bar, and 4 h	For ReS ₂ /SiO ₂ , phenol (60%), cyclohexane (20%) and others.	40
28	ReS ₂ /activated carbon	Guaiacol	Dodecane	40-80	Batch, 300 °C, 50 bar, and 4 h	See ref ⁴²	42

Table 2 (continued). State-of-the-art sulfided supported catalysts for HDO of phenolic oxygenates.

29	ReS ₂ /SiO ₂ (Al ₂ O ₃)	Guaiacol and 4,6-dimethyldibenzo thiophene	Dodecane	80	Batch, 300 °C, 50 bar, and 4 h	See ref ⁴⁴	44
30	Re/ZrO ₂ and Re/ZrO ₂ -sulphated	Guaiacol	Decaline	10-70	Batch, 300 °C, 50 bar, and 4 h	See ref ⁴³	43
31	Ni/Cu/Zn/Fe on MoS ₂ /Al ₂ O ₃	Propylguaiacol and Kraft lignin	Dodecane	99	Batch, 300 °C, 50 bar, 1000 rpm, and 4 h	See ref ⁵¹ (This thesis)	51

2.4 HDO of bio-oil model compounds over unsupported sulfided catalysts

Conventional transition metal sulfides (TMS) typically contain molybdenum disulfide supported on a high surface area catalyst support and promoted by Ni or Co as described in **Section 2.3**. Over recent decades, these traditional TMS catalysts have been tested by omitting the use of the catalyst support, resulting in unsupported TMS.

Table 3 presents the state-of-the-art of unsupported TMS for phenolic HDO. There are several methods to prepare unsupported TMS, that can be used in the hydrotreatment processes. One of these is a hydrothermal synthesis at moderate synthesis temperature (150-250 °C) and the absence of hydrogen pressure⁵²⁻⁵⁷. Wu et al. have prepared a series of hydrophobic unsupported MoS₂, NiS₂-MoS₂, and CoS₂-MoS₂ using hydrothermal synthesis with the aid of silicomolybdic acid for the HDO of 4-ethylphenol⁵⁶. The CoS₂-MoS₂ catalyst achieved a 99.9% 4-ethylphenol conversion with a 99.6% ethylbenzene selectivity after 3 h. The catalyst showed good recyclability after 3 runs at 225 °C⁵⁶. Another study by Wang et al. has proposed a reaction network for p-cresol HDO using a hydrothermally prepared CoMoS catalyst, as shown in **Figure 10**⁵². Two different deoxygenation routes for p-cresol have been proposed: the first is the DDO route, where the partially hydrogenated dihydrocresol is attacked by the dissociated H⁺ and the OH₂⁺ species is cleaved in the form of H₂O-producing toluene⁵². The second route involves HYD where the partially hydrogenated p-cresol is fully hydrogenated to 4-methylcyclohexanol and then dehydrated to 3-methylcyclohexene. The product, 3-methylcyclohexene then underwent hydrogenation and formed methylcyclohexane⁵². The study also described a p-cresol adsorption scheme on the unsupported CoMoS catalyst⁵², as shown in **Figure 11**. P-cresol could adsorb via its vertical orientation and coplanar position in relation to the DDO and HYD routes, respectively⁵².

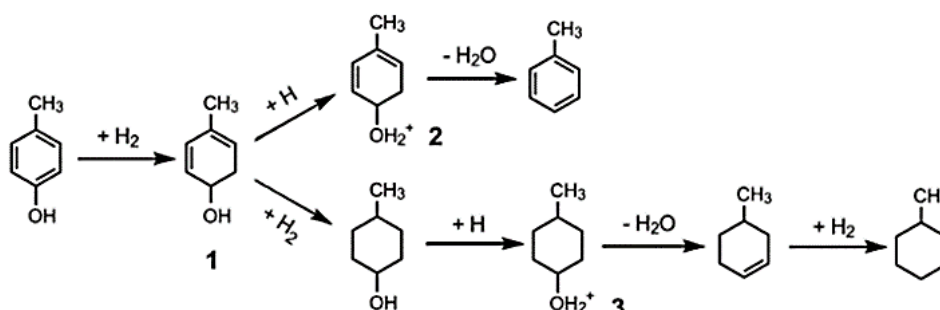


Figure 10. A reaction network for p-cresol HDO over unsupported CoMoS catalyst⁵². Reprinted (adapted) with permission from Wang, W, Zhang, K, Li, L, Wu, K, Liu, P, Yang, Y., *Ind. Eng. Chem. Res.*, 2014, 53 (49), 19001-19009. Copyright (2014) American Chemical Society.

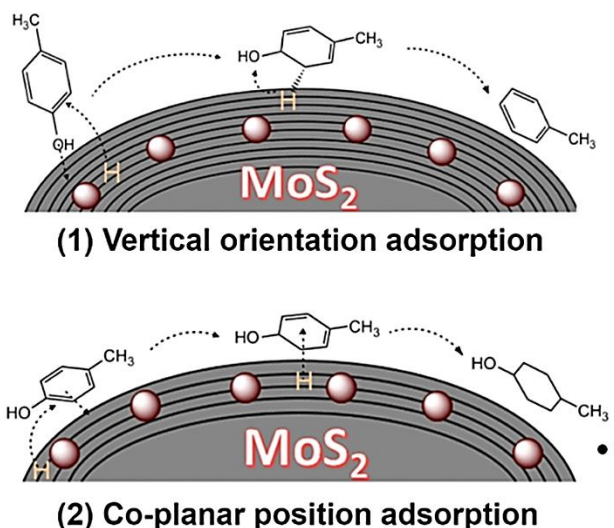


Figure 11. Adsorption scheme for HDO of p-cresol over unsupported CoMoS catalyst⁵². Reprinted (adapted) with permission from Wang, W, Zhang, K, Li, L, Wu, K, Liu, P, Yang, Y., *Ind. Eng. Chem. Res.*, 2014, 53 (49), 19001-19009. Copyright (2014) American Chemical Society.

A hard template like mesoporous silica SBA-16 has also been used to synthesize an unsupported NiMoW sulfide catalyst for the HDO of guaiacol in a fixed-bed reactor⁵⁸. The NiMoW sulfide unsupported catalyst gave a 99.6% guaiacol conversion with minimal coke formation at 400 °C⁵⁸. Adapted from the reference, shown in **Figure 12**, guaiacol underwent HDO via demethylation (DME), demethoxylation (DMO), and transalkylation⁵⁸. Phenol was formed by either the direct demethoxylation of guaiacol or the dehydroxylation of catechol; both reactions resulted in the production of benzene⁵⁸. It is worth noting that phenol was first obtained from the HDO of guaiacol as a reaction intermediate caused by the higher bond dissociation energy for the hydroxy group in the aromatic ring than in the methoxy group²⁶. Recently, in a mini-review by Cao et al., they summarized the use of unsupported MoS₂ catalysts in the deoxygenation of bio-oil model compounds such as p-cresol focusing on synthesis, defect engineering of MoS₂, and deactivation mechanism⁵⁹. It was highlighted that more efforts should be dedicated to the synthesis of single-layer MoS₂, reduced-layer-number MoS₂, and defect-rich MoS₂ that can significantly improve HDO activity⁵⁹.

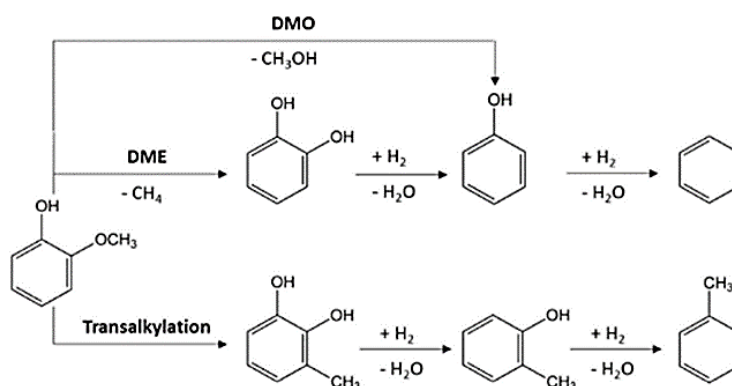


Figure 12. A proposed reaction scheme for HDO of guaiacol over NiMoW catalyst⁵⁸. This article was published in *Catalysis Communications*, Tran, C. C, Stankovikj, F, Kaliaguine, S, *Unsupported Transition Metal-Catalyzed Hydrodeoxygenation of Guaiacol*, *Catal. Commun.*, 2017, 101, 71–76, Copyright Elsevier (2017).

Table 3. State of the art of sulfided unsupported catalysts for HDO of phenolic oxygenates.

Entry	Sulfided catalyst	Model compound	Solvent	Conversion (%)	Reaction conditions	HDO product selectivity (%)	Ref.
1	MoS ₂ , NiS ₂ -MoS ₂ , and CoS ₂ -MoS ₂	4-ethylphenol and 4-propylguaiacol	Dodecane	44-81.5	Batch, 300 °C, 40 bar, 5 h and 900 rpm	See ref ⁵⁶	56
2	CoMoS nanosulfide	p-cresol, anisole, and diphenyl ether	Decalin	100 after 3 h (p-cresol)	Batch, 300 °C, 40 bar, and 4 h	Arene yield (98%)	60
3	CoS ₂ /MoS ₂	Creosol and phenol derivatives	Dodecane	18-98	Batch, 250 °C, 40 bar, and 1 h	For CoMo-0.3, toluene (99%)	61
4	MoS ₂ and CoMoS ₂	Phenol	n-decane	30-98	Batch, 350 °C, 28 bar, 150 rpm, and 1 h	See ref ⁶²	62
5	Amorphous NiMoS	Phenol	n-decane	34.5-96.2	Batch, 350 °C, 28 bar, 150 rpm, and 1 h	For NiMoS-0.3, benzene (30.4%), cyclohexane (52.4%), cyclohexene (9.8%), cyclohexanone (7.4%)	63
6	MoS ₂	Phenol, 4-methylphenol, and 4-methoxyphenol	Hexadecane	34-52	Batch, 350 °C, 28 bar, 1000 rpm, and 7 h	For phenol, benzene (36%), methylcyclohexane (6%) and cyclohexylbenzene (43%)	64
7	NiMoW	Guaiacol	-	99	Continuous, 400 °C, 28 bar, and WHSV = 2.7 h ⁻¹	Phenol (45%), creosol (15%), catechol (10%), and hydrocarbon (30%)	58
8	CoMoS	p-cresol	Dodecane	78.8-98.7	Batch, 350 °C, 28 bar, 900 rpm, and 7 h	For CoMo-0.5-200, methylcyclohexane (6.3%), methylcyclohexene (1.5%) and toluene (92.2%)	52
9	Ni-WmoS	p-cresol	Dodecane	85-97.9	Batch, 300 °C, 40 bar, 700 rpm, and 6 h	For W-Mo-0.5, methylcyclohexane (66.7%), methylcyclohexene (3.2%) and toluene (30.3%)	65
10	NiMo(W)S	4-methylphenol	Decalin	93.9-97.8	Batch, 300 °C, 30 bar, 800 rpm, and 5 h	Toluene (87.2%), methylcyclohexane (11.3%), and 4-methylcyclohexene (1.5%)	66
11	NiMoWS	4-methylphenol	Decalin	87-100	Batch, 300 °C, 30 bar, 800 rpm, and 5 h	Toluene (95.6%), methylcyclohexane (2.9%), and 4-methylcyclohexene (1.5%)	67
12	MoP, MoS ₂ , and MoO _x	4-methylphenol	Decalin	30-100	Batch, 300 °C, 30 bar, 800 rpm, and 5 h	See ref ⁶⁸	68
13	MoS ₂ (effect of adding CTAB)	p-cresol	Dodecane	42-100	Batch, 275 or 300 °C, 40 bar, 900 rpm, and 5 h	See ref ⁶⁹	69
14	NiMoS	p-cresol	Dodecane	67-100	Batch, 300 °C, 40 bar, 900 rpm, and 5 h	For NiMo-0.3, methylcyclohexane (67.1%), 3-methylcyclohexene (4.12%), and toluene (28.8%)	70
15	Fe-MoS ₂	p-cresol	Dodecane	63.3-98.3	Batch, 250 °C, 40 bar, 900 rpm, and 5 h	For FeMo-0.3, methylcyclohexane (3.7%), methylcyclohexene (1.6%), and toluene (94.7%)	71

Table 3 (continued). State of the art of sulfided unsupported catalysts for HDO of phenolic oxygenates.

16	NiMoS from oil-soluble precursors	Guaiacol	Toluene and water	100	Batch, 320-380 °C, 30-70 bar, 700 rpm, and 4-8 h (water gas shift reaction)	See ref ⁷²	72
17	Unsupported MoS ₂	Propylguaiacol and Kraft lignin	Dodecane	90%-99%	Batch, 300-340 °C, 50-76 bar, 1000 rpm, and 5 h	See ref ⁷³ (This thesis)	73

2.5 Hydrotreatment of real bio-oils and lignin over sulfided catalysts

The use of model compounds for an HDO reaction cannot fully represent the reactivity of biomass feedstocks. However, the use of model compounds allows quicker evaluation of a catalyst and the elucidation of reaction networks before examining a complex feedstock. This section presents a brief review of studies of the hydrotreatment of biomass feedstocks and lignin over sulfided catalysts, as summarized in **Table 4**.

In contrast to the pyrolysis or gasification of solid biomass, as described in **Section 2.1**, the one-pot hydrotreatment of lignin or biomass involves the simultaneous depolymerization of the complex structure of lignin into various oxygenated oligomers and fragments which then subsequently undergo full or partial deoxygenation reactions to yield deoxygenated aromatic and alkylphenolic monomers as illustrated in **Figure 13**. Besides, the depolymerized fragments from lignin may also repolymerize and form char. The undesired char byproducts are usually caused by the saturation and repolymerization of the free radicals formed during the cracking, hydrocracking, and condensation reactions. This one-step process is usually performed in the presence of a solvent under high hydrogen pressure and also high operating temperature. Joffres et al. studied the use of hydrogen donor solvents in the one-step hydrotreatment of wheat straw soda lignin over NiMoS/Al₂O₃⁷⁴. Their study highlighted that the use of hydrogen donor solvents such as tetralin is effective in depolymerizing lignin and also limiting condensation reactions⁷⁴. The low char production in their experiments can be explained by the stabilization of the free radicals resulting from the cleavage of the C-C or C-H bonds during lignin depolymerization with the hydrogen radicals from tetralin⁷⁴. Moreover, in a recent review by Stummann et al., they highlighted that using a highly active catalyst regardless of the promoter types and support acidity can suppress the char formation reactions resulting in lesser solid yield⁷⁵. A solvolytic oil from liquified lignocellulosic biomass was hydrotreated in a batch reactor setup with different hydrogen donor solvents over a series of catalysts such as NiMo/Al₂O₃ catalysts in an oxide, reduced, and sulfided form and reduced Pd/Al₂O₃ or carbon⁷⁶. The sulfided NiMo on alumina was found to give excellent liquid product yield with good rheological properties and gross calorific value⁷⁶. Levec et al., have studied the same liquified solvolysis oil hydrotreated using unsupported MoS₂, Mo₂C, MoO₂, and WS₂ catalysts⁷⁷. They have reported the synthesis of urchin-like MoS₂ interconnected with carbon materials through the sulfidation of Mo precursors, such as MoI₃ and cyclopentadiene-MoCl₄⁷⁷. Their work has demonstrated that the synthesized unsupported MoS₂ gives a high selectivity for deoxygenation and possesses a three times higher dehydroxylation rate than the commercially available bulk MoS₂⁷⁷.

Organosolv poplar lignin-derived oil has been subjected to depolymerization using MoS₂ on activated carbon (AC), which resulted in high selectivity for alkylphenols (76.2%)⁷⁸. The study highlights MoS₂/AC as an effective catalyst in simultaneous depolymerization coupled with the demethoxylation of lignin fragments, which produces alkylphenols⁷⁸. Another study has reported Kraft lignin hydrotreatment for the production of alkylphenols using a

variety of sulfided Mo and W on various supports promoted by Ni and Co⁷⁹. Sulfided NiW/AC has been found to efficiently depolymerize lignin and yielded 28 wt% of monomers. It also yielded 76% of alkylphenolics and guaiacolics in the course of an 8 h hydrotreatment⁷⁹. The study highlights a few points about lignin depolymerization, and any additional upgrading, and concludes the following items: (i) sulfided catalysts were more active than the oxide catalysts, (ii) W metal was preferred than Mo, (iii) Ni is a better promoter than Co, and (iv) support plays an important role in achieving high product yields, and acidic supports promote char formation. Mukundan et al. have studied the cleavage of C-C and C-O bonds in lignin using various model compounds and Kraft lignin over NiMoS on carbon¹¹. The catalysts demonstrated good activity in lignin depolymerization, resulting in low molecular compounds comprised of monomers and dimeric aromatics¹¹. The excellent catalytic activity was mainly attributed to the absence of support metal interaction, which promotes the formation of the NiMoS phase for deoxygenation activity¹¹.

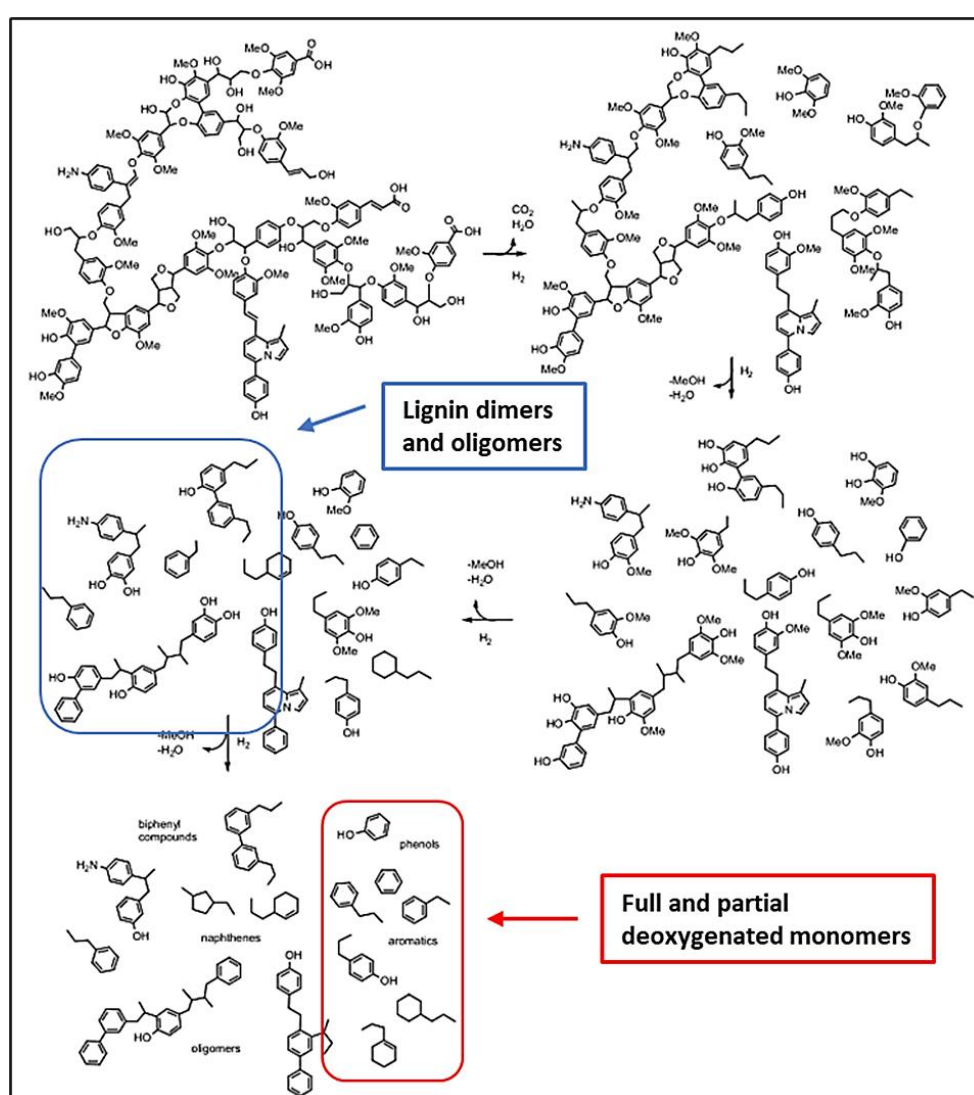


Figure 13. Reaction scheme of lignin hydroconversion over sulfided NiMo/Al₂O₃ adapted from reference⁷⁴. This article was published in *Applied Catalysis B: Environmental*, B. Joffres, M. T. Nguyen, D. Laurenti, C. Lorentz, V. Souchon, N. Charon, A. Daudin, A. Quignard, and C. Geantet., Lignin Hydroconversion on MoS₂-based supported Catalyst: Comprehensive Analysis of Products and Reaction Scheme, *Appl. Catal. B Environ.*, 2016, 184, 153–162, Copyright Elsevier (2016).

Table 4. Hydrotreatment of biomass feedstocks (real biomass/lignin-derived bio-oils) over sulfided catalysts.

Entry	Sulfided catalyst	Feedstocks	Solvent	Conversion (%)	Reaction conditions	HDO product selectivity (%) and remarks	Ref.
1	Supported oxide, reduced and sulfided NiMo, Ni, Mo, and Pd	Solvolyzed lignocellulosic biomass	Hydrogen donor solvents (Tetralin, 2-propanol, phenol, m-cresol, anthracene, cyclohexanol, xylene, and pyridine)	-	Semi-continuous, 300 °C, 80 bar, and 1 h	See ref ⁷⁶	76
2	Unsupported MoS ₂ , MoO ₂ , Mo ₂ C, and WS ₂	Solvolyzed lignocellulosic biomass	Tetralin	-	Semi-continuous, 300 °C, 80 bar, and 1 h	See ref ⁷⁷	77
3	Supported MoS ₂	Organosolv poplar lignin oil	Methylcyclohexane	-	Batch, 300 °C, 30 bar, and 10 h	Alkylphenol (76.2%), cycloalkanes (15.5%) and arenes (8.3%)	78
4	Supported NiW and NiMo	Kraft lignin	Supercritical methanol	-	Batch, 320 °C, 35 bar, and 8 h	See ref ⁸⁰	80
5	Supported NiMo and CoMo	Kraft lignin	Solvent-free	65-91	Batch, 350 °C, 100 bar, 1200 rpm, and 4 h	See ref ⁷⁹	79
6	CoMoS on alumina	Wheat straw soda lignin	Tetralin	91	Semi-continuous, 350 °C, 80 bar, 800 rpm, and 13 h	See ref ^{81,82}	81,82
7	NiMoS ₂ on carbon	Lignin model compounds and Kraft lignin	Dodecane	-	Batch, 300 °C, 50 bar, catalyst:feed ratio = 1:10, and 3 h	For Kraft lignin experiment, total monomer yield (18.98%)	11
8	Commercial sulfided NiMo	Wheat/barley straw bio-oil	-	-	Continuous, 340 °C, 40 bar, feed flow rate g.h ⁻¹ , and TOS of 80 h	See ref ⁸³	83
9	NiMoS/Al ₂ O ₃	Wheat straw soda lignin	Tetralin/Dodecane	71-35	Batch, 350 °C, 80 bar, 800 rpm, and 1/14/28 h	See ref ⁷⁴	74
10	ReS ₂ /Al ₂ O ₃	Kraft lignin	Hexadecane	> 98%	Batch, 350 or 400 °C, 56-68 bar, 1000 rpm, and 3-6 h	See ref ⁸⁴	84
11	Unsupported NiMoS-SBA catalysts	Kraft and hydrolysis lignin	Hexadecane	91-99.5%	Batch, 330-400 °C, 50-80 bar, 1200 rpm, and 5-12 h	See ref ⁸⁵	85
12	Unsupported NiMoS and NiMo-USY zeolites	Kraft lignin	Hexadecane	~99%	Batch, 400 °C, 72-80 bar, 1000 rpm, and 5 h	See ref ⁸⁶ (This thesis)	86

2.6 Slurry hydrotreatment of pyrolysis oil over sulfided catalysts

Pyrolysis oil produced from the fast pyrolysis of solid biomass contains a variety of compound groups like sugars, alcohols, phenols, ketones, aldehydes, furans, and acids. These compounds contribute to various detrimental properties of pyrolysis oil which need to be addressed before the full utilization of pyrolysis oil as a fuel or other applications by hydrotreatment in petroleum refineries. Slurry hydroconversion of challenging feedstocks like pyrolysis oils and fossil residues to renewable liquid hydrocarbon can be seen as a potential technology for the stabilization of renewable feeds before their further processing. In slurry hydroprocessing, a slurry feed containing

the liquid feedstock and a dispersed unsupported catalyst was introduced to the hydrocracker with hydrogen undergoing a hydrocracking process. Besides, many strategies have been explored for hydroprocessing FPBO, for instance, one-stage packed-bed hydroprocessing⁸⁷, two-stage mild hydrotreating followed by high-temperature hydrocracking^{88,89}, and a pre-derivatization step followed by hydrotreating in a fixed-bed hydrotreater⁹⁰.

Shumeiko et al. performed a series of screening tests of lab-synthesized and commercial sulfided NiMo catalysts for long-term hydrotreatment of wheat/barley (50/50 wt%) straw-derived pyrolysis oil in a fixed-bed reactor aiming to produce a hydrotreated pyrolysis oil that is compatible with the petroleum refinery fraction for co-processing⁸³. The assessment of their results was based on the HDO and HDS activity. Their results showed that the catalysts synthesized by co-impregnation were better than the catalysts prepared by a two-step impregnation procedure despite having the same active NiMo phase loading and the same commercial alumina support. While the commercial catalysts performed worst among all the catalysts in terms of HDO activity, they showed the best HDS performance⁸³. The difference in activity may be attributed to the different physicochemical properties of the catalysts and also preparation methods. These results suggest that the HDS activity of a sulfide catalyst is not suitable for indicating its HDO performance for pyrolysis oil. The long-term experiments (80 h) in their work were useful in understanding the deactivation of the sulfided catalysts⁸³. Their experimental results showed product quality changes, which were indicated by a gradual loss of catalyst activity with increasing time-on-stream⁸³. Thus, their work demonstrated the feasibility of using biomass-derived pyrolysis oil to obtain a compatible feedstock for co-processing in a refinery, however, the stability of the sulfided catalysts needs to be fully addressed before achieving a successful deployment of the technology.

Another study conducted by Zhang et al. looked at upgrading a pyrolysis oil produced by the fast pyrolysis of forest residues with light cycle oil (LCO) as a reaction medium using a dispersed unsupported MoS₂ catalyst⁹¹. The use of the dispersed unsupported catalysts was considered to allow better interaction between the active sites of the catalysts, hydrogen, and the heavy feedstock resulting in less solid yield. The low solid yield ranging from 0.8 to 1.8 g/100 g bio-oil at the end of their experiment showed that the use of dispersed unsupported materials can suppress the side reactions such as polymerization and re-polymerization of the large molecular weight compounds and reactive species that result in solid residues. Besides, Bergvall et al. also demonstrated the co-hydroprocessing of fast pyrolysis bio-oils (FPBO) with vacuum residues and vacuum gas oil with different feeding ratios in a continuous, as well as a semi-batch, slurry hydrocracker using *in-situ* sulfided oil-soluble molybdenum precursors¹⁷. The continuous run with 24 h time-on-stream resulted in highly deoxygenated liquid products¹⁷. Their results show that the semi-batch run of FPBO with the heavy residues resulted in coke formation and also higher gas yield as compared to the run without FPBO¹⁷. It was also mentioned that FPBO is sensitive to high temperatures which can lead to issues like coke formation and clogging within the reactor system¹⁷.

Priharto et al. studied the hydrotreatment of pyrolysis oil derived from lignin-rich digested stillage over commercial sulfided NiMo and CoMo catalysts⁹². They demonstrated the feasibility of utilizing solid waste residues from bioethanol processes for the production of pyrolysis oil. The further hydrotreatment of the pyrolysis oil also resulted in an appreciable oil yield of 60-64 wt%⁹². It should be noted that the nitrogen content in such feed should be refined employing hydrodenitrogenation (HDN), as, from their GCMS analysis, nitrogen-containing aromatic heterocyclic compounds present in the feed like indoles were converted to pyrroles. Hence, the removal of nitrogen content in pyrolysis oil by means of hydrodenitrogenation (HDN) should be addressed in

any future study with the aid of sulfided catalysts. For instance, Izhar et al. studied HDN of fast-pyrolysis oil derived from sewage sludge over a phosphorus-promoted sulfided NiMo/Al₂O₃ catalyst⁹³. The main finding from their work showed that dissolving pyrolysis oil using a non-polar solvent like xylene improved nitrogen removal compared to using protic solvents due to the competition between denitrogenation and deoxygenation reactions⁹³. It is apparent that to ensure the successful assimilation of challenging renewable feedstocks into existing infrastructures, various aspects such as the use of catalysts, co-refining techniques, process optimization, improvements, and pretreatment of feedstocks, etc. are needed.

2.7 Strategy to suppress char formation reactions – use of co-solvent, co-reactant, or capping agent

Exploring different approaches that can limit and avoid the condensation and repolymerization reactions that occur under the liquefaction of lignin sources employing different depolymerization methods (i.e. solvolysis, base-catalyzed, hydrothermal liquefaction (HTL), oxidative, and reductive) could provide an opportunity for the production of lignin-derived monomers. Kim et al. have summarized in a mini-review discussing the possible undesired secondary reactions during the liquefaction process of lignin and also efforts to suppress those undesired reactions and in turn, maximize the yield of low molecular weight products⁹⁴. The undesired secondary reactions like condensation already occurred during the fractionation and pretreatment of biomass limiting the production of the low molecular weight lignin fraction. It was mentioned that reactive intermediates such as carbocation and quinone methides induced the repolymerization reactions and resulted in the formation of condensed lignin⁹⁴. Lignin condensation can be classified into benzylic carbocation-induced diarylmethane (DCM) condensation, aldehyde-induced DCM, radical-induced coupling reactions, and carbonyl-induced aldol condensation⁹⁵. Lan et al. presented an overview of different ways to avoid the recondensation of lignin, and these ways can be divided into two major groups, the first group focuses on trapping the reactive lignin intermediates *in-situ* and forming a more stable lignin molecule, and the second group focuses on preventing the formation of reactive intermediates by physical or chemical stabilization of lignin linkages⁹⁶. Another review work outlines the strategies using chemical functionalization as a means to stabilize the reactive intermediates resulting from the condensation pathways during the defragmentation of biomass⁹⁷. One of the char mitigation methods is to supply or co-feed a second reactant during the liquefaction of lignin, this second reactant/co-solvent can function as a capping agent, which can chemically trap the reactive intermediate resulting from the depolymerization and prevent charring reactions. There are also studies showing the use of phenol as a protecting agent in the base-catalyzed lignin depolymerization^{98,99} and also hydrothermal liquefaction of lignin exhibited a positive influence in terms of achieving high bio-oil yields and also suppressing repolymerization of large lignin fragments¹⁰⁰. **Table 5** presents an overview of literature related to various strategies in suppressing the undesired secondary reactions during lignin valorization using a co-solvent, co-reactant, or capping agent.

Table 5. Literature overview related to the use of co-solvent, co-reactant, or capping in lignin valorization for char suppression.

Co-solvent or reactant	Reaction system	Finding	Ref.
Methanol	Sodium lignosulfonate (SL) depolymerization in continuous mode	-SL was found depolymerized thermally, without any catalyst, and independent of the solvent mixture. -The MeOH/water solvent system resulted in higher monomer yield and lower molecular weight products.	101
Ethanol/Methanol	Soda lignin depolymerization	-The capping effect of ethanol resulted in the stabilization of reactive phenolic intermediates by O-alkylation of OH groups and C-alkylation of aromatic rings. -Ethanol was found to be more efficient than methanol.	102
Ethanol/Methanol	Lignin depolymerization/hydrogenolysis	-Ethanol as a solvent system resulted in a higher monomer yield than methanol. -Ethanol scavenges lignin-derived formaldehyde which is known to be involved in undesired repolymerization reactions.	103
Phenol/Boric acid	Base-catalyzed lignin depolymerization in water	-Boric acid and phenol as a capping agent yielded different products distribution during lignin depolymerization. -Using phenol as a capping agent resulted in higher phenolic compound yield and low char yield.	98
Phenol and methanol	Hydrolytic treatment of black liquor using NaOH as a catalyst	-Supplementing phenol reduces the repolymerization and condensation reactions during Kraft lignin depolymerization in black liquor.	104
Phenol	Phenol-assisted lignin depolymerization	-Phenol acts as a solvent for lignin dissolution. -Phenol scavenged the methylene linkages (C-C linkage) in condensed lignin facilitating lignin depolymerization	105
Formaldehyde	Extraction of lignin under acid condition	-Formaldehyde reacts with 1,3 diol structure of β -O-4 linkages to form acetals and prevents the formation of a reactive carbocation intermediate inhibiting the condensation reactions.	106
Boric acid	Base-catalyzed lignin depolymerization	-Boric acid inhibited the addition and condensation reactions by capping the phenolic OH group by forming boric ethers and increasing oil yield.	107
Aniline	Oxidative lignin depolymerization	-Aniline can stabilize vanillin by protecting the carbonyl group through the reversible formation of imine.	108
Isopropanol	Hydrothermal liquefaction (HTL) of softwood Kraft lignin	-Isopropanol as a co-solvent presented a capping effect such as the reduced molar mass of both char and also precipitated solids. -The char-suppressing effect of isopropanol is less effective as compared to phenol under similar reaction conditions.	109
Ethylene glycol (EG) and ethanol (EtOH)	Reductive solvolysis of lignosulfonate	-The depolymerized fragments of lignin oil in EtOH had a lower molecular weight compared to the oil product in EG. -EG inhibited condensation reactions.	110
Lignin-derived phenolic oil	Base-catalyzed lignin depolymerization	-The organosolv lignin was depolymerized into phenolic oil and used as a renewable capping agent in base-catalyzed lignin depolymerization. -The usage of a capping agent favored the demethoxylation of guaiacyl units, and reduced the repolymerization reactions and thus the solid char yield.	99
p-hydroxybenzyl alcohol (HBA)	Acid-catalyzed lignin depolymerization	-HBA is a novel capping agent. -HBA was able to limit condensation reactions resulting in a high yield of depolymerized ethyl acetate soluble lignin with high antioxidant ability.	111
Formic acid	Mild catalytic reductive Kraft lignin depolymerization in ethanol/water	-Formic acid generates in-situ hydrogen. -The addition of 3.6 vol% formic acid in the process provided smaller depolymerized lignin fragments with more phenolic OH functionalities	112
Glycerol	HTL of Kraft lignin	-Glycerol decreased the molecular weight of the liquid product but increases the char yield. -The addition of NaOH in the process, improved the yield of monoaromatics. -Short residence time is beneficial in minimizing char formation.	113

3 Experimental

This chapter of the thesis describes the catalyst synthesis methods, catalyst characterization methods, catalytic test measurements, and product analytics methods.

3.1 Catalyst synthesis

3.1.1 Supported sulfided catalysts

Unpromoted Mo supported on γ -alumina (**Paper I**) was prepared using a conventional wet impregnation method following the procedure reported earlier by our group¹¹⁴. This unpromoted Mo γ -alumina-supported catalyst was then further loaded with a second transition metal, such as Nickel (Ni), Zinc (Zn), Iron (Fe), or Copper (Cu), via a conventional incipient wetness impregnation method. For instance, a solution of 3 wt% of $\text{Ni}(\text{C}_5\text{H}_7\text{O}_2)_2$ in 20 mL of ethanol was first prepared for the Ni-promoted catalyst. The unpromoted Mo supported on γ -alumina catalyst was dissolved in 25 mL of ethanol. The nickel precursor solution was added dropwise to the solution of the Mo catalyst prepared in the previous step. 10 mL of ethanol was used to wash off the residue in the beaker containing the Ni precursor solution to ensure that all solutions had been transferred. The catalyst slurry was then stirred overnight under a fume hood to evaporate all the ethanol. The dry catalyst was calcined at 400 °C for 4 h in air. The same procedure was followed for the preparation of FeMo, ZnMo, and CuMo on γ -alumina. Iron (III) acetylacetonate (99%), $\text{Fe}(\text{C}_5\text{H}_7\text{O}_2)_3$, Zinc acetylacetonate hydrate (99.995%), and copper (II) nitrate hemipentahydrate (98%) were used as Fe, Zn, and Cu precursors, respectively. These catalysts were sulfided before the catalytic tests and will from this point on be denoted as the Mo, NiMo, ZnMo, FeMo, and CuMo catalysts.

The description of the supported catalyst preparation method for **Paper III** is presented in **Section 4.3, Table 11**.

3.1.2 Unsupported sulfided catalysts

A facile hydrothermal synthesis inspired by various studies was followed in the second study to prepare an unsupported MoS_2 (**Paper II**)^{115,55}. The preparation steps were modified taking into account the different apparatus available in our laboratory. 0.35 g of ammonium heptamolybdate tetrahydrate (>99%) and 1.3 g of thiourea (>99%) were both first dissolved in 55 mL of distilled water with gentle stirring. The pH of the solution was then adjusted to 0.8 using hydrochloric acid (35 wt%). This pH alteration step was omitted for one catalyst sample to evaluate the influence of pH adjustment on catalyst properties. After the pH adjustment, the mixed solution was divided equally and transferred to a 70 mL Teflon liner. The filled Teflon liner was then placed and sealed in a stainless-steel autoclave. The mixed solution was heated to 200 °C in an oven for either 12 h or 24 h; taking 20 minutes for the oven to reach the desired temperature. After 12 h or 24 h of heating, the oven was cooled to room temperature, and the as-synthesized catalyst (black) was collected by filtering and washing the resulting solution in the Teflon liner several times with absolute ethanol. The filtered and washed catalyst was covered and dried under a vacuum at 50 °C overnight. After vacuum drying, the freshly prepared as-synthesized catalysts were tested in the model reaction without any further treatment. These as-synthesized catalysts were denoted as MoS_2 -12 and MoS_2 -24, corresponding to the synthesis time. For a second set of samples, the as-synthesized catalysts underwent an annealing pre-treatment at 400 °C for 2 h under nitrogen flow prior to their implementation in the model reaction. These pretreated catalysts were then denoted as MoS_2 -12a or MoS_2 -24a. Commercially available bulk MoS_2 from

Sigma-Aldrich in powdered form with a particle size of $\sim 6 \mu\text{m}$ (max. $40 \mu\text{m}$) and a sulfided Mo-supported catalyst were also used in the second study for comparison.

For the third and fourth studies in this work, the unsupported NiMoS catalyst (**Paper III** and **Paper IV**) was synthesized using a hydrothermal method with further modification reported in the second study. Precursors for Ni, S, and Mo were Nickel (II) nitrate hexahydrate, thiourea, and ammonium heptamolybdate tetrahydrate respectively. The metal precursors were weighted according to the molar ratio of Ni:Mo of 1:2 and with 4.25 g of thiourea, they were dissolved in 180 mL of distilled water. Then 7 mL of HCl (36 wt%) was slowly added into the solution to adjust the pH to approximately pH 1. The sample solution was transferred into a Teflon liner and put into the autoclave before closing the lid. The oven was set at $200 \text{ }^\circ\text{C}$ for 12 h. After 12 h, the sample was cooled down, it was filtered, and washed with MilliQ water several times, followed by absolute ethanol. The solid catalyst that was collected on filter paper was covered with aluminum foil and dried under vacuum in an oven at $50 \text{ }^\circ\text{C}$ overnight. The dried catalyst was ground in a mortar to refine the particles and break any solid clumps, weighted, and stored in a dry cabinet.

3.2 Kinetics measurements

The HDO kinetics measurement experiments were carried out in a 300 mL stainless steel batch reactor (Parr instruments). The reactor was equipped with a magnetically driven internal stirrer, an inlet that was connected to an H_2/N_2 gas line, an outlet for gas release, and a sampling line for reaction liquid sample collection (0.5 – 2 mL). The reactor setup is shown in **Figure 14**.

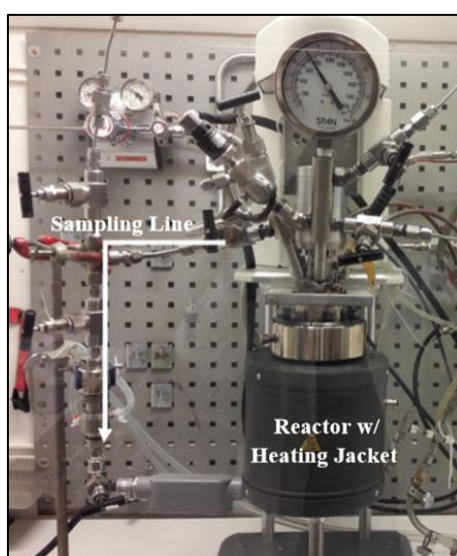


Figure 14. The batch reactor set-up.

Prior to the activity test, 0.5 g of catalyst was sulfided in the batch reactor using 0.5 mL of dimethyl disulfide (DMDS, $\geq 99.5\%$, Sigma-Aldrich) with 20 bar of H_2 at $340 \text{ }^\circ\text{C}$ for 4 h. The reactor was loaded with 1 g of reactant, 0.5 g of pre-sulfided catalyst, 0.1 mL of DMDS, and 100 mL of dodecane for a typical experiment. After loading the reactor with all the reactants, the reactor was first flushed with N_2 three times to remove air, followed by three flushings with 5 bar of H_2 . The final reaction conditions for all experiments were set at $300 \text{ }^\circ\text{C}$, 50 bar H_2 , and 1000 rpm. Reaction samples were collected at 0.5 h, 1 h, 2 h, 3 h, 4 h, and 5 h. The sampling line was purged with

N₂ before collecting the reaction sample. After each reaction sample collection, a small drop in pressure approx. 1 bar was observed. The pressure drop was immediately compensated by repressurizing the reactor to maintain the same pressure. When the reaction was finished, the reactor was rapidly cooled to room temperature with a water bath. The spent catalyst was recovered, filtered, centrifuged, and washed with acetone to remove adhering reactants and products. It was then dried under atmospheric conditions for further analysis. The same procedures were followed in the second study. However, 66 mg of unsupported catalyst was used in these experiments.

Parts of the first, second, third, and fourth studies involved the hydrotreatment of Kraft lignin (KL). The hydrotreatment reaction was carried out in the same batch reactor described above. Prior to the reaction experiment, the reactor was loaded with 0.75 g of catalyst, 2.25 g of KL (Sigma-Aldrich), and 75 mL of hexadecane as a solvent. The catalyst and lignin mass ratio was maintained at 1:3. The final reaction conditions were 340 °C or 400 °C, a total of 70-76 bar of H₂ pressure depending on the catalyst was used, and stirring speed 1000 rpm. The hydrotreatment reaction was monitored for 3 h, 5 h, 6 h, or 8 h once the reaction temperature was reached. The heating period took approx. 40 minutes to reach the desired temperature. No reaction samples were collected for these experiments. The liquid product rich in hexadecane obtained after the hydrotreatment was regarded as bio-oil in all the studies. The solid residues obtained after the filtration contained char residues and also spent catalysts. The solid residues were washed with acetone several times to remove the residual hexadecane and dried in an oven overnight. The dried solid was then washed with dimethyl sulfoxide (DMSO) to dissolve unconverted lignin. The yield of lignin-derived char residue was determined based on the initial lignin feed by subtracting the catalyst weight and the unconverted lignin from the total dried weight of the solid products.

A pilot slurry hydrocracking (SHC) facility located in RISE Research Institutes of Sweden ETC, Piteå was used for a first stage of hydrotreatment of FPBO (**Figure 15**) in **Paper V**. The SHC pilot plant consisted of a stirred tank batch reactor with a total volume of 2.6 dm³, a slurry preparation tank, a double-syringe pump, a High Pressure-High Temperature (HP-HT) separator, a Low Pressure-Low Temperature (LP-LT) separator, actuators, and product collection tanks equipped with scales. At the beginning of the campaign, the reactor was filled with 1.67 g of unsupported NiMoS catalysts (referred to as unsupported NiMoS in **Papers III** and **IV**) and 500 g of hexadecane. The batch system was leak proofed and pressurized with hydrogen to 100 bar and heated to 410 °C with a heating rate of 200 °C/h. The stirring rate was set at 1340 rpm and a continuous hydrogen flow of 1800 Ndm³/h was fed throughout the experiment. In the slurry preparation tank, 9.867 kg of FPBO, 33 g (contains 30% Mo, based on total catalyst weight) of unsupported NiMoS, and 1 g of DMDS were input into the tank to create the slurry feed. When the desired reaction temperature was reached in the main reactor, a continuous feed of FPBO slurry (0.33 wt% catalyst concentration) with a flow rate of 1 dm³/h was used throughout the experiment. The average residence time was 2.6 h and a liquid hourly space velocity (LHSV) of 0.385 h⁻¹ resulted from the liquid flow rate. The slurry feed and H₂ were fed into the bottom of the reactor vessel that had reached the reaction temperature.

The liquid and gas samples were continuously withdrawn during the experiment from the top of the reactor to a high-pressure high-temperature (HP-HT) separator. In the HP-HT separator, the water and light volatile organic compounds were evaporated while the remaining heavy liquid product was withdrawn through the bottom of the separator and directed to the collection tank. The evaporated product was directed to a low-pressure low temperature (LP-LT) separator where the products were separated into water fractions and light oil products and

directed to the collection tanks. The mass flow of the gas stream was continuously measured using a Coriolis mass flow meter and further analyzed by a micro-GC with dual thermal conductivity detectors (TCD). The product collection tanks were placed on scales for continuous monitoring of the masses of final products. The feeding of the slurry started at 09:45 (07-06-2022), and after 3.75 h, the heavy product tank was emptied. The collected products were centrifuged and separated into a water phase, an oil phase, and a hexadecane phase (initially present in the main reactor). The continuous feeding of the slurry proceeded for another 4 h and the heavy product was again collected. The collected heavy product was then centrifuged and separated into a water phase and an oil phase. These collected heavy liquid products were then dewatered by distillation to separate the remaining water. The resulting light oil product collected from the collection tank was then mixed with the dewatered heavy product and further filtered with a 10-20 μm filter, creating a stabilized slurry FPBO for further hydrotreatment in a fixed bed reactor.

The fixed-bed hydrotreater used in **Paper V** is located in the mini-refinery in RISE, Södertälje. The fixed-bed reactor is equipped with a thermometer slit, and a furnace, and has the dimensions: 0.5 inch (12.7 mm) external diameter, 0.4 inch (10.22 mm) internal diameter, 916 mm bed height, and 75.1 mL bed volume. The catalytic bed was first dried under nitrogen at 10 bar and 250 °C. The catalyst used was pelletized supported NiMo on δ -alumina (HDC-10) from Hulteberg Chemistry and Engineering. The catalyst was then sulfided using a flow of light gas oil (LGO) with 4 wt% dimethyl disulfide (DMDS) at 70 bar hydrogen pressure and 350 °C for 4 h. The continuous reaction was performed with the stabilized feed from the SHC at 80 bar H_2 with a liquid flow corresponding to an LHSV of 0.5 h^{-1} and a gas-to-oil volumetric feed ratio of 1000:1. 11 liquid samples were collected at different times on stream during the hydrotreatment with varying reaction temperature.

Six liquid samples were fractionated into aqueous and organic phases. The organic phases were pooled and underwent distillation into three main fractions as follows: a fraction with a boiling point below 177 °C collected at atmospheric pressure, a fraction with a boiling point between 177-343 °C, and a fraction with a boiling point above 343 °C (distillation residue). These distillate fractions were further analyzed to understand their composition and functionality.

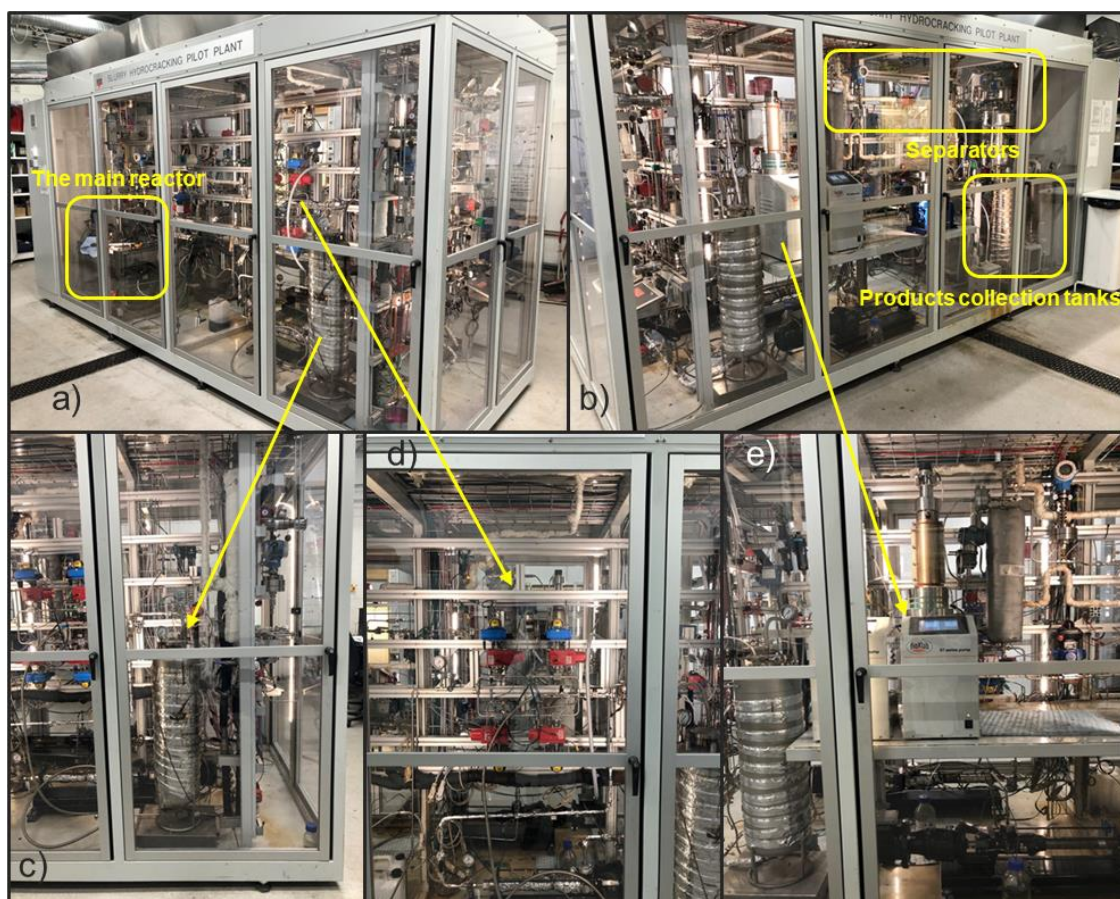


Figure 15. Slurry hydrocracker (located in RISE ETC, Piteå) used in **Paper V** a) front view of SHC, b) back view of SHC, c) slurry feed tank, d) actuators, and e) double-syringe pump.

3.3 Product analysis

For the first study, the liquid reaction samples were analyzed with a GC-MS (Agilent 7890-5977A). The GC-MS was equipped with a non-polar HP-5 column (30 m × 250 μm × 0.25 μm), a Flame Ionization Detector (the setpoint was 335 °C), and a mass spectrometer for compound identification via a NIST library. The initial oven temperature was 100 °C for 1 minute and then the temperature was increased to 190 °C at a rate of 10 °C/min. The temperature was increased to 300 °C at a heating ramp of 30 °C/min and was maintained constant for 1.333 minutes.

External calibration curves were obtained for 4-propylguaiacol, propylcyclohexane, 4-propylphenol, propylbenzene, 4-propylresorcinol, 1,2-dimethoxy-4-propenylbenzene, gamma terpene, 4-tertbutylanisole, and 2-methyl-6-propyl phenol using commercial chemicals.

The unit for the concentration of reactant and reaction products is expressed in molar percent (mol%). The following definitions were used in this study:

PG conversion was calculated as

$$C_{PG}(\%) = \frac{C_0 - C_t}{C_0} \times 100 \quad (1)$$

where C_0 is the initial concentration of PG and C_t is the concentration of PG at the reaction time equal to t .

Reaction product yields were calculated as

$$Y_{product}(\%) = \frac{C_{product,t}}{C_0} \times 100 \quad (2)$$

where $C_{product,t}$ is the concentration of the reaction product at the reaction time t .

Reaction product selectivities were calculated as

$$S_{product}(\%) = \frac{C_{product,t}}{C_0 - C_t} \times 100 \quad (3)$$

The molar balance was calculated to evaluate the material balance in the liquid phase of the HDO reaction. The molar balance was calculated by dividing the sum of the concentration of all identified reaction products and the initial feed at reaction time t by the concentration of the initial feed at time zero. The carbon balance on the liquid phase was checked for all reported experiments and found to be in the range between 95% and 99%. The missing carbon from the balance calculations could be attributed to the experimental errors and also small amounts of light hydrocarbons and carbon oxide byproducts in the gas phase after the reaction.

The same GC-MS was used in the second study to analyze the bio-liquid products from the catalytic hydrotreatment of KL. The initial GC oven temperature was 50 °C for 5 minutes and then the temperature was increased to 300 °C at a rate of 10 °C/min. This was maintained constant for 5 minutes. The solid residues obtained from the filtration of the bio-liquid were washed first with acetone and then dried in an oven at 80 °C overnight. The unconverted lignin retained in the dried solid was dissolved with dimethyl sulfoxide (DMSO) washing. After dissolving the unconverted lignin with DMSO, the solid product was dried again in an oven at 80 °C overnight.

The bio-liquid products were also in some cases analyzed with 2D GC × GC-MS FID (Agilent 7890-5977A) gas chromatography equipped with an oven, a flow splitter, a modulator, and a flame ionization detector. The injector temperature was 280 °C and the sample injection volume was 1 μL. Helium gas was used as a carrier gas with a flow rate of 1 mL/min with a split ratio of 30. The chromatographic separation involved two columns: a mid-polar phase column VF-1701MS (30 m × 250 μm × 0.25 μm) and a non-polar phase column DB-5MS UI (1.2 m × 150 μm × 0.15 μm). The modulation time on the modulator was 8 s. The oven temperature was initially set at 40 °C for 1 min and then heated up to 280 °C at a rate of 2 °C/min. The flame ionization detector temperature was set at 250 °C. The hydrogen flow rate was 30 mL/min and the airflow rate was 350 mL/min. The analysis was performed using the GCImage software for multidimensional chromatography. The individual product selectivities in the liquid were calculated by dividing the corresponding MS blob volume of a product by the total MS blob volume for all identifiable products in the liquids.

For the third study (**Paper III**), the 2D GC analysis was done using the same method as in **Paper I** and **II**, with greater effort being placed on the quantification of individual components of the bio-oils. The bio-oil yields were measured using external standard calibrations. Dihexyl ether was used as an internal standard. Calibration curves were obtained using different commercially available individual compounds with five known concentrations (wt%) points such as n-butylbenzene, benzene, toluene, ethylbenzene, xylene, propylbenzene, 1,2,3-trimethylbenzene, propylcyclohexane, cyclopentane, cyclohexane, methylcyclohexane, cyclohexanol, propylcyclohexanol, 4-propylphenol, guaiacol, p-cresol, creosol, 2-ethylphenol, 4-propylguaiacol, 4-

ethylguaiacol, 1,3-dimethylnaphthalene, propylanisole, butylanisole, methylnaphthalene, 1,5-dimethyltetralin, 2-methyl-1,1'-biphenyl, phenol, biphenyl, and phenanthrene. All detected compounds by GC were accounted for when calculating the total yields of bio-oils and were grouped into deoxygenated cycloalkanes, aromatics like alkylbenzenes, alkylphenolics, and also polyaromatics like indanes and naphthalenes.

For the co-hydrotreatment in which Kraft lignin and pyrolysis oil or oxygenated monomers were used (**Paper IV**), the bio-oil yield was calculated based on the total initial loaded reactants (both Kraft lignin and pyrolysis oil/monomers). The 2D GC analysis in **Paper IV** was done using the same method as in **Paper III**. The fraction of bio-oil yield derived from Kraft lignin and monomer after the hydrotreatment was not determined since the oxygenate monomers could also have been derived from lignin and pyrolysis oil itself. In the co-hydrotreatment of Kraft lignin (KL) and oxygenated model compounds, different monomers such as 4-propylguaiacol (PG), 4-propylphenol, phenol, methylguaiacol, 4-ethylguaiacol, p-propylanisole, anisole, 4-propylcyclohexanol, benzaldehyde, cyclohexanol, acetic acid, hydroxyacetone, and guaiacol were selected as the co-reactants. The feed mass ratio (KL: PG, w/w) was also varied to study its influence on char and bio-oil yields.

The initial solid residues obtained after filtration should contain spent catalyst, solid char, and unconverted lignin. The weight of the solid was recorded after each drying. Kraft lignin conversion was calculated based on the difference between the initial Kraft lignin feed and the unconverted lignin divided by the initial lignin feed.

Char amount (g) = Total solid residues (g) – 0.75 g of catalyst – unconverted lignin (g)

Char yield (%) = Char amount (g) / 2.25 g of initial Kraft lignin feed × 100%

The analytical methods used for the analysis of the liquid products from the SHC process and also the fixed-bed hydrotreating in **Paper V** are as followed:

- Elemental (C, H, N, and S content) analysis and Unterzaucher pyrolysis for O content determination
- ¹H-NMR for the determination of mol% of hydrogen associated with alkanes, alkenes, aromatics, alcohols/ethers, or carboxylic acids/aldehydes/phenols
- ³¹P-NMR for the determination of the hydroxyl groups in mmol/g associated with aliphatic alcohols, phenolics, and carboxylic acids
- ¹³C-NMR was used to qualitatively provide carbon information on the raw FPBO, the slurry-product, and the FB-product.
- ASTM E3146-18a for carbonyl content determination
- ASTM D664 for total acid number determination
- SS12916:2019 for aromatic contents determination
- GC-Simdist (ASTM D2887) for boiling point distribution (fixed bed hydrotreated products) and TGA for the slurry feed
- Two-dimensional GC × GC-MS FID, the same method as in previous studies

3.4 Catalyst characterizations

3.4.1 Nitrogen (N₂) physisorption

Textural properties, such as specific surface area, pore volume, and the pore size of the catalysts, were measured with N₂ physisorption at -196 °C using a Tristar 3000 gas analyzer. The supported catalysts (approximately 0.3 g) were degassed in a quartz tube at 250 °C for 2 h under N₂ flow to remove moisture, and the unsupported catalysts (approximately 0.15 g) were degassed at 300 °C overnight. The specific surface area and pore sizes of the catalysts were calculated by the Brunauer-Emmett-Teller (BET) method and Barrett-Joyner-Halenda (BJH) method, respectively.

3.4.2 X-ray powder diffraction (XRD)

XRD was used to identify the crystalline phases of the synthesized catalysts in this work. X-ray diffractograms for all catalysts were obtained using an X-ray powder diffractometer operated at 40 kV and 40 mA (Bruker AXSD8 Advance) with a CuK α monochromatic radiation ($\lambda=1.542 \text{ \AA}$) source in the 2θ range of 10°-80°.

3.4.3 X-ray photoelectron spectroscopy (XPS)

The chemical state and composition of the catalysts were measured with XPS. The measurements were carried out using a Perkin Elmer PHI 5000 VersaProbe III Scanning XPS Microprobe. The monochromatic Al-K α X-ray source with a binding energy of 1486.6 eV was operated in the analysis chamber. The core-level spectra of Mo 3d, O 1s, S 2p, and C 1s were recorded with a step size of 0.1 eV. The software Casa XPS with the C 1s binding energy at 284.8 eV as a reference was used to analyze the raw data with a Shirley background.

3.4.4 Raman spectroscopy

Raman spectra were obtained using a WITec alpha300 R Confocal Raman microscope equipped with a thermoelectrically cooled (-60 °C) EMCCD detector. A 532 nm CW diode laser at 0.3 mW was used for excitation and the light was focused on the sample with a 100X/NA0.9 objective. The Raman scattering was collected using the same objective and was spectrally resolved using an 1800 grooves/nm grating. The position of the Raman spectra bands was calibrated using the silicon peak at 519.3 nm.

3.4.5 Electron microscopy (SEM & TEM)

The morphologies and structure of the catalysts were investigated using scanning and transmission electron microscopy, SEM, and TEM. The SEM images for the unsupported MoS₂ in the second study were acquired using a JEOL 7800F Prime scanning electron microscope. The particle diameter of over two hundred MoS₂ particles from the SEM images was measured with ImageJ software and further calculated to obtain the average particle sizes.

The TEM images for both studies were acquired using an FEI Titan 80-300 transmission electron microscope (TEM) operated at an accelerating voltage of 300 kV. A high-angle annular dark-field (HAADF) was used to acquire scanning TEM (STEM) images. Energy dispersive X-ray (EDX) analysis was performed using an Oxford X-sight detector in STEM mode to identify the chemical elements in the catalyst samples. TEM Imaging & Analysis (TIA) software was used for data analysis and spectrum acquisition. 15-25 representative images were used for data analysis. The ImageJ software was used to measure and process approximately 300-350 MoS₂ slabs.

The following equations were used to calculate the average MoS₂ slab length (ΔL) and stacking number (Δn)¹¹⁶:

$$\text{Average MoS}_2 \text{ slab length } (\Delta L) = \frac{\sum_i^n x_i l_i}{\sum_i^n x_i} \quad (4)$$

$$\text{Average stacking number } (\Delta n) = \frac{\sum_i^n x_i N_i}{\sum_i^n x_i} \quad (5)$$

where n is the total number of MoS₂ slabs. X_i is the number of MoS₂ slabs with N_i layers of length l_i . N_i is the stacking number, and l_i is the MoS₂ slab length.

The MoS₂ dispersion (f_{mo}) of the catalysts was calculated with the following equation reported in the literature¹¹⁶:

$$\text{MoS}_2 \text{ dispersion } (f_{mo}) = \frac{Mo_{edge}}{Mo_{total}} = \frac{\sum_i^m 6(n_i - 1)}{\sum_i^m (3n_i^2 - 3n_i + 1)} \quad (6)$$

where Mo_{edge} is the number of Mo atoms located on the edges of the MoS₂ slabs, and Mo_{total} is the total number of Mo atoms. N_i is the number of Mo atoms along the edge of the MoS₂ slabs with its length obtained by calculation ($L = 3.2(2n_i - 1)$ Å), and m is the total number of MoS₂ slabs obtained from the TEM images of different catalysts.

The edge-to-corner ratio of MoS₂ slabs was calculated based on the following equation¹¹⁷:

$$\frac{f_{edge}}{f_{corner}} = \frac{5\Delta L}{3.2} - 1.5 \quad (7)$$

3.4.6 Temperature Programmed desorption (TPD) and reduction (TPR)

To measure the acidities of the supported impregnated catalysts in the third study, ammonia (NH₃) and ethylamine (C₂H₅NH₂) TPD measurements (**Paper III**) were performed in a setup consisting of a manifold of mass flow controllers (MFC), a quartz tube with catalyst sample (~25 mg), a temperature-controlled oven (Setaram Sensys differential scanning calorimeter) and a mass spectrometer (Hidden HPR-20 QUI) to analyze the products in the outlet carrier gas. The total flow rate through the tube was maintained at 20 NmL/min.

For ethylamine TPD, the samples were first degassed (110 °C for 1 h and at 250 °C for 3 h) in a flow of Ar. Then the samples were reduced at 600 °C by 13% H₂ for 2 h followed by cooling to 100 °C. At this temperature, the sample was exposed to 543 ppm of ethylamine for 3 h to complete the adsorption. The sample was then flushed with Ar for 2 h to remove the loosely bound ethylamine. Finally, the temperature was ramped to 600 °C at a rate of 5 °C/min to desorb the ethylamine. Quantification of the Brønsted acidity is based on the evolved signal of ethylene, C₂H₄ (formed from the decomposition), and measured calibrations for C₂H₄ and ethylamine in the mass spectrometer.

For NH₃-TPD, the sample was degassed at 300 °C for 0.5 h followed by NH₃ adsorption (1000 ppm) at 100 °C for 1.5 h. After that, the sample was flushed with Ar that continued for 1 h to remove the physically adsorbed NH₃. The sample was then heated to 700 °C with a ramp of 10 °C/min. The time evolution of the NH₃ desorption peak was used to quantify the total acidity of the catalyst using a standard calibration for NH₃. A similar procedure was used for ethylamine TPD measurements.

TPR was performed for supported and unsupported catalysts (**Paper III** and **Paper IV**) using the same setup as TPD. A small amount of sample (10-20 mg) was degassed at 300 °C for 0.5 h under Ar flow. The temperature of the sample was then cooled to 25 °C. Afterward, 1 vol% of H₂ in Ar flowed through the sample followed by a

temperature increase to 800 °C at a rate of 10 °C/min. The H₂ peak in the MS was followed to compare the H₂ uptake profiles of the tested catalyst.

3.5 Solid lignin and lignin-derived solid char characterization

The solid residues consisting of the spent catalyst and lignin-derived char resulting from the hydroprocessing were analyzed using Fourier transform infrared spectroscopy (FTIR, Bruker Vertes70v spectrometer). The spectra were recorded in the range of 400-4000 cm⁻¹ in a transmittance mode with a resolution of 4 cm⁻¹ and 63 scans per sample. Some selected solid residues were examined using solid-state cross-polarization (CP) ¹³C NMR measurements using a 4 mm CP MAS probe on the Bruker AVIII 500MHz spectrometer with the following conditions: ¹³C CP-MAS at 10 kHz, with Tset =298K, a ¹H excitation 90°-pulse of P3=3.0 μs, a contact time of P15=1.5 ms, with CP at ¹³C 60.0 kHz (PLW1=109 W) and ¹H optimized ramp 45-90 kHz (SPW0=110 W) followed by SPINAL64 decoupling at 83 kHz (PCPD2=6.0 μs, PLW12=96 W) during acquisition and a relaxation delay of d1=2.0 s with 4000 scans.

4 Results and discussion

This chapter presents the results and a discussion based on all the independent although related studies presented in **Papers I, II, III, IV, and V** in this thesis. In the first study (**Paper I**), the effect of Ni, Fe, Zn, and Cu on a conventional MoS₂ supported on γ -alumina catalyst was studied in a model reaction, the HDO of PG at 300 °C, 50 bar H₂ pressure, and 1000 rpm for 5 h. The PG conversion, reaction product yield, and selectivity for all catalyst systems were examined. The characterization results are reported here to explain the different properties of the catalysts. A reaction network for the HDO of PG over the sulfided catalysts and kinetic modeling were performed to validate the experimental data. The influence of the impregnation of the transition metals on the rates of different reactions in the HDO of PG was studied. In the second study (**Paper II**), the activity and selectivity of the as-synthesized and annealed unsupported MoS₂ catalysts prepared using a hydrothermal method were studied for the HDO of PG. The effect of synthesis parameters, such as synthesis time and pH adjustment, on the unsupported MoS₂ catalyst, was investigated. The activity of an annealed unsupported MoS₂ catalyst in the hydrotreatment of Kraft lignin was demonstrated. A comparison was made between a bulk MoS₂ catalyst in the HDO of PG and the hydrotreatment of Kraft lignin. In the third study (**Paper III**), NiMo sulfides on ultra-stable Y zeolites with a silica/alumina mole ratio of 30 and also unsupported NiMoS catalysts were tested in a one-pot Kraft lignin hydrotreatment. Moreover, desilicated and dealuminated zeolites were also tested in the hydrotreatment. Efforts were put into understanding the role of the catalyst support and the NiMoS active phase in lignin depolymerization and stabilization of lignin fragments. In the fourth study (**Paper IV**), experiments related to the pyrolysis-oil assisted lignin hydrotreatment using the unsupported NiMoS were performed to mimic the co-hydrotreatment of Kraft lignin with oxygenates. The work further investigated various potential bio-derived monomers as co-reactant during the depolymerization of Kraft lignin. The mass ratio between Kraft lignin and oxygenates was determined and optimized using PG as the co-reactant. The effect of several reaction parameters such as temperature, time, and catalyst loading on the hydrotreatment was studied in terms of the yield of bio-crudes and also the char residues. In the fifth paper (**Paper V**), the synthesized unsupported NiMoS was used in the slurry hydrocracking process of biomass-derived pyrolysis oil. The stabilized slurry feed was then hydrotreated in a fixed bed unit under continuous mode over a commercial-supported NiMo sulfide catalyst. The hydrotreated products also underwent fractional distillation resulting in fractions corresponding to boiling point ranges. The stabilized slurry feed from SHC, the hydrotreated products from the fixed bed hydrotreaters, and the distillate fractions were thoroughly analyzed to obtain a deeper understanding of their chemical properties. In the sixth paper (**Paper VI**), a comprehensive review and summary were written collaboratively with colleagues focusing on the use of metal sulfides as catalysts in the valorization of renewable feedstocks such as bio-oils model compounds (monomers and dimers), lignin feeds, and pyrolysis oil. The work will not be further discussed in this thesis (refer to the manuscript and the background chapter above). Various aspects such as catalytic roles (both in supported and unsupported form), reaction network and mechanism, reaction kinetics, and also catalyst deactivation were discussed. In addition, the challenges and future needs of research in the field were addressed.

4.1 Role of transition metals on MoS₂-based supported catalysts for hydrodeoxygenation (HDO) of Propylguaiacol

4.1.1 HDO of PG over supported Mo sulfided catalysts

The effect of Ni, Fe, Zn, and Cu on γ -alumina-supported MoS₂ was studied using the HDO of PG in a batch reactor. **Figure 16** shows the conversion of PG for Mo, NiMo, FeMo, ZnMo, and CuMo sulfided catalysts. Complete PG conversion was obtained after 2-3 hours for all catalysts.

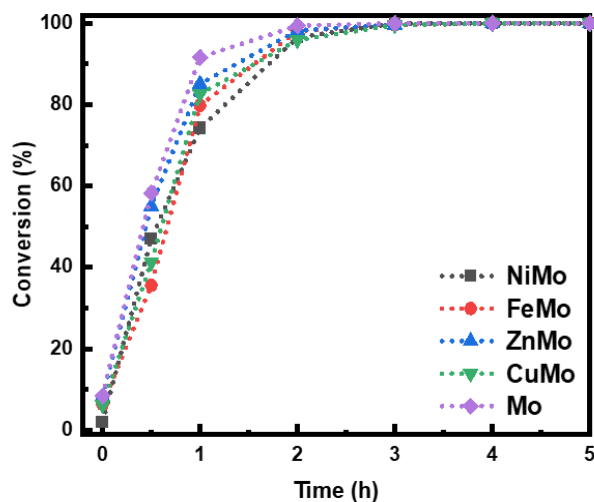


Figure 16. PG conversion (%) versus time (h). Reaction conditions: 300 °C, 50 bar H₂, 1000 rpm, and 5 h reaction.

One hour was the reference time for comparison, and a 91% PG conversion was achieved for the sulfided Mo catalyst, which was the highest conversion of all the catalysts. In contrast, the NiMo sulfided catalyst showed a 74% PG conversion after 1 h. A decrease in the PG conversion after 1 h was observed in the order of Mo > ZnMo > CuMo > FeMo > NiMo. The results show that the bimetallic catalysts had a lower conversion after 1 h; the NiMo had the lowest conversion. The lower conversion for the bimetallic catalysts at the earlier stage of the reaction (1-2 h) can be attributed to the slower rate in the demethoxylation of PG, forming 4-propylphenol as the first step in the deoxygenation route. Different reactions, such as demethoxylation, dehydroxylation, hydrogenolysis, hydrogenation, transalkylation, and isomerization, occurred at different times during the 5-hour reaction. A pool of products was formed, including partially deoxygenated compounds such as phenolics, deoxygenated aromatics, and cycloalkane compounds. To facilitate the analysis, the reaction products and intermediates were grouped into different classes that included compounds with two oxygen atoms, phenolics, aromatics, and cycloalkanes, as listed in **Figure 17**.

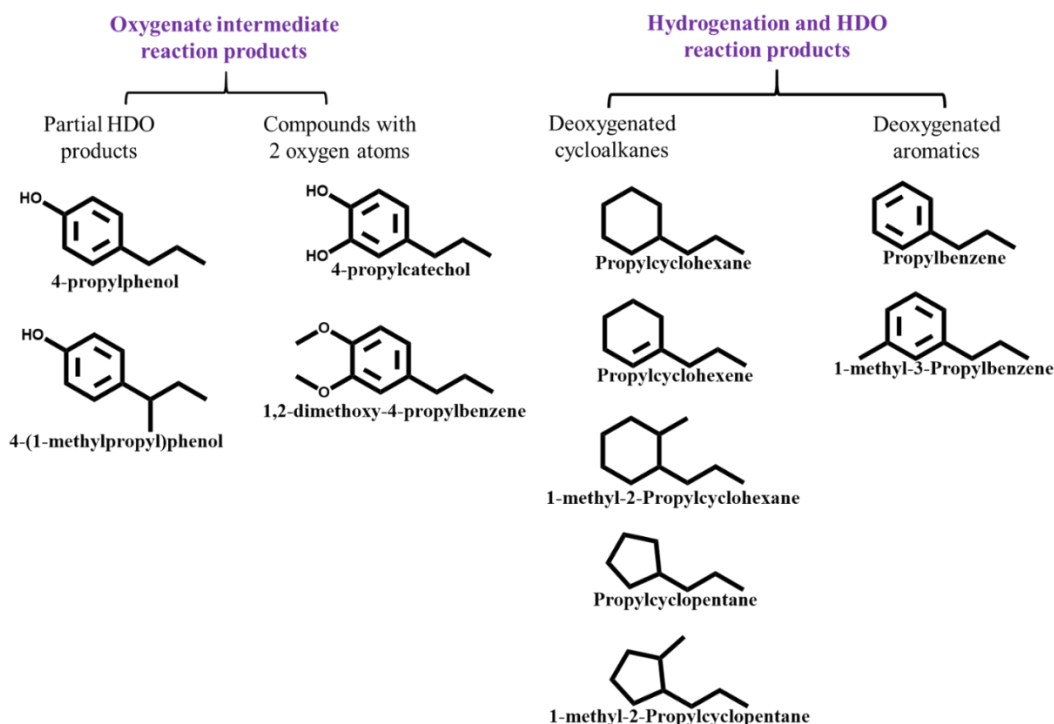


Figure 17. Classes for reaction products and intermediates from HDO of PG: oxygenate intermediates and hydrogenation and HDO reaction products.

The evolution of products and intermediates versus reaction time for the HDO of PG over all the studied catalysts is illustrated in **Figure 18**. The demethoxylation of PG that formed 4-propylphenol was the first step in the deoxygenation route as the yield of the phenolics (mainly 4-propylphenol) increased to a maximum after 1-2 hours of reaction time. The suppression of the yield of phenolics that occurred afterward can be explained by the dehydroxylation of 4-propylphenol, which underwent hydrogenation and produced propylcyclohexane and propylcyclohexene. It has been reported in the literature that intermediates such as 4-propylcyclohexanone, resulting from the keto-enol tautomerization of partially hydrogenated 4-propylphenol, has been found in the HDO of isoeugenol using non-sulfided catalysts^{118,119}. However, we did not find 4-propylcyclohexanone when sulfided catalysts were used, indicating that the primary route for the formation of propylcyclohexane was from the dehydroxylation of 4-propylphenol and the further hydrogenation of propylbenzene. This result implies that direct deoxygenation (DDO) is the dominant deoxygenation pathway for HDO of PG over these bimetallic sulfided catalysts which was consistent with the findings from literature studies^{39,52}. Trace amounts of two-oxygen-atom compounds, such as 4-propylcatechol and 1,2-dimethoxy-4-propylbenzene, were detected after 30 minutes for all catalysts and were suppressed after 2-3 hours (see **Figure 18**). 9% of oxygenates were found in the liquid products when using sulfided Mo catalysts, and 19% were found when using NiMo catalysts after 30 minutes.

The yield of deoxygenated cycloalkanes was studied for each catalyst (see **Figure 18**). The cycloalkanes detected in all the experiments included propylcyclohexane, propylcyclohexene, propylcyclopentane, 1-methyl-2-propylcyclopentane, 1-methyl-2-propylcyclohexane. Propylcyclohexane was the major compound detected in all the catalyst systems. The production of deoxygenated cycloalkanes dominated in the latter part of the reaction for all catalysts, except for the CuMo catalyst. For example, a 70.2% cycloalkane yield was achieved for the Mo catalyst after 5 h, as shown in **Figure 18 a**). 4.5% of 1-methyl-2-propylcyclopentane was formed after 5 h, which

resulted from the ring contraction that occurred during the reaction in addition to deoxygenation and ring hydrogenation. The same cyclopentane-derived compound was obtained for the NiMo, ZnMo, and FeMo catalysts, which gave a final yield of 3%, 4.6%, and 4.5%, respectively. A comparison between the catalysts showed that the sulfided NiMo catalyst gave the highest yield of deoxygenated cycloalkane at 94%. In contrast, the total deoxygenated cycloalkane yield was 58.1%, 67.2%, and 44.4% for FeMo, ZnMo, and CuMo catalysts, respectively. The results show that the sulfided NiMo catalyst was the most efficient at deoxygenation of all catalysts, and the impregnation of Fe, Zn, and Cu slowed the deoxygenation rate; Cu was the most inefficient. The better HDO activity for the NiMo catalyst was attributed to the high dispersion of active particles, as found in the TEM analysis in **Section 4.1.2**. However, a better MoS₂ dispersion may not be the only deciding factor to achieve better HDO activity when relating the catalytic activity results obtained using ZnMo, FeMo, and CuMo sulfided catalysts in HDO of PG. For instance, the ability of the added metal to interact with Mo and promote the formation of sulfur vacancy sites may be of primary importance¹²⁰.

All classes of compounds produced using HDO were considered during the study. It is worth mentioning the importance of the production of aromatic compounds as they can be blended with gasoline to improve the octane number¹²¹. Aromatic compounds can serve as an important feedstock for bulk chemical production¹²². **Figure 18 a)** shows that the Mo catalyst reached a final yield of aromatic compounds of 12% which contains propylbenzene and 1-methyl-3-propylbenzene. The sulfided FeMo and ZnMo catalysts afforded a final deoxygenated aromatic yield of 16% and 19%, respectively. In contrast, the high aromatic hydrogenation activity for sulfided NiMo catalysts resulted in only 7% of deoxygenated aromatics. The results show that the incorporation of Fe and Zn into the traditional hydrotreating catalyst can suppress the hydrogenation activity of the catalyst, yielding more deoxygenated aromatics. The sulfided Mo catalyst provided a deoxygenated compound yield of 82.1%. The sulfided NiMo catalyst exhibited complete deoxygenation after 5 h. The deoxygenated compounds yield was 86.6%, 74.3%, and 50.1% for sulfided ZnMo, FeMo, and CuMo catalysts, respectively. These findings indicate that the sulfided NiMo catalyst was able to deoxygenate efficiently, while the sulfided ZnMo catalyst was able to improve PG deoxygenation better than the sulfided Mo catalyst. In contrast, the sulfided FeMo and CuMo catalysts repressed the formation of deoxygenated compounds.

The evolution of phenolics was investigated for all catalyst systems. **Figure 18 b)** shows that the yield of phenolics reached a maximum of 34% after 2 h for NiMo catalysts. The Mo catalyst had a maximum yield of 44% of phenolics, as shown in **Figure 18 a)**. This result explains the faster demethoxylation rate of PG for the unpromoted catalysts than for the Ni-promoted catalyst. The same result was found for sulfided ZnMo (**Figure 18 d)**), which had a 36% yield after 1 h. CuMo sulfided catalysts had a steady increase in phenolic yield to 53.8% in 3 h (**Figure 18 c)**), but the final yield was 47%. The sulfided FeMo catalyst (**Figure 18 e)**) had a maximum of 54% phenolic yield after 2 h, and this decreased to 26% at the end of the reaction. The sulfided CuMo catalyst had the highest phenolic yield, implying that it had the lowest deoxygenation activity of all the sulfided catalysts.

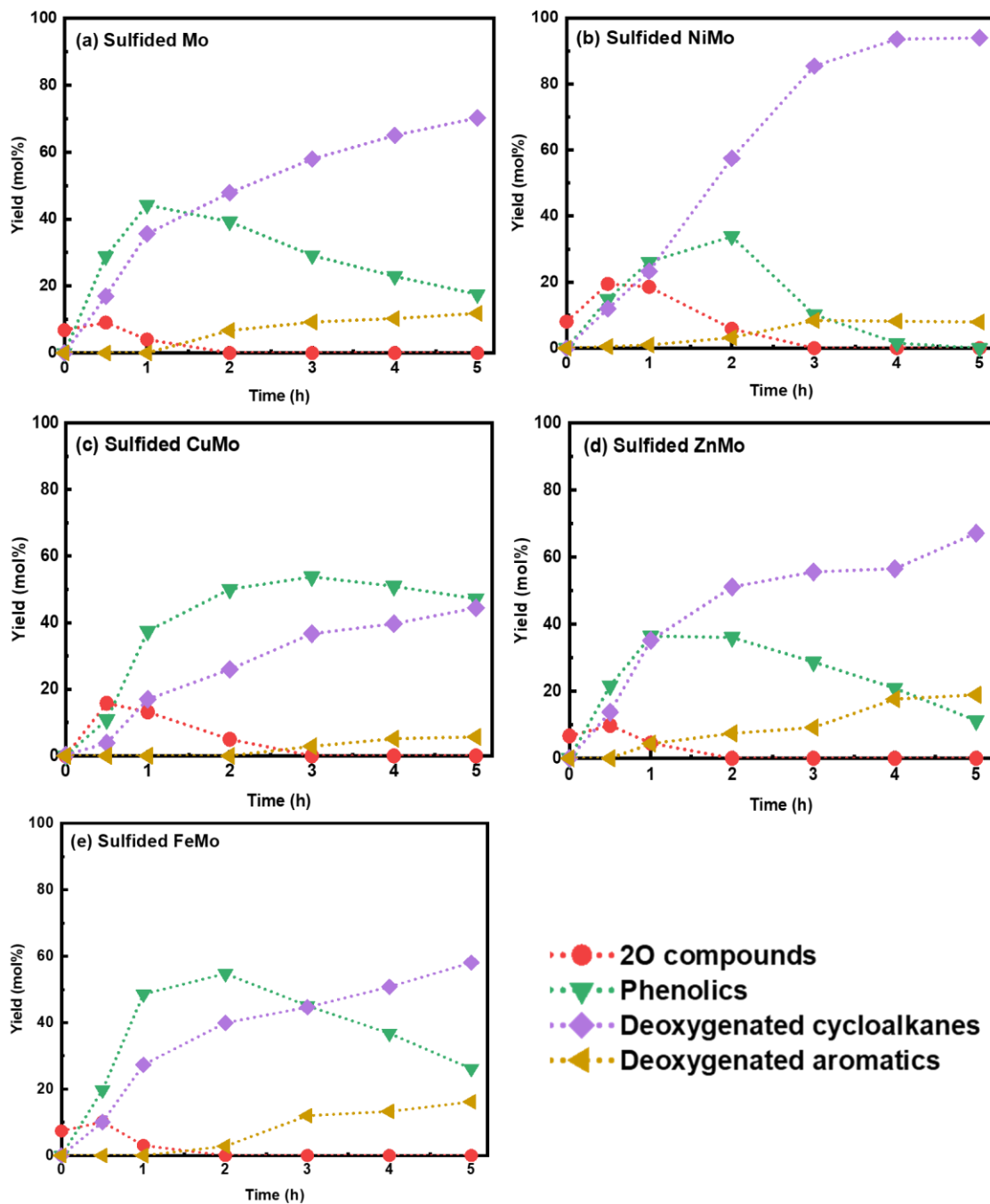


Figure 18. Reaction product evolution for HDO of PG over (a) Mo, (b) NiMo, (d) ZnMo, and I FeMo catalysts. Reaction conditions: 300 °C, 50 bar H₂, 1000 rpm, and 5 h reaction. Markers present the experimental points.

4.1.2 Catalyst characterization

The metal loadings and textural properties of the as-synthesized catalysts were verified with ICP-MS and N₂ physisorption, as shown in **Table 6**. The specific surface area and pore volume of the catalysts were reduced after the metal impregnation, indicating pore blockage.

Table 6. Elemental composition (wt%) and N₂ physisorption results for the as-synthesized catalysts.

Catalyst	Elemental composition, (wt%)					N ₂ physisorption		
	Mo	Ni	Cu	Fe	Zn	S _a *	V _p *	d _p *
Mo	13.2	-	-	-	-	155	0.36	93.2
NiMo	13.4	3.47	-	-	-	133	0.29	87.2
CuMo	12.4	-	3.32	-	-	144	0.32	89.2
FeMo	12.3	-	-	2.47	-	139	0.34	97.7
ZnMo	11.0	-	-	-	2.23	141	0.34	96.3

*S_a = BET surface area (m²/g), V_p = Pore volume (cm³/g), d_p = Average pore size (Å)

The XRD patterns in **Figure 19** represent the freshly sulfided catalysts and γ -alumina. All diffraction peaks corresponding to γ -alumina were visible in all catalysts¹²³. In contrast, there were no diffraction peaks related to MoS₂, indicating a well-dispersed MoS₂ phase on the support and lower crystallinity for the supported catalysts. Metal sulfided phases, such as NiS, FeS, FeS₂, and CuS, were not identified in the diffractograms, which could mainly be attributed to the low metal loading of the catalysts. Interestingly, the sulfided ZnMo catalyst had three characteristic peaks at $2\theta = 28.6^\circ$, 47.6° , and 56.5° , corresponding to (111), (220), and (311) planes, showing the presence of the ZnS phases¹²⁴.

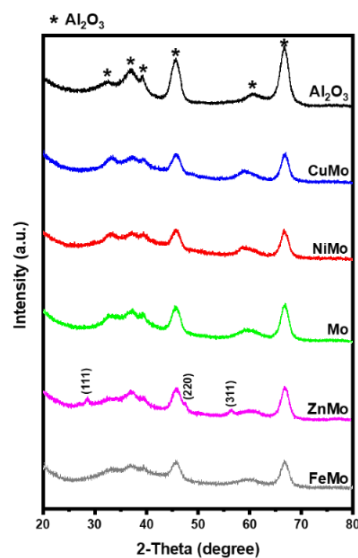


Figure 19. XRD analysis for all sulfided catalysts and alumina.

XPS measurements were performed to understand the chemical and electronic state of the sulfided catalysts. All representative spectra for the sulfided catalysts are shown in Supporting Information in **Paper I. Table 7** shows the Mo degree of sulfidation for all sulfided catalysts. This was calculated based on the contribution of Mo⁴⁺ over the total Mo species (Mo⁴⁺, Mo⁵⁺, and Mo⁶⁺) determined from the Mo 3d core-level spectrum. The presence of Mo⁵⁺ and Mo⁶⁺ was attributed to the surface re-oxidized MoS₂ during the analysis and the incomplete sulfidation

of the catalysts. Ni species, such as Ni²⁺, NiMoS, and NiS_x, were visible in the Ni 2p spectrum of the sulfided NiMo catalyst¹²⁵. Cu⁺ species and pure Cu metal were visible in the Cu 2p spectrum of the sulfided CuMo catalyst¹²⁶. The Fe 2p spectrum also had binding energies of Fe²⁺ and Fe³⁺, indicating the presence of both species⁷¹. Characteristic peaks corresponding to Zn²⁺ species were visible, corroborating the results from XRD and showing the presence of ZnS.

Table 7. Mo 3d XPS results for supported sulfided catalysts

Catalyst	Mo _{sulfidation} (%)	Binding energy (eV)					
		Mo ⁴⁺		Mo ⁵⁺		Mo ⁶⁺	
		3d _{5/2}	3d _{3/2}	3d _{5/2}	3d _{3/2}	3d _{5/2}	3d _{3/2}
Mo	69.2	228.7	231.8	-	-	232.4	235.5
NiMo	57.9	229.3	232.4	-	-	232.5	235.6
CuMo	28.4	229.3	232.4	230.6	233.7	233.7	236.9
FeMo	92.3	229.1	232.5	-	-	233.7	236.1
ZnMo	83.1	228.9	232.1	-	-	233.7	235.6

The morphologies of all sulfided catalysts were examined with TEM, as shown in **Figure 20**. Typical linear and curly MoS₂ black fringes scattered around were visible in all TEM images, as shown in **Figure 20** (a-e). The interplanar distance of 0.64 nm corresponding to the characteristic basal plane of MoS₂ can be seen in the TEM images. **Table 8** presents the statistical results for the average slab length and average stacking layer for MoS₂, MoS₂ dispersion, and the edge-to-corner ratio for a MoS₂ slab. The distributions for the number of MoS₂ stack layers and slab lengths are shown in **Figure 21**. The number of stacks in all the catalysts was in the range of one to six; one was the most frequent. Slab lengths were mostly between 4 nm and 6 nm. It is clear that the doping of different metals on the Mo catalyst reduced the slab length and increased the stacking layer of MoS₂, as shown in **Table 8**. This could result from the metal species hindering the growth of MoS₂ fringes during sulfidation. Overall, the increase in the average stacking layer of the metal-doped catalysts and the reduction in slab lengths improved the dispersion of MoS₂. The better dispersion of MoS₂ was also confirmed by the absence of MoS₂ peaks in the XRD analysis. Improvement in MoS₂ dispersion also increased the exposure of active edges to the catalytic reaction. Elemental mapping was performed on a selected area at the edge of the NiMo catalysts, as shown in **Figure 20** f), and the results indicate that there was an even distribution of Ni, Mo, and S elements on the catalyst surface. The better dispersion of the active particles for the NiMo catalyst as compared to the base Mo catalyst may contribute to improved HDO activities, as demonstrated by the NiMo catalyst in **Section 4.1.1**.

Table 8. TEM analysis of sulfided catalysts.

Sulfided Catalysts	Average slab length (ΔL), nm	Average stacking degree (Δn)	MoS ₂ Dispersion (f_{Mo})	Mo edge-to-corner ratio (f_{edge}/f_{corner}) _{Mo}
Mo	5.643	1.952	0.139	7.317
NiMo	5.099	2.162	0.146	6.467
CuMo	5.018	1.958	0.153	6.341
FeMo	5.145	1.870	0.149	6.539
ZnMo	4.232	2.074	0.168	5.113

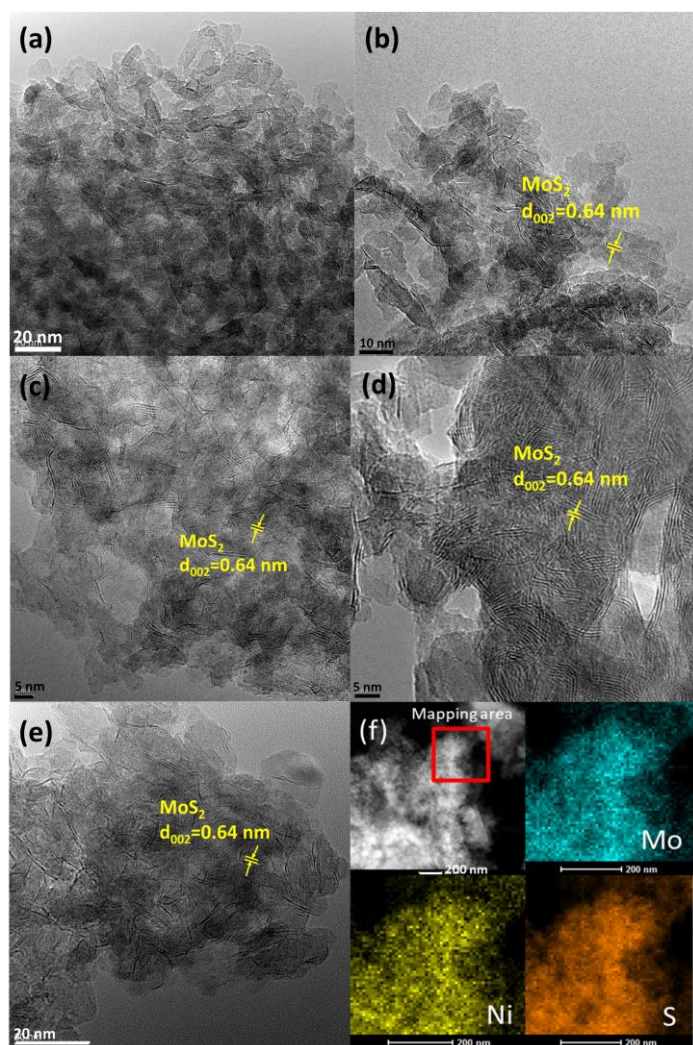


Figure 20. TEM images of (a) Mo, (b) NiMo (c) CuMo, (d) ZnMo, (e) FeMo sulfided catalysts, and (f) HAADF STEM-EDX images of NiMo sulfided catalyst.

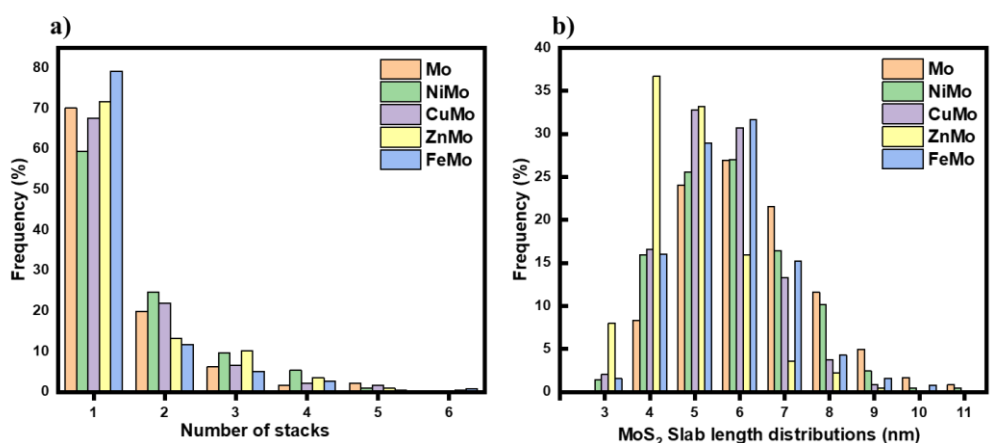


Figure 21. The (a) number of stacks and (b) distribution of MoS₂ slab lengths for all sulfided catalysts.

4.1.3 Modeling the reaction network for HDO of PG over sulfided catalysts

A reaction network for the HDO of PG over different sulfided catalysts was proposed, as shown in **Scheme 3** based on the kinetics results and research articles on phenolics HDO. Under the studied reaction parameters, PG underwent demethoxylation, producing 4-propylphenol as a major intermediate that was seen in all the catalytic reactions. A trace amount of two-oxygen-containing compounds, such as 4-propylcatechol and 1,2-dimethoxy-4-propylbenzene, were also visible at the onset of the reaction, but when the reaction had progressed, the corresponding yield of these compounds decreased. Since the concentration of these compounds was low at the beginning of the reaction, they were lumped together as a sum to study the evolution of such products. The production of dimethoxy-4-propylbenzene can be explained by the intermolecular transfer of the methyl group to the hydroxyl group^{127,128}. 4-propylphenol was then further converted to propylbenzene through hydrogenolysis and deoxygenation reactions. Deoxygenated cycloalkanes, such as propylcyclohexane, were formed through the hydrogenation of propylbenzene. A partially hydrogenated compound like propylcyclohexene was also observed during the reaction. Some alkylated products, such as 4-(1-methylpropyl)phenol and 1-methyl-3-propylbenzene, were detected in low concentrations during the reaction¹²⁹. Different reaction products detected during the 5 h reaction were grouped into phenolics, partial HDO products, deoxygenated cycloalkanes, and aromatics, as shown in **Figure 17**.

One of the objectives of this study was to understand the reaction network of bio-oil model compounds when sulfided catalysts are used. Another objective was to study how the doping of different transition metals into conventional hydrotreating catalysts can affect the rates of different reactions that take place during the HDO of PG. Hence, a simple modeling study of the HDO of PG was performed based on the kinetic results obtained in the experimental work. Several studies have reported the kinetics for phenolics HDO using zirconia-supported Rh catalysts¹³⁰, Pt- and Ir-modified bifunctional catalysts¹³¹, carbon-supported metal catalysts¹³², and sulfated Ni promoted zirconia on SBA-15¹¹⁹. Studies on the reaction behaviors of phenolics using sulfided catalysts coupled with modeling are scarce.

A simple pseudo-first-kinetic model was used to fit the experimental data for the PG HDO obtained in the batch setup. The low complexity and the low numbers of parameters to be estimated were the reason for the model selection. The hydrogen concentration and catalyst mass in all experiments were assumed to be constant throughout the reaction and were lumped together in the apparent rate constants, as listed below in the rate equations. All reaction parameters were kept constant for all experiments for comparable kinetic constants.

The development of the kinetic model first involved the construction of a simple model by considering a simplified route as ‘a: 4-propylguaiaicol → b: 4-propylphenol → c: propylbenzene → d: propylcyclohexane’ based on the proposed reaction route in **Scheme 3**. The rate equation corresponding to each reaction was defined and a set of ordinary differential equations (ODE) for the batch reactor material balance was considered.

These ODEs were then solved numerically with the MATLAB ode15s function. Experimental results for the kinetic model were fitted to estimate the kinetic constant for all involved reactions during the HDO of PG. The residual sum of squares (Sres) was minimized and defined as follows:

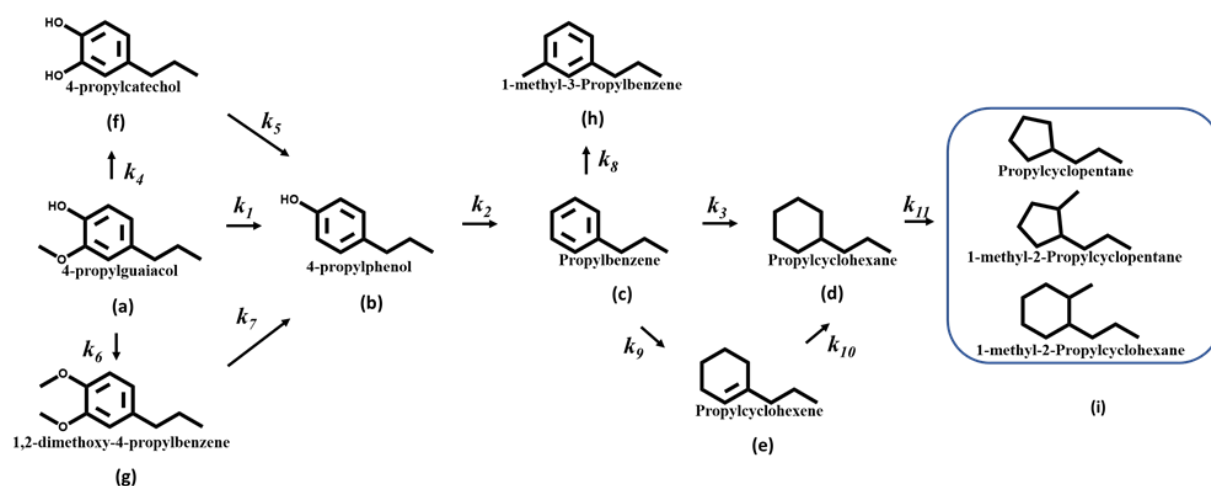
$$S_{res} = \sum (C_{exp,t} - C_{model,t})^2 \quad (8)$$

where $C_{exp,t}$ is the concentration of different reaction products obtained from experimental values, and $C_{model,t}$ is the estimated concentration from the kinetic model.

The coefficient of determination (R^2) was defined as follows:

$$R^2 = \left(1 - \frac{\sum(C_{exp,t} - C_{model,t})^2}{\sum(C_{exp,t} - C_{mean})^2}\right) \times 100 \quad (9)$$

where C_{mean} is the mean value of the parameter. The coefficient of determination was used as an indication of the feasibility of the kinetic model when applied to all sulfided catalyst systems.



Scheme 3. A proposed reaction network for HDO of PG over different sulfided catalysts.

Figure 22 shows the kinetic fitting results obtained using the simplified kinetic model and illustrates the concentration trend of PG, 4-propylphenol, propylbenzene, and propylcyclohexane. The plot of the simplified kinetic model was able to describe the deoxygenation route of PG. The deoxygenation route for PG first involved the cleaving of the methoxy group and followed by the formation of propylphenol, then there was a further cleaving of the hydroxyl group, which produced propylbenzene. 90.5% of the coefficient of determination was obtained for this simple model, indicating a good description of experimental data. However, the side reactions were omitted from this model, and some clear deviations in the data points can be seen in **Figure 22**.

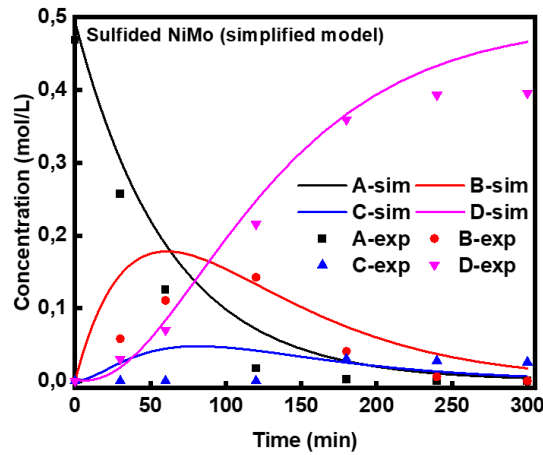


Figure 22. Product concentration profiles for PG HDO over sulfided NiMo catalyst using the simplified model. A: PG, B: 4-propylphenol, C: Propylbenzene, and D: Propylcyclohexane. The solid line represents the modeling results, and the symbol represents the experimental results.

The simplified model was then improved by considering all the side reactions that occurred during the HDO of PG as shown in **Scheme 3**. A full set of rate equations was defined for the side reactions as follows:

$$r_4 = k_4 c_a \quad (10)$$

$$r_5 = k_5 c_f \quad (11)$$

$$r_6 = k_6 c_a \quad (12)$$

$$r_7 = k_7 c_g \quad (13)$$

$$r_8 = k_8 c_c \quad (14)$$

$$r_9 = k_9 c_b \quad (15)$$

$$r_{10} = k_{10} c_e \quad (16)$$

$$r_{11} = k_{11} c_d \quad (17)$$

where k_i corresponds to the apparent rate constants of the reaction steps in **Scheme 3**. The notations for all compounds in the rate equation were as follows: a: 4-propylguaiaicol, b: 4-propylphenol, c: propylbenzene, d: propylcyclohexane, e: 4-propylcyclohexene, f: 4-propylcatechol, g: 1,2-dimethoxyl-4-propylbenzene, h: 1-methyl-3-propylbenzene, and i: side products. The concentrations of propylcyclopentane, 1-methyl-2-propylcyclopentane, and 1-methyl-2-propylcyclohexane were low and consequently were lumped together as one and labeled as c_i . The complete mass balance equations for the improved kinetic model include the following:

$$\frac{dC_a}{dt} = -r_1 - r_4 - r_6 \quad (18)$$

$$\frac{dC_b}{dt} = r_1 + r_5 + r_7 - r_2 \quad (19)$$

$$\frac{dC_c}{dt} = r_2 - r_8 - r_3 - r_9 \quad (20)$$

$$\frac{dC_d}{dt} = r_3 + r_{10} - r_{11} \quad (21)$$

$$\frac{dC_e}{dt} = r_9 - r_{10} \quad (22)$$

$$\frac{dC_f}{dt} = r_4 - r_5 \quad (23)$$

$$\frac{dC_g}{dt} = r_6 - r_7 \quad (24)$$

$$\frac{dC_h}{dt} = r_8 \quad (25)$$

$$\frac{dC_i}{dt} = r_{11} \quad (26)$$

where C_a is the concentration of the initial feed (4-propylguaiacol) expressed in mol/L, C_x is the concentration of compound x (4-propylphenol or any side products) and t is the reaction time.

The improved model took all side reactions into account. The kinetic fitting results for all sulfided catalysts are shown in **Figure 23**. The fitting results were generally improved, and the experiments agreed well with the pseudo-first-order kinetic model. The best description of the concentration profile was obtained with the sulfided NiMo catalyst, which had a 95% coefficient of determination. It was concluded that the proposed model was well described by the experimental data points and modeling results. The estimated parameters for the apparent kinetic rate constant with a 95% confidence interval are presented in Supplementary Information in **Paper I**. The high estimated confidence intervals could be attributed to the small experimental sets and that the parameters were highly correlated.

The current modeling results for the HDO of PG revealed that the same reaction routes can be applied to all the studied catalysts. The influence of the added transition metals was reflected in the modeling results. For instance, the results showed that adding promoters to the Mo catalyst did not change the reaction routes significantly. The rate constant k_1 represents the rate for the demethoxylation step of PG, and the Mo catalyst had the highest value ($k_1 = 1.86 \times 10^{-2} \text{ min}^{-1}$) of all the catalysts. This result explains the faster demethoxylation rate for the unpromoted Mo catalyst as compared to the others, and it can also be related to the faster initial PG conversion of the Mo catalyst during the first 1-2 h of the reaction. Besides, the kinetic rate constants k_3 ($8.50 \times 10^{-2} \text{ min}^{-1}$) and k_9 ($9.92 \times 10^{-2} \text{ min}^{-1}$) were the highest for the sulfided NiMo catalyst. These results correlate with the highest rate of the hydrogenation of propylbenzene to propylcyclohexane and propylcyclohexene given the highest yield of deoxygenated products achieved by the NiMo catalyst as shown previously (**Section 4.1.1**). It was found that both the CuMo and FeMo catalysts, had a lower rate constant, k_2 , than the Mo catalyst, suggesting that they inhibited the dehydroxylation of 4-propylphenol. The ZnMo catalyst had a higher rate constant k_2 ($1.05 \times 10^{-2} \text{ min}^{-1}$) than the Mo catalyst, but a lower k_3 ($1.65 \times 10^{-2} \text{ min}^{-1}$) and k_9 ($6.73 \times 10^{-2} \text{ min}^{-1}$) rate constant relative to the Mo catalyst, hence corroborating its highest aromatics production. The lowest rate constant, k_3 , for the FeMo catalyst also verified its low rate of propylbenzene hydrogenation in HDO of PG which resulted in a 16% aromatic yield at the end of the reaction.

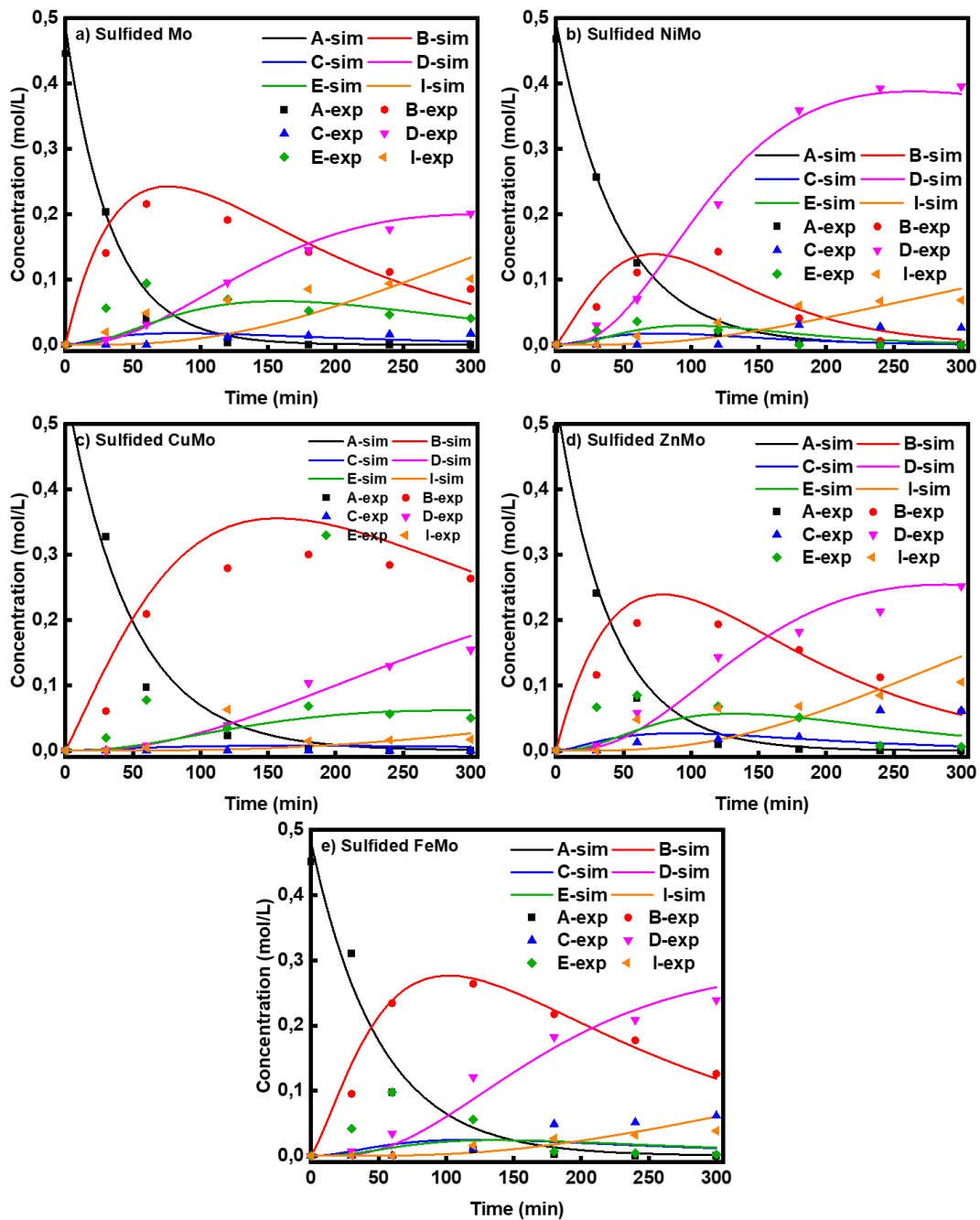


Figure 23. Kinetic fitting results for HDO of PG over sulfided a) Mo, b) NiMo, c) CuMo, d) ZnMo, and e) FeMo. The solid line denotes the modeling results and the points represent experimental data. Notation: A = PG, B = 4-propylphenol, C = propylbenzene, D = propylcyclohexane, E = propylcyclohexene, and I = side products.

4.2 Annealing treatment of unsupported MoS₂ for hydrodeoxygenation of propylguaiacol and hydrotreatment of Kraft lignin

4.2.1 Hydrothermal synthesis of unsupported MoS₂ for HDO of PG

An unsupported MoS₂ catalyst was synthesized in the second study and tested in HDO of PG. The effect of the annealing treatment on the synthesized sample was investigated and found to be crucial to enhance HDO activity. The effect of hydrothermal synthesis time and the pH adjustment with the annealing treatment on the catalytic activity was studied using the model reaction. The annealed MoS₂ and bulk MoS₂ catalysts were then further evaluated in the hydrotreatment of Kraft lignin.

The effects of hydrothermal synthesis time and the annealing pretreatment were studied on the model reaction. **Figure 24** shows the comparison between the annealed MoS₂ and as-synthesized MoS₂ with synthesis time of 12 h and 24 h in terms of product selectivity and PG conversion at 4 h. Increasing the synthesis time from 12 h to 24 h improved the PG conversion for the as-synthesized MoS₂ catalyst. The selectivity for deoxygenated cycloalkanes, such as propylcyclohexane and propylcyclohexene, was 27.5% and 43.4% for MoS₂-12 and MoS₂-24, respectively. While for an intermediate like propylphenol, the selectivity remained in the range of 47-48%. A 24.7% selectivity for a compound with two oxygen atoms like propylcatechol (2O compound), was found for MoS₂-12 after 4 h. Increasing the synthesis time to 24 h, decreased the selectivity of the propylcatechol (2O compound) to 8.3%.

The as-synthesized catalysts underwent additional annealing treatment at 400 °C for 2 h under a nitrogen flow. The selectivity and PG conversion after 4 h for the annealed and as-synthesized catalysts are shown in **Figure 24**. It can be seen in **Figure 24** that both annealed catalysts (MoS₂-12a and MoS₂-24a) had the same PG conversion after 4 h. The MoS₂-12a and MoS₂-24a had a 64% and 55% selectivity for deoxygenated cycloalkane, respectively, after 4 h. It can be seen in **Figure 24** that both annealed samples had a higher selectivity for deoxygenated cycloalkanes than the as-synthesized samples. The selectivity for phenolics was also reduced for both annealed samples. Interestingly, aromatics, such as propylbenzene, were found in the annealed samples with a selectivity of 18-20%. The 2O compounds were not detected in the reaction medium using either annealed sample (MoS₂-12a and MoS₂-24a) after 4 h. The results indicate that a shorter synthesis time was better for the PG deoxygenation when using annealed catalysts. A longer synthesis time was preferable for the as-synthesized catalysts to attain better deoxygenation activity. The difference in results can be attributed to that the 12 h synthesis time was enough to nucleate sufficient MoS₂ crystallites, and the annealing treatment facilitated the growth of MoS₂ crystals.

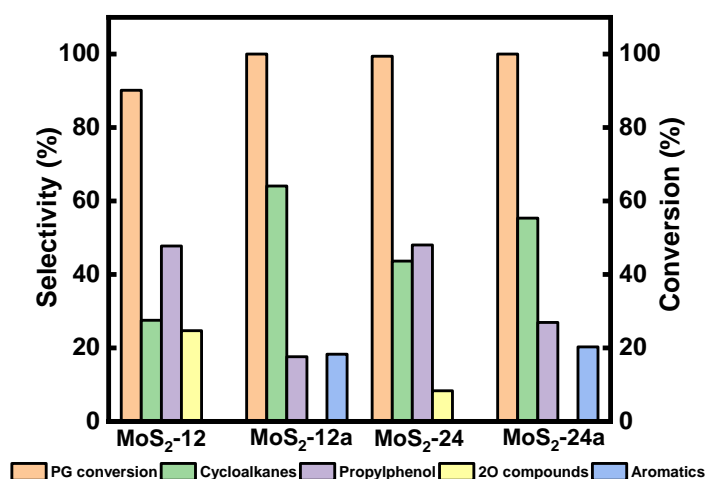


Figure 24. Comparison between selectivity for reaction product and PG conversion after 4 h for HDO of PG over MoS₂-12, MoS₂-12a, MoS₂-24, and MoS₂-24a at 50 bar total H₂ pressure, 300 °C, and 1000 rpm.

The effect of not adding acid during the synthesis of unsupported MoS₂ was investigated in the HDO of PG. The product distribution for both as-synthesized and annealed catalysts prepared without adding acid is shown in **Figure 25**. A final PG conversion of 86.6% was obtained after 5 h for the as-synthesized MoS₂ prepared without the addition of acid. Besides, the selectivity for 4-propylphenol increased to 42.5% after 2 h and stabilized at 40.8% after 5 h. A downward trend was found also for the selectivity for oxygenated intermediates (2O-compounds) which gave a final selectivity of 19.5% (**Figure 25 a**). A gradual increase in the selectivity for deoxygenated cycloalkanes was found, which gave a final selectivity of 40%. For a fair comparison, the fresh as-synthesized MoS₂ (without acid addition) underwent an annealing treatment similar to the one described previously (**Section 3.1.2**) and was applied in the HDO of PG. Surprisingly, the annealing treatment had a negative effect on the PG conversion, showing a final PG conversion of 74.2% (**Figure 25 b**). In contrast, a slight increase in the selectivity for deoxygenated cycloalkanes selectivity was found, which gave a final selectivity of 46.6% (**Figure 25 b**). A decreasing trend was found for the selectivity for phenolics with reaction time, which gave 36.6% selectivity for 4-propylphenol and 15.8% selectivity for 4-propylcatechol (2O-compounds) after 5 h. The clear difference in the product distribution of the HDO of PG between the unsupported MoS₂ catalysts prepared with and without the addition of acid shows that an acidic environment while synthesizing unsupported MoS₂ is crucial to produce MoS₂ with a smaller particle size (evident in SEM images, **Figure 28**). The resulting MoS₂ particle size had a direct effect on the HDO selectivity. This result is in line with the conclusion by Zhang et al.¹³³, which shows that higher HDS and hydrogenation activities can be achieved using MoS₂ prepared with low pH values. The smaller MoS₂ particles synthesized in an acidic environment had more active sites, which led to higher selectivity for HDO. It is worth mentioning that the annealing treatment proposed in this study positively enhanced the PG HDO activity when MoS₂ catalysts prepared with pH adjustment were used. The MoS₂ prepared without any pH adjustment had the opposite effect, especially on the PG conversion, and did not facilitate the growth of MoS₂ crystals.

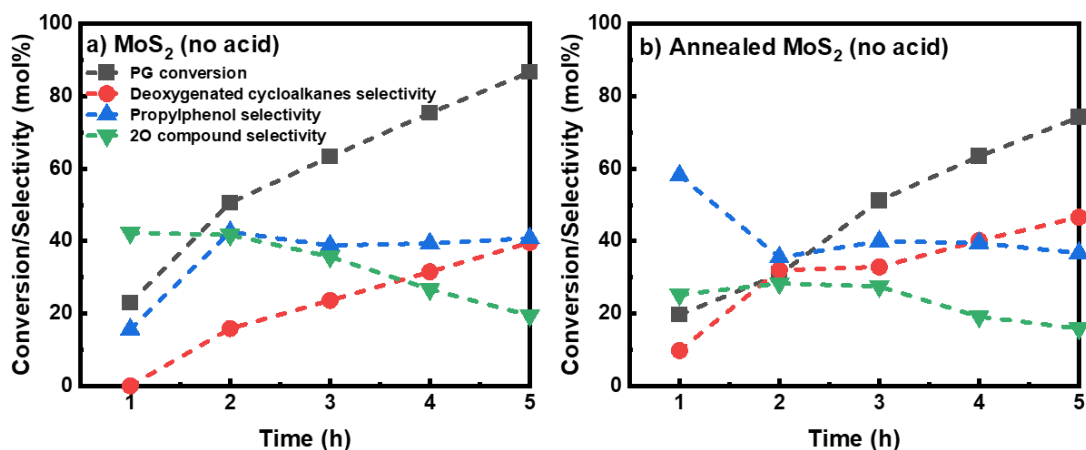


Figure 25. Reaction product distribution for HDO of PG over a) MoS₂ prepared without acid adjustment and b) annealed MoS₂ without acid adjustment at 50 bar total H₂ pressure, 300 °C and 1000 rpm.

4.2.2 Catalyst characterization

The specific surface area, pore volume, and pore size of the unsupported MoS₂ and bulk MoS₂ catalysts are listed in **Table 9**. The specific surface area of the catalysts was ranked in decreasing order: MoS₂-24a > MoS₂-12a > MoS₂-24 > MoS₂-12 > bulk MoS₂. It was found that prolonging the synthesis time from 12 h to 24 h had a negligible effect on the specific surface area of the catalyst and gave a range between 15-16 m²/g for MoS₂-12 and MoS₂-24. In contrast, both annealed samples (MoS₂-12a and MoS₂-24a) gave a higher specific surface area than the as-synthesized catalysts. The N₂ adsorption-desorption isotherms for all the catalysts are provided in Supporting Information in **Paper II**. The isotherms for the annealed MoS₂ catalysts were characterized as type IV isotherms according to the IUPAC classification¹³⁴. A prominent H3-type hysteresis loop was also found for both annealed MoS₂ samples. This loop featured slit-shaped pores created by the build-up of MoS₂ layers. The as-synthesized and bulk MoS₂ type-II isotherms had a distinctive form indicating a non-porous character. This observation can be explained by the agglomeration of particles that formed larger lumped particles with reduced porosity, as shown in the SEM images (**Figure 28**). These findings suggest that an annealing treatment can significantly increase the specific surface area and the porosity of the as-synthesized catalysts. It is important to highlight that this porosity was created by the shrinkage of particles during annealing and the resulting formation of MoS₂ crystals (see the XRD analysis, **Figure 26 a**). They were re-coordinated and agglomerated to generate cavities. It is also worth noting that MoS₂-12a had the highest pore volume and the lowest pore size of all the unsupported catalysts.

Table 9. Physical properties (surface area, pore-volume, and pore size) of synthesized unsupported catalysts.

Catalysts	Surface area (m ² /g)	Pore volume (cm ³ /g)	Pore size (Å)
MoS ₂ -12	15.4	0.34	108
MoS ₂ -12a	27.8	0.60	83.8
MoS ₂ -24	16.2	0.13	317
MoS ₂ -24a	37.1	0.11	105
Bulk MoS ₂	4.70	0.03	177

Figure 26 a) shows the XRD diffractograms for the MoS₂ unsupported catalysts. The XRD patterns show that the as-synthesized samples had low crystallinity with a peak at $2\theta = 14^\circ$, representing the typical (002) plane of hexagonal MoS₂. The results also confirm that prolonging the synthesis time from 12 h to 24 h did not improve the crystallinity of the samples resulting in the same XRD pattern (**Figure 26**). Prominent peaks were visible at $2\theta = 14^\circ, 33^\circ, 39^\circ,$ and 59° for both annealed MoS₂ catalysts attributed to the (002), (100), (103), and (110) planes of MoS₂¹³⁵. The improved crystallinity of the as-synthesized MoS₂ after a simple annealing treatment suggests that the annealing process at 400 °C for 2 h can promote the growth of MoS₂ crystals. In comparison, the bulk MoS₂ was highly crystalline, as shown in **Figure 26 a)**.

Raman spectroscopy was performed to understand the chemical state of the as-synthesized and annealed catalysts. The Raman spectra of MoS₂-24 and MoS₂-24a were obtained at the 532 nm CW laser excitation mark with an average power of 0.3 mW, as shown in **Figure 26 b)**. For MoS₂-24a catalysts, four main Raman peaks located at 379 cm⁻¹ (E_{2g}^1), 404 cm⁻¹ (A_{1g}), 283 cm⁻¹ (E_{1g}) and 454 cm⁻¹ (E_{1g}) indicate that the usual 2H-MoS₂ phase was present¹³⁶. Two low-intensity Raman peaks at 219 cm⁻¹ and 335 cm⁻¹ were identified in the spectra for MoS₂-24a, proving the existence of the 1T phase of MoS₂¹³⁶. The results indicate that the annealing pre-treatment changed the structure of the as-synthesized catalysts and resulted in mixed 1T and 2H phases for MoS₂. In contrast, for MoS₂-24 catalysts, three peaks were identified, as shown in **Figure 26 b)** with a relatively lower intensity. This proves the lower crystallinity of the as-synthesized catalyst. The results from Raman spectroscopy analysis corroborate with the results obtained from XRD analysis.

The chemical state and composition of the unsupported MoS₂ catalysts before and after the annealing treatment were determined with XPS (**Figure 27**). The Mo 3d spectra in **Figure 27 a)** and **Figure 27 c)** were deconvoluted into three Mo 3d_{5/2} – Mo 3d_{3/2} doublets for the as-synthesized samples. The presence of the Mo⁴⁺ oxidation state indicated by two characteristic peaks at 229.3 eV and 232.5 eV binding energies, proved the existence of the MoS₂ species¹³⁷. Characteristic peaks at the binding energies 230.0 eV and 233.0 eV were found for the Mo⁵⁺ oxidation state, which demonstrated the presence of intermediate oxysulfide species (MoO_xS_y) in the as-synthesized catalysts¹³⁸. An additional doublet at 233.4 eV and 235.8 eV associated with the Mo⁶⁺ oxidation state which is associated with the MoO₃ species was also found¹³⁹. **Table 10** shows the Mo 3d composition of the Mo states obtained from the XPS data. The sulfidation degree based on the Mo⁴⁺ content increased for both annealed MoS₂ more than for the as-synthesized unsupported catalysts. MoS₂-24a had the highest degree and correspondingly lowest degree of oxidation of Mo. The presence of oxysulfide species in the as-synthesized catalysts was caused by one of the reactions that are expected to occur during the synthesis of MoS₂, where (NH₄)₆Mo₇O₂₄ reacts with H₂S and forms MoO_xS_y, ammonia, and water. However, no oxysulfide species were found in either annealed catalyst. This finding suggests that the MoO_xS_y phase may have been completely converted into MoS₃, and the annealing pretreatment facilitated the thermal decomposition of MoS₃ to MoS₂.

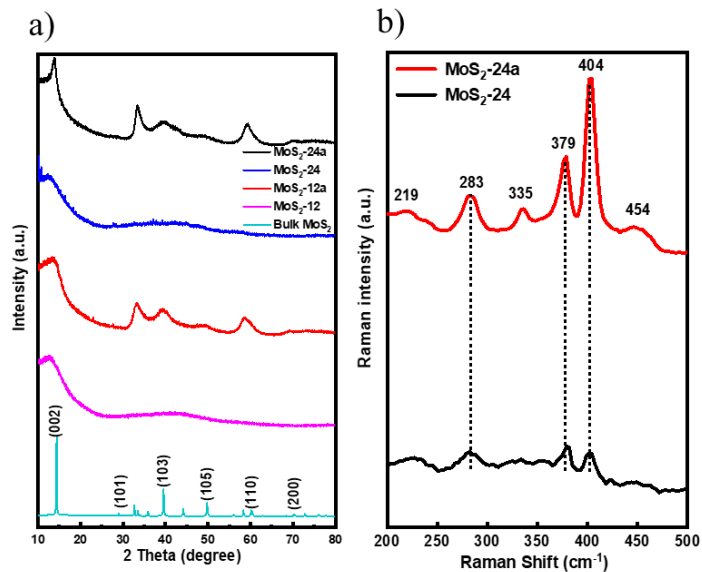


Figure 26. a) XRD patterns for MoS₂-12, MoS₂-12a, MoS₂-24, MoS₂-24a and bulk MoS₂ and b) Raman spectra for MoS₂-24 and MoS₂-24a catalysts.

Table 10. Mo 3d composition for MoS₂-12, MoS₂-12a, MoS₂-24, and MoS₂-24a.

Catalyst	Mo 3d composition (area %)		
	Mo ⁴⁺	Mo ⁵⁺	Mo ⁶⁺
MoS ₂ -12	62.9	22.2	14.9
MoS ₂ -12a	88.6	-	11.4
MoS ₂ -24	82.9	11.3	5.8
MoS ₂ -24a	93.1	-	6.9

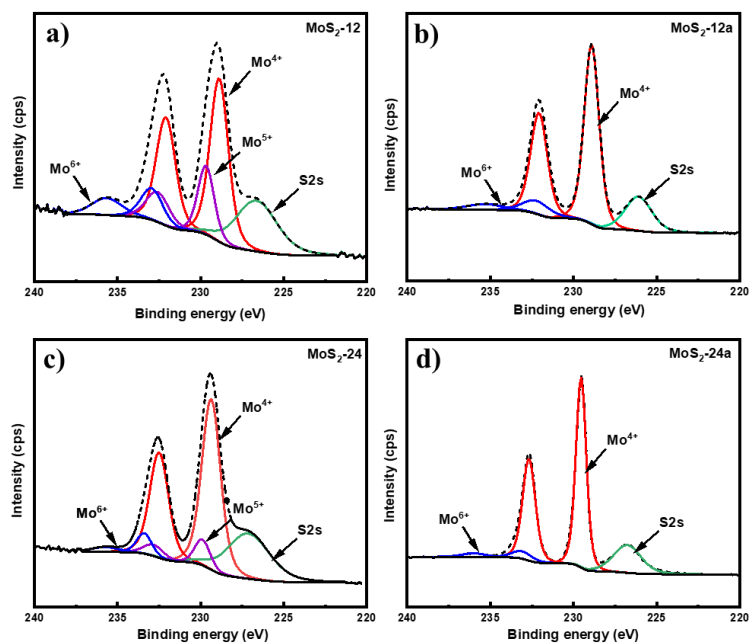


Figure 27. XPS spectra of Mo 3d for a) MoS₂-12, b) MoS₂-12a, c) MoS₂-24, and d) MoS₂-24a.

The structure and morphologies of the unsupported catalysts synthesized in this work were examined with SEM. The laminar growth of the MoS₂ during hydrothermal synthesis resulted in the formation of spherical particle agglomerates, shown in the SEM images in **Figure 28**. The average particle diameter was measured based on all the SEM images using ImageJ software. The distribution of particle size is shown in the insets of **Figure 28**. As can be seen in **Figure 28** e) and f), the MoS₂-24 catalyst consisted of a mixture of larger and smaller particles with an average particle diameter of 305 nm. Similar morphology was found for MoS₂-12 (**Figure 28** a) and b)). The MoS₂-24a catalyst had more dispersed and uniformly distributed MoS₂ particles than the as-synthesized catalyst with a smaller average particle diameter of 190 nm as shown in the SEM images in **Figure 28** g) and h). In general, the annealed catalysts had a more defined morphology. The SEM analysis also showed that the annealing treatment reduced the MoS₂ particle diameter and size distribution of particles.

To understand the effect of pH adjustment during synthesis on the morphology of the MoS₂ catalyst, a batch of unsupported MoS₂ was prepared following the same procedure but omitting the acid adjustment step, as described in **Section 3.1.2**. The subsequent batch was then examined with SEM, and the results are shown in **Figure 29**. The particles in **Figure 29** show an apparent flower-like morphology with a larger average particle diameter of 2 μm. It is worth noting that this is almost the average particle size for the bulk MoS₂ sample (6 μm, max 40 μm). The characterization results presented here are also in line with the findings by Zhang et al.¹³³. The pH adjustment step in the catalyst synthesis was important to facilitate the growth of MoS₂ micelles, which eventually formed smaller crystallites in the MoS₂ catalysts (**Figure 28** and **Figure 29**). A material with a larger particle size was formed for the MoS₂ catalyst prepared without acid addition (**Figure 29**).

High-resolution transmission electron microscopy (HRTEM) was also performed to better understand the effect of annealing on the structure of an unsupported catalyst, and the images are presented in **Figure 30**. The usual thread-like fringes with an interplanar distance of 0.64 nm, corresponding to the (0 0 2) basal planes of the MoS₂ catalysts, were identified in all of the HRTEM images. One of the main differences was from the HRTEM images for the annealed catalysts in which the edges showed a spiky feature that was not visible in the as-synthesized catalysts, see **Figure 30**. The changes in the structure near the edges of the catalyst after the annealing process could be due to the enhancement of the growth of the smaller MoS₂ crystallites in the as-synthesized catalysts. This demonstrates the importance of the annealing treatment in changing the structure of the catalysts. Consequently, the spiky edges of the annealed unsupported catalysts contributed to their higher specific surface area and the exposure of more active sites to the H₂O reaction.

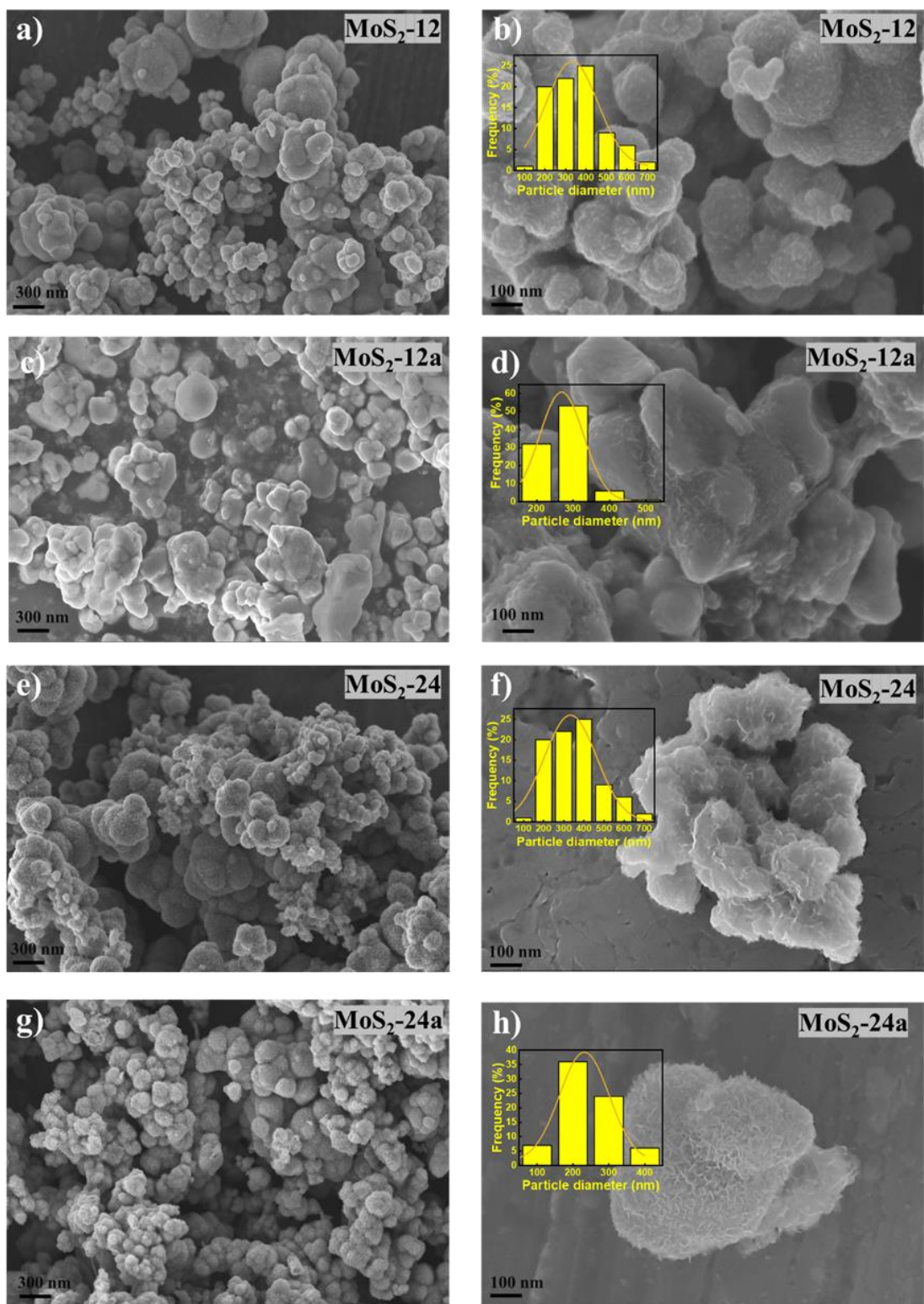


Figure 28. SEM images of (a and b) MoS₂-12, (c and d) MoS₂-12a, (e and f) MoS₂-24, and (g and h) MoS₂-24a.

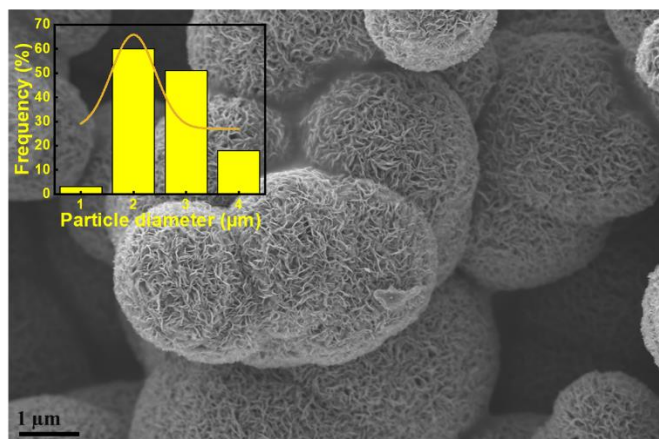


Figure 29. SEM image of MoS₂ prepared without pH adjustment.

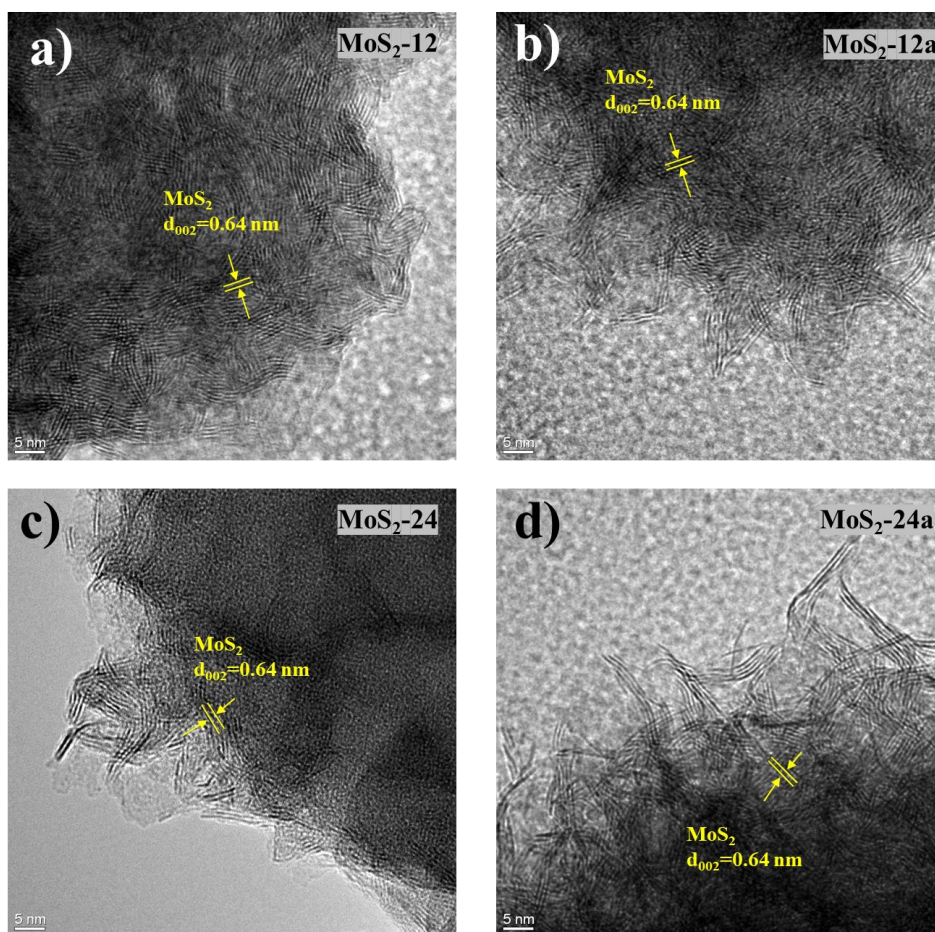


Figure 30. HRTEM images of a) MoS₂-12, b) MoS₂-12a, c) MoS₂-24, and d) MoS₂-24a.

4.3 Elucidating the role of ultra-stable Y (USY) supported and unsupported NiMoS catalysts during the hydrotreatment of Kraft lignin

It has been shown in the previous study that one of the major hurdles in Kraft lignin hydrotreatment was the production of undesired char residues during depolymerization. The resulting side product from the hydrotreatment hampers the implementation of kraft lignin as a solid feedstock in many current refining facilities. Moreover, in previous studies conducted in our group, it has been demonstrated that NiMo sulfides on Y zeolites enhanced the cleavage of C-O-C and the more recalcitrant C-C linkages in lignin dimer compounds^{140,141}. The enhancement was attributed to the synergistic effect of the active sulfide phases and also the acidic nature of the catalysts^{140,141}. Therefore, the focus of this study aimed to elucidate the role of sulfided NiMo-impregnated USY zeolites for the reductive liquefaction and deoxygenation of Kraft lignin and also the stabilization of lignin fragments in suppressing repolymerization reactions, in turn, reducing the char formation. The physical mixing of unsupported NiMoS and Y zeolites as a catalyst system was also tested in Kraft lignin hydrotreatment to clarify their roles in the depolymerization and repolymerization reactions influencing product selectivity and production of char residues. The effect of the desilication and dealumination treatment on the USY zeolites, which changes their pore sizes and acid site density was also investigated. The catalysts used in this study are abbreviated as NiMo(D)YXX, where Ni stands for nickel, Mo stands for molybdenum, Y stands for USY, and XX stands for the silica-alumina ratio. **Table 11** gives the descriptions of catalysts used in **Paper III**.

Table 11. Description of catalysts in **Paper III**.

Catalysts	Description
Y30	-Commercial ultra-stable zeolites, USY (Zeolyst international) Molar SiO ₂ /Al ₂ O ₃ = 30
Y80	-Commercial ultra-stable zeolites, USY (Zeolyst international) Molar SiO ₂ /Al ₂ O ₃ = 80
Y150	-Dealuminated using 3 M oxalic acid at 70 °C, stirring rate 500 rpm for 16 h ¹⁴²
Y200	-Dealuminated using 3 M oxalic acid at 70 °C, stirring rate 500 rpm for 95 h ¹⁴²
DY80	-Y80 was desilicated using 0.2 M (NaOH + tetrapropylammonium bromide, TPABr (PDA)) at 25 °C for 0.5 h. -The desilicated sample was further exchanged with 0.5 M NH ₄ NO ₃ at 60 °C for 1 h.
NiMoY30/Y80/Y150/Y200/DY80	-Ni and Mo were loaded on the designated USY support via a wet impregnation method
UNiMoS	-Unsupported catalysts synthesized by a hydrothermal method ^{52,73}

4.3.1 Kraft lignin hydrotreatment using sulfided NiMo-impregnated USY zeolites

The kraft lignin-derived yields of liquid products (wt%) and char residues (wt%) during hydrotreatment over sulfided NiMo impregnated Y zeolites and also blank run (non-catalytic) at 400 °C, 35 bar H₂ (at 25 °C), and 1000 rpm for 5 h is presented in **Figure 31**. In the non-catalytic run, Kraft lignin undergoes reductive thermal depolymerization and results in a high char residue yield (47%) and a low bio-oil yield (~18%) after 5 h. This higher char residue yield for the blank run could be explained by the extensive reactions between the reactive depolymerized lignin fragments which further lead to the generation of repolymerization products. The thermal disintegration of lignin and repolymerization starts as early as during the heating phase of the hydrotreatment in a batch reactor, hence, the presence of an active catalyst is crucial to stabilize these fragments. As shown in **Figure 31**, the presence of only USY zeolites (Y30 or Y80) reduces the yield of char residues to 37.1% and 44.4% for Y30 and Y80, respectively. The bio-oil yield for hydrotreatment when using Y30 was 21%, which possesses a

slight increase in bio-oil yield in comparison to the blank run. For all the runs using sulfided NiMo-impregnated USY zeolites (either desilicated or dealuminated), the solid char yield reduces to within 20% to 24%, indicating the catalytic suppression of repolymerization reactions. It can be observed that the bio-oils yields dropped for the dealuminated catalysts from 30.5% to 20.1%, for NiMoY30 and NiMoY200, respectively. Furthermore, an opposite trend for the yield of char residues (increased from 23.8% to 26.7%) can be observed. Among all the studied catalysts, NiMoY30 gives a notable liquid yield (30.5%) and also yields the lowest char residues (23.8%). These results prompted further investigation of the role of the NiMoS and Y30 as catalyst components in the depolymerization and deoxygenation of Kraft lignin. The impregnated form of the catalysts and also in their separate forms (physical mixture of unsupported NiMoS and Y30) were investigated in the hydrotreatment to gain further insight.

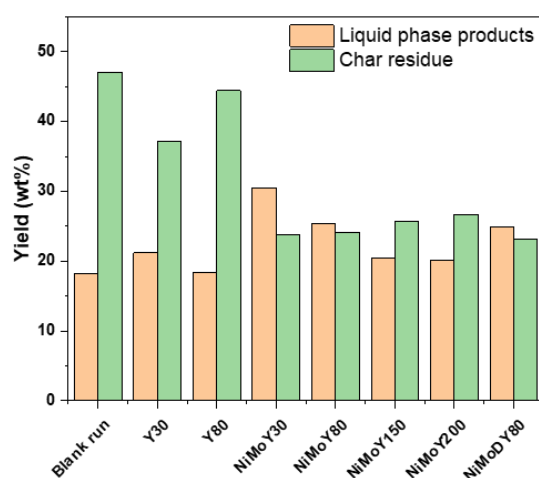


Figure 31. The kraft lignin-derived liquid product yields (wt%) and char residues (wt%) during Kraft lignin hydrotreatment over sulfided NiMo impregnated Y zeolites and also blank run (non-catalytic) at 400 °C, 35 bar H₂ (at 25 °C), and 1000 rpm for 5 h.

4.3.2 The role of NiMoS and Y30 in Kraft lignin hydrotreatment

Figure 32 illustrates a 2D GC × GC-MS chromatogram of the product distribution from Kraft lignin hydrotreatment over NiMoY30 after 5 h. As can be observed from **Figure 32**, several product groups can be identified such as cycloalkanes, alkylbenzenes, phenolics, indanes, naphthalenes, biphenyl-derived compounds, and other oxygenates (ketones, aldehydes, and alcohols). The comparison between different catalyst systems in terms of liquid product selectivity is demonstrated in **Figure 33**. The selectivity was calculated based on all the identified and detectable products from the 2D GC × GC-MS chromatogram. In the thermal depolymerization of lignin (absence of catalyst), the depolymerized lignin fragments further undergo depolymerization resulting in the formation of phenolics and cycloalkanes monomers with the selectivity reaching 60% and 10%, respectively. Apart from the depolymerization, the disintegration of the lignin framework also results in the formation of free radicals that undergo coupling and recombination reactions, leading to the formation of char residues during the hydrotreatment. With the presence of Y30 as a catalyst, the selectivity of cycloalkanes and alkylbenzenes increases and the selectivity of phenolics decreases indicating the deoxygenation activity commences, however, to a lesser extent when compared to other catalyst systems. When using NiMo-impregnated Y30 catalyst, the deoxygenated fraction (cycloalkanes and alkylbenzenes) selectivity doubled showing ~61% (comprised of ~24% cycloalkanes

and ~37% alkylbenzenes). The greater amount of alkylbenzenes indicates the direct deoxygenation routes for the depolymerized oxygenate fragments during the hydrotreatment.

It should be noted that the amount of UNiMoS used for the hydrotreatment has a similar nominal loading of Ni and Mo to that when using the NiMoY30 catalyst. In the experiment using only UNiMoS catalysts, a deoxygenated product selectivity of 42% and a 25% phenolics selectivity was obtained. On the other hand, when a physical mixture of UNiMoS and Y30 catalyst was used, the deoxygenated product selectivity was lower (~30%) and a slightly higher phenolics selectivity (~27%) was achieved. One of the notable observations from both experiments was that the use of both the unsupported NiMoS active phase components and also the Y30 support are crucial in stabilizing the lignin fragments and hindering the formation of char residues. Especially in the case of using the physical mixture of both catalyst components, a lower char yield of 16.7% was achieved indicating the greater accessibility of active sites to the depolymerized lignin fragments that resulted in efficient depolymerization. It also shows that the acidic sites of the Y30 and metallic NiMoS sites presented a synergistic effect in stabilizing the lignin fragments and limiting the reaction routes toward char formation. This was further clarified when using the NiMo-impregnated Y30 in which the metallic and acidic sites are less accessible resulting in a higher char yield (23.8%). However, the higher bio-oil yield with NiMoY30 compared to other catalyst systems can be attributed to the close surface proximity of NiMoS and acidic sites resulting from the impregnation. In terms of hydrocracking activity, both experiments (UNiMoS alone and physical mixing of UNiMoS and Y30) show a higher polyaromatics selectivity (21-24%) as compared to the use of NiMoY30 catalysts (9%) indicating lower hydrocracking activity. This implies that the close contact between the deoxygenation sites and acidic sites as in the impregnated catalysts, prevents the formation of polyaromatics to a greater extent. In the event of extending the reaction time to 8 h and also increasing the loading of NiMoY30 catalyst, a noticeable improvement in the selectivity for deoxygenated monocyclic and alkylbenzene (79%) products was obtained with an improved bio-oil yield of 38.9%. The solid char residues of 16.4% were obtained after 5 h. A low selectivity of polyaromatics (4.9%) was achieved in this case further signifying the importance of the proximity of the metallic and acidic sites.

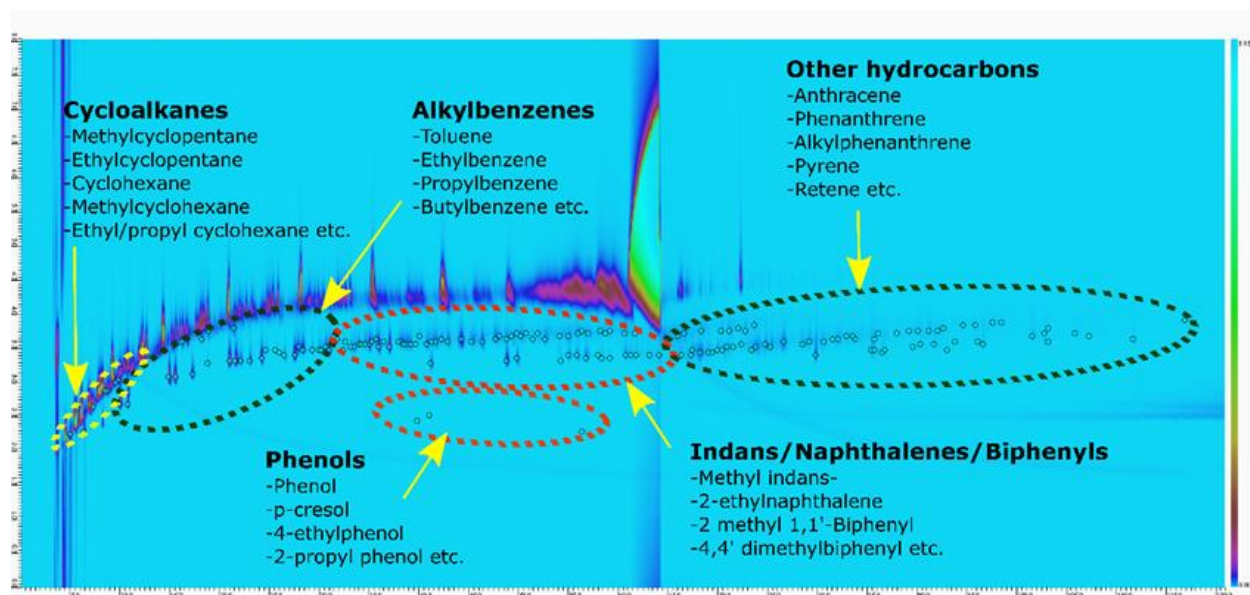


Figure 32. 2D GC × GC-MS chromatogram of the liquid phase products distribution from the Kraft lignin hydrotreatment over NiMoY30 after 5 h.

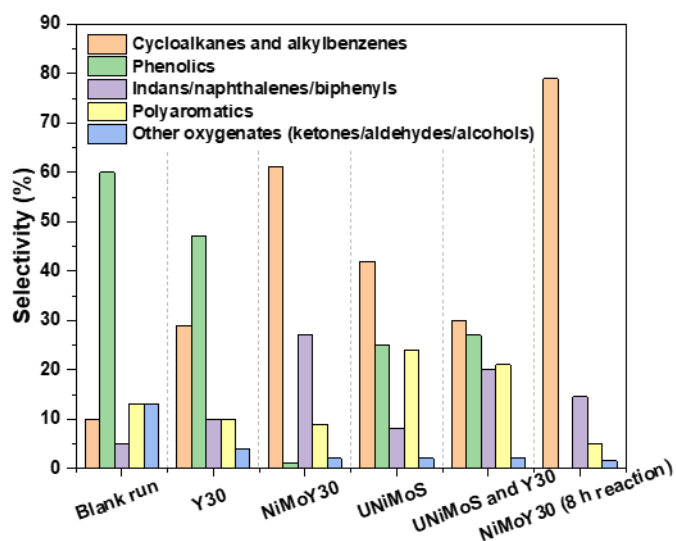


Figure 33. The liquid product selectivity (wt%) for Kraft lignin hydrotreatment over sulfided NiMo impregnated Y zeolites, unsupported NiMoS, and also blank run (non-catalytic) at 400 °C, 35 bar H₂ (@25 °C), and 1000 rpm for 5 h.

4.3.3 Catalyst characterizations

The elemental composition and textural properties of the synthesized catalysts used in **Paper III** are presented in **Table 12**. It can be observed that both the total specific and external surface area of the impregnated catalysts is lower compared to the bare catalyst support, indicating the blockage of pores by NiMo. A similar observation was seen for the pore size in **Table 12**. It can be observed that oxalic acid treatment used for dealumination efficiently removes the aluminum framework, resulting in a higher silica to alumina ratio for Y150 and Y200 samples. The increment in the pore sizes especially in the case of NiMoY30 and NiMoDY80 (via dealumination and desilication) could allow better access for the large depolymerized lignin fragments to reach the NiMo active sites for further conversion. This can be reflected in the decrease in the selectivity of the polyaromatic compounds and the increase in the selectivity for monomers (e.g. cycloalkanes, alkylbenzenes, and phenolics) for the impregnated catalysts. NiMoY30 showed an external surface area of 126 m²/g and an average mesopore size of 4.4 nm. The UNiMoS catalyst had a specific surface area of 49 m²/g with a larger average pore size of 11.5 nm. The ICP-MS analysis shows that the Mo and Ni loading remains in the range of 12-13 wt% and 3.7-4.5 wt%, respectively, giving the range of Ni/(Ni + Mo) atomic ratio 0.33-0.37 for the supported catalysts. For unsupported NiMoS, the ratio was kept at 0.31.

Table 12. Composition and textural properties of the synthesized sulfided catalysts used in **Paper III**.

Catalyst	Elemental composition (wt%)				N ₂ physisorption			
	SiO ₂ /Al ₂ O ₃ ^b	Mo	Ni	Atomic ratio Ni/(Ni+Mo)	S _{a,total} (m ² /g)	S _{a,external} (m ² /g)	V _{p,total} (V _{p,meso}) (cm ³ /g)	d _p (Å)
Y30	25	-	-	-	801	234	0.54 (0.26)	40.9
NiMoY30	-	12.7	4.5	0.37	514	126	0.33 (0.14)	44.3
Y80	88	-	-	-	808	243	0.56 (0.29)	39.3
NiMoY80	-	13	4.4	0.36	500	165	0.33 (0.17)	37.8
Y150	146	-	-	-	792	279	0.57 (0.32)	41.3
NiMoY150	-	12.8	4.4	0.36	398	175	0.33 (0.20)	41.6
Y200	212	-	-	-	737	268	0.57 (0.34)	43.8
NiMoY200	-	12.6	4.4	0.36	423	148	0.32 (0.19)	43.8
DY80	69	-	-	-	662	353	0.68 (0.53)	49.3
NiMoDY80	-	12.4	3.7	0.33	344	213	0.40 (0.34)	50.3
UNiMoS	-	29.8	8.4	0.31	49	49	0.22	115.2

* S_a=BET surface area. V_p = Pore volume. D_p = Average pore sizes for mesopores. ^b = measured by ICP-SFMS.

The total acidity and Brønsted acidity of the synthesized catalysts measured by NH₃ and ethylamine temperature-programmed desorption are presented in **Table 13**. It can be observed that the total acidity of the parent Y zeolites is lower and it is attributed to their far lower Lewis acidity (**Table 13**). Impregnation of the NiMo on the support increases the total acidity, seemingly due to the formation of new Lewis acid sites. It was mentioned in a review paper by Guan et al. that the two main factors playing an important role in preventing the formation of coke and char during the depolymerization of lignin and further upgrading is acid sites and pore structure¹⁴³. As reflected by the catalytic data (**Figure 31** and **Figure 33**), these acidic sites strongly contribute to the different extents of hydrogenolysis, isomerization, transalkylation, hydrocracking, and dehydration reactions in the one-pot lignin conversion.

The correlation of the acidity of the catalysts to the liquid product yield (wt%) and the char yield (wt%) was investigated (**Figure 34** a) and b)). It could be observed that the liquid product yield correlated well with the total and Brønsted acidities, with the increasing acidic site density enhancing the lignin depolymerization and resulting in improved monomer yield. On the other hand, a poorer correlation between the char yield and variation of acid site density was observed. In addition, it appears that the lower polyaromatic yield for NiMoY150 and NiMoY200 compared to NiMoY80 suggests that larger pores permitted more hydrocracking activity of the larger compounds. **Figure 34** c) shows a good correlation between the pore volume of catalysts and the yield of liquid, with the desilicated sample (NiMoDY80) deviating the most. Overall, NiMoY30 appeared to offer an optimized and balanced Brønsted and Lewis acid site density to achieve a higher yield for depolymerized fractions along with high selectivity for deoxygenated products.

Table 13. The total acidity and Brønsted acidity of the synthesized catalysts were measured by NH₃ and ethylamine temperature-programmed desorption.

Catalyst	Total acidity (NH ₃ -TPD) (μmol g ⁻¹)	Brønsted acidity (C ₂ H ₅ NH ₂ -TPD) (μmol g ⁻¹)	Lewis acidity* (μmol g ⁻¹)
Y30	478	386	92
NiMoY30	608	300	308
Y80	248	221	27
NiMoY80	424	217	207
NiMoY150	397	123	274
NiMoY200	348	102	248
NiMoDY80	515	222	293
UNiMoS	158	-	-

*Estimated from the difference between the total and Brønsted acidity.

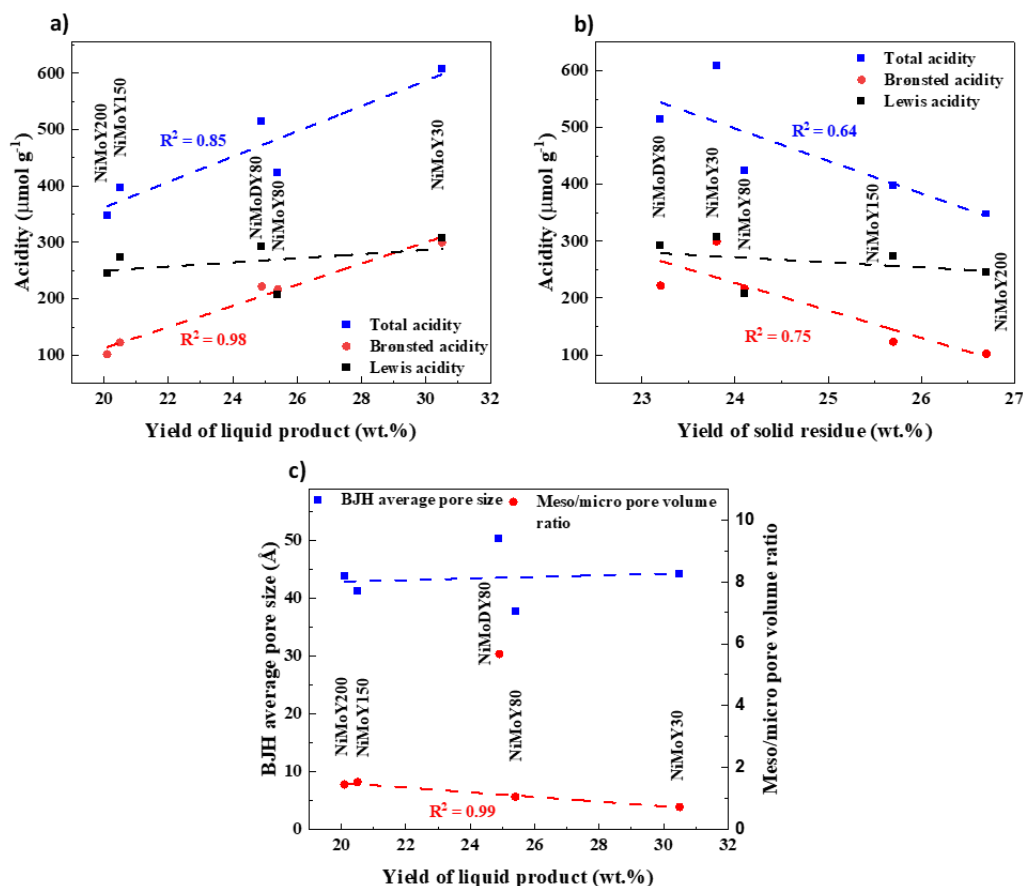


Figure 34. Correlation of the acidity of the catalysts to the a) liquid product yield (wt%) b) char yield (wt%), and c) the correlation of the catalyst's textural properties to the yield of liquid product after the hydrotreatment over sulfided impregnated catalysts. Dashed lines represent linear correlation along with the coefficient of determination (R^2 value).

The XRD patterns (refer to the published article) of the studied catalysts in **Paper III** indicate the absence of the diffraction peaks representing Ni and Mo for the impregnated catalysts. This indicates that the NiMo phases are well dispersed, and/or possess low crystallinity. For the unsupported NiMoS, prominent peaks can be observed at 2-theta values corresponding to the (0 0 2), (1 0 5), and (1 0 3) characteristics planes of 2H-MoS₂¹³⁵. Moreover, the characteristics peaks correspond to the (1 1 1), (2 0 0), (2 1 1), (2 2 0), (3 1 1), and (2 3 0) planes also indicating the presence of NiS_x⁷⁰.

The hydrogen uptake characteristics of unsupported NiMoS, the sulfided and as-synthesized form of NiMoY30 are presented in **Figure 35**. For instance, the unsupported NiMoS catalyst starts consuming H₂ at a higher temperature (415 °C) while the sulfided NiMoY30 at a lower temperature (330 °C). At the same time, the release of hydrogen sulfide occurred indicating the creation of sulfur vacancies which are responsible for the deoxygenation and hydrogenolysis reactions¹¹⁴. The differences between the two sulfided catalysts for the H₂ uptake temperatures could be attributed to their differences in structural composition and morphology arising from the different synthesis methods. It should be noted that lignin starts disintegrating at ~200 °C¹⁴⁴. This also suggests that the repolymerization and recombination reaction of depolymerized lignin fragments occurred and/or dominated at lower temperatures leading to the formation of char residues. While in the presence of the H₂-

activated supported and unsupported NiMoS, the depolymerized lignin fragments undergo stabilization which ensures further depolymerization. To justify this, an additional hydrotreatment experiment with Kraft lignin was performed by heating the reactor filled with sulfided NiMoY30 to 400 °C and then rapidly cooled down to room temperature. The result was a liquid product yield of 13.4% and a massive amount of char residues (35%) indicating the dominance of the repolymerization of large lignin fragments at low temperatures when the catalyst is less active. On the other hand, when lowering the lignin to catalyst (NiMoY30) mass ratio, a significant increase in bio-oil yield with 79% selectivity for deoxygenated products was obtained indicating the importance of the amount of catalytic active sites.

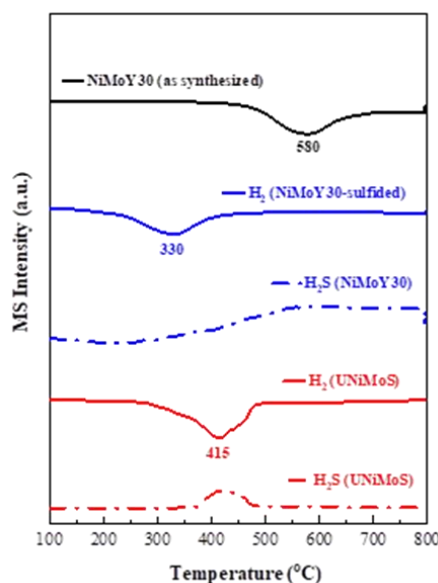


Figure 35. Hydrogen temperature program reduction (TPR) analysis for UNiMoS, as-synthesized and sulfided NiMoY30.

Table 14 presents the XPS results on the sulfided-impregnated NiMoY30 and UNiMoS (unsupported) catalysts. Sulfide phases such as MoS₂ (228.6 ± 0.1 eV), NiS_x (852.8 ± 0.1), and NiMoS (854.2 ± 0.2) were identified for the impregnated NiMoY30 and unsupported NiMoS catalysts. A higher percentage of Mo-oxysulfide phase (Mo⁵⁺) for UNiMoS was evident compared to the supported catalyst. While a higher fraction of NiS_x was observed for NiMoY30. Interestingly, the surface Ni/(Ni+Mo) ratio was found to be low for UNiMoS as compared to NiMoY30 showing that Ni was more concentrated in the bulk of the unsupported catalyst. HRTEM images of the NiMoY30 and UNiMoS catalysts are shown in **Figure 36**. As can be seen from the SEM images resulting from the STEM-High angle annular dark field (HAADF) and STEM-EDX mapping, a uniform distribution of Ni, Mo, and S over a representative area for both catalysts was obtained. The typical fringes and also the layered structure of MoS₂ with the characteristic interlayer distance of 0.62 nm which corresponds to the (0 0 2) MoS₂ crystal plane can also be identified in the bright-field (BF) TEM micrograph. As shown in **Table 14**, it was found that the calculated average slab length for UNiMoS was higher than the supported NiMoY30 and vice versa for the average stacking. On the other hand, the supported NiMoY30 shows a 63% higher MoS₂ dispersion than the unsupported catalyst. However, UNiMoS showed more edge Mo atoms than the corner sites which should promote higher hydrogenolysis activity than the NiMoY30. In addition, different features of the MoS₂ morphology can be observed

for both catalysts. A more rounded or curved MoS₂ layer can be observed for NiMoY30 mainly attributed to the influence of the support. While sharper, bending, and curvy features can be observed for the unsupported NiMoS.

From both the XPS and TEM analysis, it can be noted that both sulfided-supported NiMoY30 and unsupported NiMoS contain NiS_x and MoS₂ phases. This result is also consistent with the XRD pattern for UNiMoS. It is worth highlighting that the presence of NiS_x has been found to enhance the hydrogenation activity of MoS₂¹⁴⁵. Moreover, the synergistic effect between NiS₂ and MoS₂ was found to be another factor in improving the hydrogenation and deoxygenation⁵⁶. It was also found that excessive NiS_x species can hinder access to MoS₂, and thus curtail the activity. H₂-TPR shows that Ni integration lowers the hydrogen uptake temperature more for NiMoY30 than UNiMoS. The higher yield and selectivity over the use of NiMoY30 during hydrotreatment, according to the catalyst characterizations (H₂-TPR, XPS, and TEM), was mainly attributed to the low-temperature H₂-activation leading to enhanced stabilization of depolymerized lignin fragments. Moreover, the higher MoS₂ dispersion for the supported catalyst gave rise to a higher amount of edge Mo atoms rather than corners atoms, which improves the hydrogenolysis and hydrogenation reaction activity. The acidic nature of the NiMoY30 also contributes to isomerization, hydrocracking, and dehydration reactions. Nonetheless, the textural properties of the supported catalyst presumably inhibit the accessibility of the bulky lignin molecules and fragments to the active sites, which enhances the formation of char residues.

Table 14. XPS and TEM analysis results for the supported and unsupported NiMoS.

Catalysts	Mo sulfidation (%)	Ni sulfidation (%)			Ni/(Ni+Mo) atomic ratio	Average slab length (nm)	Average stacking	MoS ₂ dispersion, f_{Mo}	Edge-to-corner ratio
		Mo ⁴⁺ /Mo ⁵⁺	NiS _x	NiMoS					
UNiMoS	68/20	7	72	21	0.05	6.3	2.9	0.156	8.4
NiMoY30	75/13	24	66	10	0.22	4.3	3.8	0.254	5.2

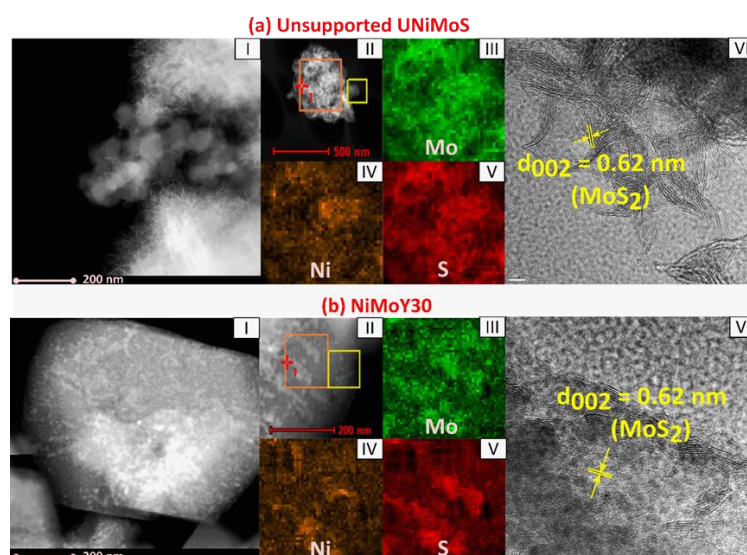


Figure 36. HAADF-STEM/HRTEM images of a) unsupported NiMoS and b) NiMoY30. (I) Materials overall, (II) overview of the analysis area (orange box), (III) Molybdenum (Mo), (IV) Nickel (Ni), (V) Sulfur (S), EDX mapping, and (VI) TEM micrograph.

4.4 Slurry Co-hydrotreatment of Kraft lignin and pyrolysis oil over unsupported NiMoS catalyst: a char suppression strategy

In the previous study (section 4.3), the use of supported and unsupported NiMoS was investigated in the hydrotreatment of Kraft lignin. A combination of depolymerization, hydrogenolysis, and hydrodeoxygenation (HDO) reactions occurred under this catalytic reductive approach for lignin liquefaction which gives a wide spectrum of products. Various compositions of the liquid products consisting of phenolics, deoxygenated cycloalkanes, and aromatics were obtained along with, insoluble solid char residues after the hydrotreatment. One observation that can be obtained from the previous work was the presence of diffusion resistance for the polymeric Kraft lignin over the supported catalysts. The inaccessibility of the larger lignin fragments to reach the NiMoS active sites induced undesired reactions such as radicals coupling, recombinations, and condensation that subsequently enhanced the formation of char residues.

Exploring different approaches that can limit and avoid the condensation and repolymerization reactions that occur under the liquefaction of lignin sources could provide an opportunity for the production of lignin-derived monomers. Table 5 in section 2.7 presented an overview of a literature survey related to various strategies in suppressing the undesired secondary reactions during lignin valorization using a co-solvent, co-reactant, or capping agent. Thus, in this study, for the first time, we have presented a study that covered the co-hydroconversion of Kraft lignin and pyrolysis oil (co-reactants) using hexadecane as a non-polar solvent over a hydrothermally synthesized unsupported NiMo sulfide catalyst. We have shown that co-processing pyrolysis oil with Kraft lignin during catalytic hydroconversion can completely suppress the char formation. To further investigate the role of pyrolysis oil co-processing for char suppression, multiple model compounds for pyrolysis oil were examined, including a wide variety of chemical species like aldehydes, ketones, carboxylic acids, furans, and phenolics, in terms of their global oil yield (wt%) and production of the undesired solid char residues (wt%). The effect of adding monomers containing different functional groups like hydroxyl (-OH), methoxyl (-OCH₃), alkyl chain (-C_xH_y), carbonyl (-R₂C=O), formyl (-R-CH=O), and carboxyl (-COOH) on the rate of liquefaction and depolymerization of lignin was studied. The effect of the ring saturation was also examined using co-reactants like propylcyclohexanol and cyclohexanol in the lignin hydrotreatment. It was found that the most efficient model compound was 4-propylguaiaicol (PG) and further detailed studies were therefore performed on PG. Finally, a reaction network was proposed describing the effects of pyrolysis oil and its oxygenated monomers on char suppression during its co-processing with Kraft lignin.

4.4.1 Pyrolysis-oil-assisted Kraft lignin hydrotreatment

Pyrolysis oil (PO), is a liquid product derived from the pyrolysis of lignocellulosic biomass that represents a complex multi-component mixture including furans, furfurals, ketones, aldehydes, alcohols, acids, esters, ethers, sugars, and phenolic compounds¹⁴⁶. Different capping agents have been examined during lignin depolymerization (Table 5), such as phenols⁹⁸, ethanol¹⁰², isopropanol¹⁰⁹, and p-hydroxybenzyl alcohol¹¹¹. Since pyrolysis oil includes phenolic compounds as well as alcohols, we have therefore examined the effect of co-processing pyrolysis oil and Kraft lignin (KL), intending to use the pyrolysis oil as a capping agent. To avoid extensive repolymerization and charring reactions, we experimented by hydrotreating only PO (2.2 g) in the presence of unsupported NiMoS without the KL lignin in a similar fashion as described in the previous section. A total liquid product yield of 27.9% was achieved after 6 h as shown in Figure 37. Among the detected compounds, 13.1% of the liquid yield

was contributed by cycloalkane-derived compounds. Traces of other compounds such as pentanoic acids, sulfurous acids, carbonic acids, hexanoic acids, benzaldehyde-derived compounds, and alcohols like pentanol amounting up to 9.9% could also be detected by the 2D GC × GC-MS in the hydrotreatment of PO. Another interesting observation when running only PO hydrotreatment was that there were no solid char products obtained at the end of the hydroprocessing. In contrast, for the KL lignin hydrotreatment, a high char yield of 14.7% was obtained. This result led to further investigation by increasing the amount of PO used in the hydrotreatment of PO (4.4 g). An increase in the liquid product yield (44.3%) could be obtained from doubling the loading of PO but with otherwise the same experimental conditions. Similarly, in this experiment, no solid char product could be detected when hydrotreating an increased amount of PO (**Figure 37**).

Then the concept of co-hydroprocessing lignin and pyrolysis oil with different ratios was implemented. These experiments showed a promising result in terms of the apparent ability of co-feeding pyrolysis oil to suppress the formation of undesired solid char products. Different ratios of lignin and pyrolysis oil (PO) were tested in the co-hydrotreatment, and solid residues and bio-oil liquid products are shown in **Figure 37**. With a 1:0.1 weight ratio of KL lignin and PO, an observable amount of solid char products up to 16.8% was obtained at the end of the hydrotreatment. The char-suppressing effect of PO in the KL lignin hydrotreatment was not observed, instead, the char yield increased slightly from the reference experiment at 14.7% (only KL lignin) to 16.8%. The bio-oil yield obtained in this hydrotreatment (KL:PO 1:0.1) was 29.6%, of which 27.2% of it was composed of cycloalkanes and alkylbenzenes. Unexpectedly, an increasing amount of co-processing feed of PO (KL:PO at 1:0.5) in the co-hydroprocessing decreased the solid yield by approximately 10%. This result shows that the co-feeding of a suitable amount of pyrolysis oil in the hydrotreatment of Kraft lignin was able to reduce the production of recondensation products indicated by the reduced solid char yield. More interestingly, when the KL:PO feed weight ratio was increased to 1:1, an undetectable level of solid char and 42.8% of bio-oil yield was achieved. This experiment was repeated and indeed, the same results were retrieved with no solid formation.

The current results from the co-hydrotreating of KL lignin and PO suggest that Kraft lignin is mostly responsible for the insoluble solid char residue formation during the hydrotreating process. The results also inferred that an optimal amount of PO supplemented in the KL lignin hydrotreatment was able to reduce and suppress the rate of condensation and repolymerization of the large lignin-derived fragments. The presence of various pyrolysis oil compounds with certain advantageous functional groups at the beginning of the co-hydrotreatment was able to stabilize the lignin-derived intermediates before they repolymerized to condensed solid char and also ultimately improve the rate of Kraft lignin liquefaction by facilitating the depolymerization resulting in an improved liquid oil yield.

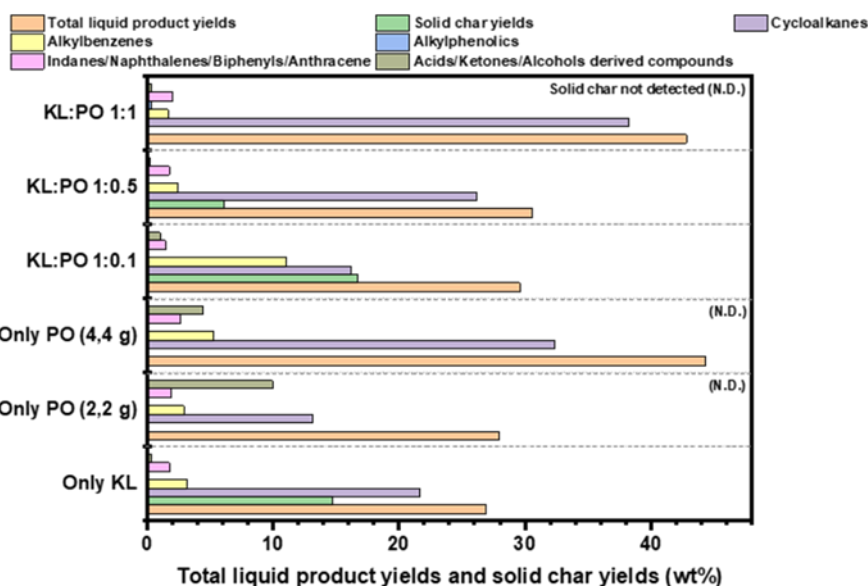


Figure 37. Co-hydroconversion of Kraft lignin (KL) and pyrolysis oil (PO) over an unsupported NiMoS. Operational parameters: 400 °C, 6 h, 75 bar total hydrogen pressure, 1000 rpm, and 75 mL of hexadecane as solvent. The KL lignin amount was fixed at 2.25 g and PO amount was varied. The weight percentage (wt%) reported was calculated based on the total reactant (KL and PO) input.

4.4.2 Investigating the effect of model pyrolysis oil compounds as co-reactants in Kraft lignin hydrotreatment

Co-processing of pyrolysis oil and Kraft lignin exhibited excellent results and was even able to completely suppress the solid char formation. To deepen the understanding of the co-hydroprocessing of Kraft lignin with pyrolysis oil, we examined the hydrotreatment of Kraft lignin with several model compounds representative of different compounds found in pyrolysis oil. Firstly, different phenols (phenol and propylphenol) and saturated cyclohexanol compounds (cyclohexanol and propylcyclohexanol) were studied in the co-hydrotreatment of Kraft lignin. An increasing trend in terms of bio-oil yields could be observed in the order of: propylphenol (14.7%) < propylcyclohexanol (37.8%) < phenol (44.6%) < cyclohexanol (49.7%). Both saturated molecules, 4-propylcyclohexanol, and cyclohexanol, gave a lower char yield of 9% and 6.8%, respectively, compared to their unsaturated ring counterparts. This could be attributed to the saturated rings of both compounds providing hydrogen radicals that react with lignin fragments and radicals, subsequently blocking the radical coupling that otherwise forms C-C bonds.

The effect of a larger pool of model pyrolysis oil compounds was selected for comparison according to: 4-propylguaiacol (hydroxyl, methoxy, and propyl groups), guaiacol (hydroxyl, and methoxy groups), phenol (only hydroxyl group), anisole (only methoxy group), benzaldehyde (only formyl group), acetic acid (only carboxyl group), and hydroxy acetone (only carbonyl group). The effect of the functional groups (hydroxyl, methoxy, alkyl, carbonyl, formyl, and carboxyl) on the yield of bio-oils and solid chars for co-hydrotreatment with Kraft lignin is presented in **Figure 38 b**). The experiment where only Kraft lignin was used as a sole reactant in the hydrotreatment was taken as a reference for comparison (**Figure 38 b**). The condensation rate of large polymeric lignin fragments was found to be extensively suppressed by the presence of three different functional groups (such as hydroxyl,

methoxy, and propyl-) in the case of 4-propylguaiacol (PG), evidently from the scarcely low char yield (3.7%) compared to all others. Noteworthy, in the reference experiment where no co-reactant was used, the catalytic Kraft lignin hydrotreatment gives a relatively high char yield of 14.7%, and a bio-oils yield of 26.9% (from 2D GC × GC-MS) in which the yields for cycloalkanes and alkylbenzenes are 21.6% and 3.2%, respectively.

Apart from PG, co-reactants like phenol and benzaldehyde were also found to enhance the depolymerization of Kraft lignin, resulting in higher bio-oil yields of 44.6% and 40.3%, respectively. Both tests also resulted in a slightly lower solid char production (11.9% for phenol and 13.3% for benzaldehyde) as compared to the reference experiment with only Kraft lignin. Interestingly, for benzaldehyde, a high yield of alkylbenzenes (23.3%, yellow bar in **Figure 38 b**) was observed, which was not the case for PG and phenol where the major product was cycloalkane-derived compounds. Whereas for guaiacol, anisole, acetic acid, and hydroxy acetone, comparatively low bio-oil yields could be observed compared to the bio-oil yield achieved in only Kraft lignin hydrotreatment (**Figure 38 b**). For instance, anisole as a co-reactant in the Kraft lignin co-hydrotreatment gave a poor bio-oil yield of 17.5% and also a higher char yield of 16.9%. These results provide an important insight into the presence of multiple functional groups in the co-reactant, for instant PG, appearing to have a synergistic effect in limiting the rate of lignin fragment repolymerization during the hydroconversion process over an unsupported NiMoS catalyst.

Figure 38 c) gives an overview of the ranking of the different molecules with different functional groups in terms of bio-oil and solid char yields. Several observations can be made from **Figure 38 c**), firstly, anisole as a co-reactant gives the highest char yield of 17% as compared to all other co-reactants and also only Kraft lignin hydrotreatment. While other co-reactants like PG, guaiacol, hydroxy acetone, phenol, benzaldehyde, and acetic acid provide a lesser char yield (scattered in **Figure 38 c**) as compared to the reference experiment (only Kraft lignin). These reactants were found to be beneficial in terms of reducing the char formation reactions, with PG showing the best char-suppressing capability during co-hydrotreatment with lignin. In terms of the bio-oil yields, PG, phenol, and benzaldehyde show a higher liquid yield as compared to the others including the reference experiment. A ranking considering the char-reducing potential of the individual compounds with different functional groups is as follows: PG (hydroxyl, -OH, methoxy, -OCH₃, and propyl, -C₃H₇) > guaiacol (hydroxyl, -OH, methoxy, -OCH₃) > hydroxyacetone (carbonyl, -R₂C=O) > phenol (hydroxyl, -OH) > benzaldehyde (formyl, -R-CH=O) > acetic acid (carboxyl, -COOH) > anisole (methoxy, -OCH₃). A summary of the GC × GC-MS detectable yields of bio-oil products and the char yields obtained from the co-hydroprocessing of Kraft lignin and various oxygenated monomers over an unsupported NiMoS catalyst are shown in **Paper IV** (refer to the manuscript). The other products are the non-detectable compounds by GC such as heavy lignin oligomers, water molecules, and light gaseous products. Since 4-propylguaiacol (PG) was the model compound that gave the lowest char production as well as the highest bio-oil yield, its combination of functional groups under varying conditions was further studied.

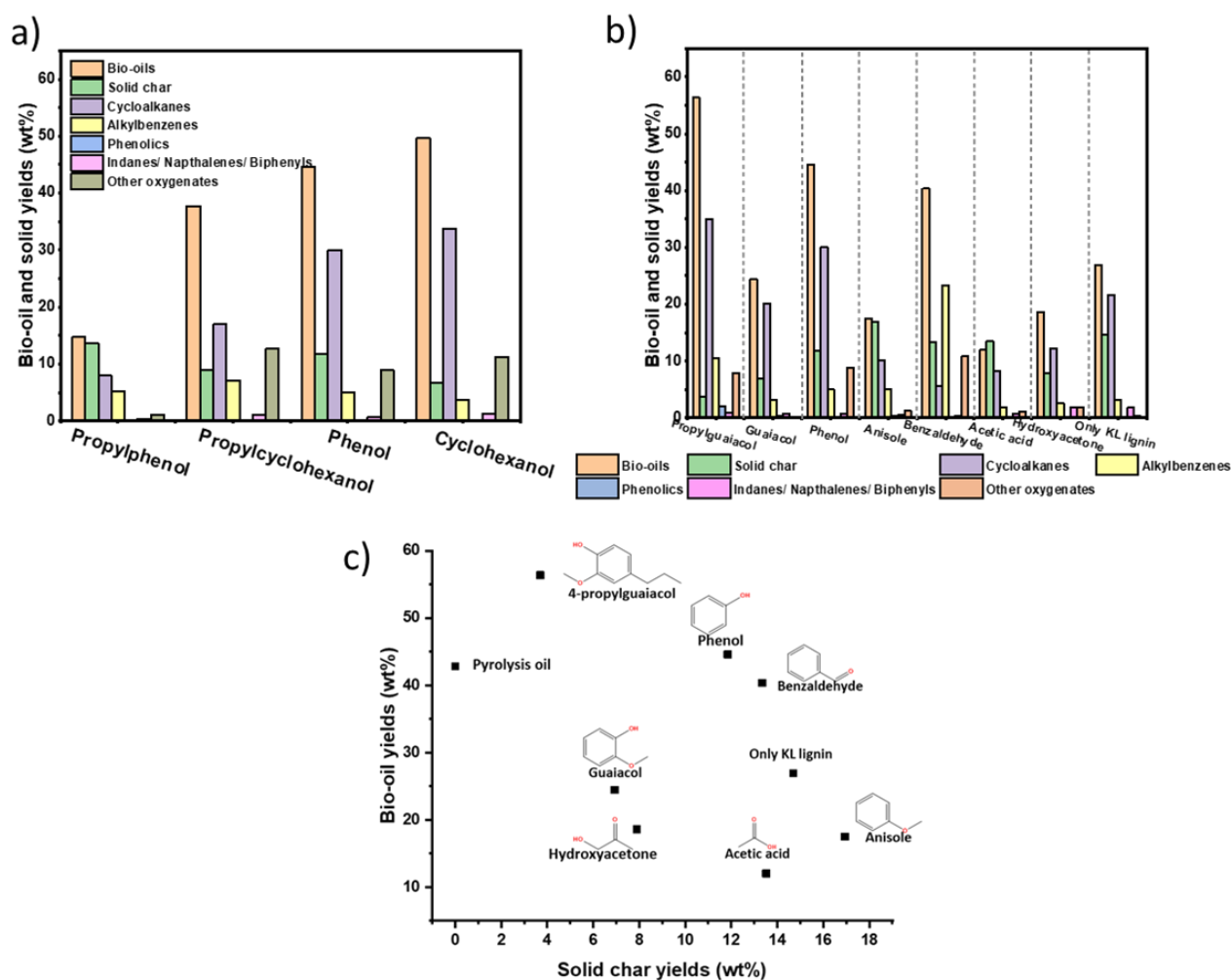


Figure 38. Co-hydrotreatment of Kraft lignin with different model compounds. a) Effect of ring saturation b) Effect of various functional groups on the bio-oil yields and solid residues. Reaction conditions: 400 °C, 75 bar total H₂ pressure, 1000 rpm, 6 h, and KL:monomer (1:1). Monomers selection: 4-propylguaiaicol, guaiacol, phenol, anisole, benzaldehyde, acetic acid, and hydroxy acetone c) An overview of the ranking of the different molecules with different functional groups in terms of bio-oil yields and solid char yields in the co-hydrotreatment with Kraft lignin.

4.4.3 Influence of mass ratio of Kraft lignin versus 4-propylguaiaicol during co-processing

The influence of the feed mass ratio between Kraft lignin (KL) and propylguaiaicol (PG) was studied using the ratios KL:PG of 1:2, 1:1, 1:0.5, and 1:0. The experiments were performed using hexadecane as a solvent over an unsupported NiMoS catalyst at the reaction condition of 400 °C, 75 bar total H₂ pressure for 6 h (**Figure 39 a**). Blank experiments, in which the hydrotreatment was performed without a catalyst were also conducted as reference experiments. As expected, the undesired repolymerization of the reactive intermediates formed during the non-catalytic depolymerization of lignin resulted in a high solid residue yield of 54.8% and a low bio-oil yield of 17.9% (**Figure 39 a**), Exp 6). The total bio-oil yield, determined by GC × GC-MS, includes cycloalkanes, alkylbenzenes, phenolics, indanes/naphthalenes/biphenyls and other oxygenates such as alcohols and ketones. Interestingly, the solid residue yield (57.9%) is even higher when co-feeding both lignin and PG without catalysts

(**Figure 39 a**), Exp 5), as compared to the experiment in which only lignin was used. This is evidently from the images of solid char residues remaining in the bottom of the autoclave and around the stirrer in **Figure 40**. The higher solid residue yield could be explained by the extensive reactions between the depolymerized lignin fragments and also the added propylguaiacol via repolymerization, radical coupling, and condensation without the activation of hydrogen provided by the presence of the catalyst. The importance of the catalyst for facilitating hydrogenation reactions that stabilize reactive intermediates and eventual hydrodeoxygenation reactions is evident by the high selectivities for phenolics and other oxygenate compounds in the experiments without catalyst and only KL, and then even higher with PG co-reactant without the presence of a catalyst (**Figure 39 a**), Exp 5 and 6).

Further catalytic experiments were performed to understand the influence of adding PG as a co-reactant during lignin hydrotreatment. There was a significant drop in undesired solid product yield when PG was co-feed in the catalytic hydrotreatment. KL:PG ratio of 1:1 gives the lowest solid yield (3.7%), which is close to the ash content (3.4%) of the Kraft lignin used. Moreover, it gives a notable bio-oil yield (~56.4%). It was worth noting that for the mass ratio of KL:PG 1:2 and 1:0.5, both co-hydrotreatment tests also give a low solid residue yield of 4.4% and 7.5%, respectively.

Figure 39 b) shows the reaction product selectivities among the catalytic and non-catalytic hydrotreatment of Kraft lignin and PG in different mass ratios. The non-catalytic hydrotreatment of Kraft lignin and lignin + PG resulted in phenolics selectivity of 12.0% and 62.8%, respectively. Other oxygenates such as alcohol-derived compounds and ketones were in the range of 11-12% for both of these non-catalytic tests. On the other hand, for the catalytic Kraft lignin hydrotreatment, HDO activity was apparent, and for the case with KL:PG ratio of 1:1 no phenolics were detected and 66.9% cycloalkanes and 19.2% alkylbenzenes product selectivity was achieved. In KL:PG mass ratio of 1:0.5, the product selectivity was similar as for only Kraft lignin hydrotreatment with cycloalkanes showing 66.9% as shown in **Figure 39 b**). While alkylbenzenes and polyaromatics product selectivities were 17.3% and 15.2%, respectively. When the feed of PG increased as KL:PG mass ratio decreased from 1:0.5 to 1:2, more phenolics were detected, giving a phenolics selectivity of 9.8% in the case of the KL:PG of 1:2 mass ratio. This could be reasoned by the contribution of derivatives from PG in the co-hydrotreatment as previously discussed and is evident by comparison of the GC × GC-MS spectrums in **Figure 41 d**) without PG and **Figure 42 d**) with PG. Since the mass ratio of KL:PG 1:1 hydrotreatment provided the lowest undesired insoluble char products and reasonable total bio-oil yields, the same mass ratio between Kraft lignin and co-reactant model compounds was selected for further experiments.

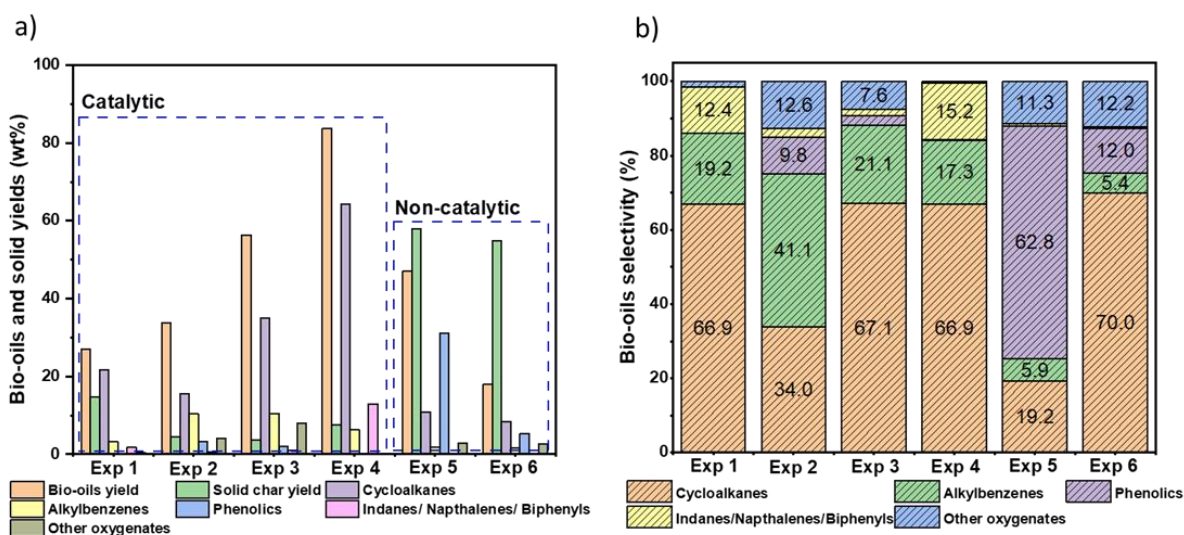


Figure 39. a) Comparison of bio-oil yield and solid yield from experiments with different feed mass ratios between propylguaiacol (PG) and Kraft lignin (KL) (Catalytic run: Experiment (Exp) 1: Only lignin, Exp 2: KL:PG 1:2, Exp 3: KL:PG 1:1, Exp 4: KL:PG 1:0.5, Non-catalytic run: Exp 5: KL:PG 1:1 and Exp 6: Only lignin) b) Products selectivity (cycloalkanes, alkylbenzenes, phenolics, indanes, naphthalenes, biphenyls and other oxygenates) comparison for co-hydrotreatment of lignin with PG.



Figure 40. Solid residues resulting from non-catalytic experiments of co-hydrotreatment of KL. Left: inside of the reactor vessel. Right: reactor head with a stirrer, thermocouple, dip tube, and cooling coil.

4.4.4 Effect of reaction time on co-hydrotreatment of Kraft lignin with 4-propylguaiacol

The influence of the reaction time on the co-hydroprocessing of Kraft lignin and 4-propylguaiacol (PG) was also investigated by performing the experiments for 0 h, 3 h, 6 h, and 8 h at 400 °C, with the total H₂ pressure of 75 bar and using the unsupported NiMoS catalyst. It should be noted that the notation of 0 h means the hydrotreatment reaction was stopped once the reaction temperature of 400 °C was reached and then immediately cooled down (cooling takes 25 minutes) to room temperature. The purpose of performing this experiment (0 h) was to understand more about the solid char formation during the heating and cooling of the reactor system. **Figure 43** compares the bio-oil yield calculated based on the identified liquid products from the 2D GC × GC-MS analysis

and also solid char yields obtained after different reaction times with PG and without PG. The results show that as much as 30.6% (for KL+PG) and 35% (KL) solid char were formed during the heating of the reactor to 400 °C (time =0 h). As expected during the heating period, Kraft lignin was depolymerized and the depolymerized lignin fragments start to undergo coupling reactions at low temperatures which eventually resulted in high solid char formation. These results are in line with the report earlier about lignin pyrolysis. Hosoya et al. reported that the condensation reaction was a major pathway in the early stage of the lignin dimer pyrolysis process and it was effective at a lower pyrolysis temperature¹⁴⁷. Some of the depolymerized lignin has also been further reacted and formed different liquid products. These products included alkylated phenolics, cycloalkanes, aromatics, and polyaromatics as can be seen in the 2D GC × GC-MS spectra shown in **Figure 41 a)** and **Figure 42 a)**. This can be reasoned by that Kraft lignin will start to decompose thermally at 250 °C in which the ether linkages, β-O-4 bonds will be cleaved to form monolignols¹⁴⁸. PG in the co-hydrotreatment was also partially reacted and underwent demethoxylation to form propylphenol as is prominent in the 2D GC × GC-MS spectra in **Figure 42 a)**.

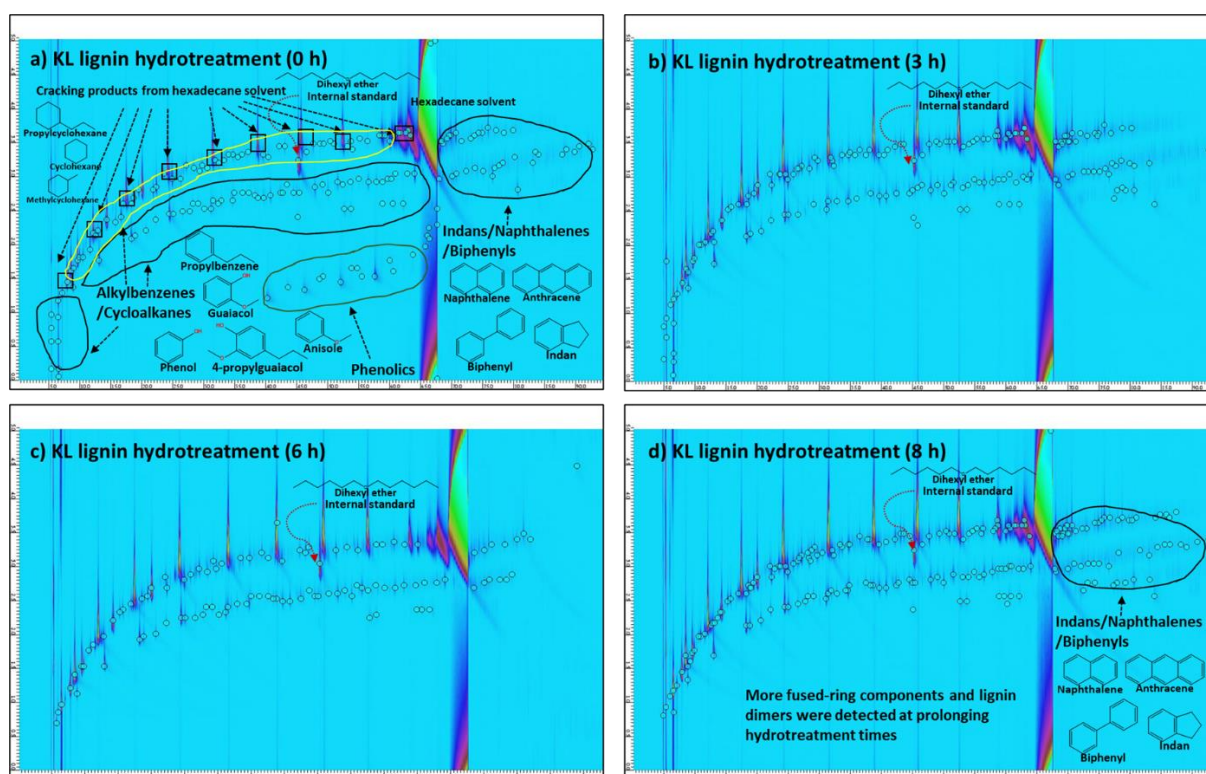


Figure 41. 2D GC × GC-MS chromatogram of the detectable liquid phase products evolved during different reaction times a) 0 h, b) 3 h, c) 6 h, and d) 8 h from the Kraft lignin hydrotreatment. Reaction conditions: 400 °C, total H₂ pressure of 75 bar, 0.75 g of NiMoS catalyst, 2.25 g of KL lignin, 1000 rpm, and 75 mL of hexadecane solvent.

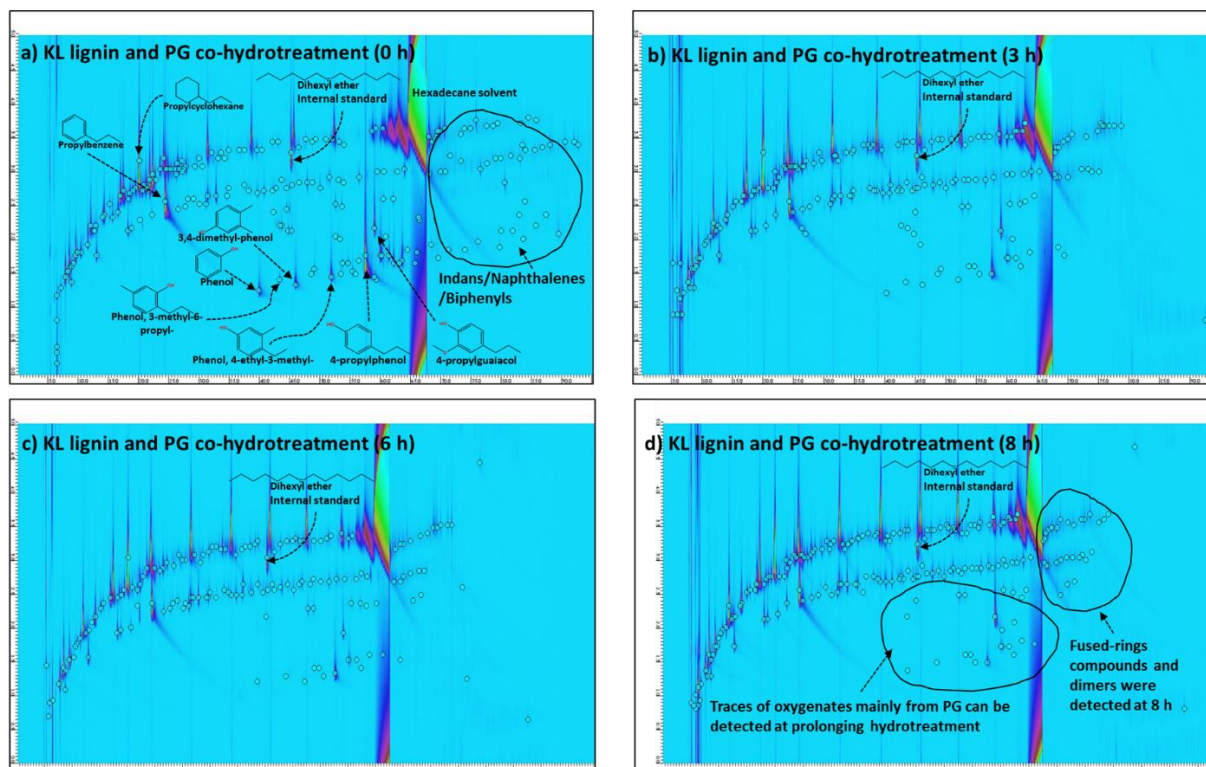


Figure 42. 2D GC \times GC-MS chromatogram of the detectable liquid phase products evolved during different reaction times a) 0 h, b) 3 h, c) 6 h, and d) 8 h from the Kraft lignin and PG co-hydrotreatment. Reaction conditions: 400 $^{\circ}$ C, total H_2 pressure of 75 bar, 0.75 g of NiMoS catalyst, 2.25 g of KL lignin, 1000 rpm, and 75 mL of hexadecane solvent.

As the reaction progresses, the char yields dropped drastically from 0 h to 6 h in both the Kraft lignin hydrotreatment and also co-hydrotreatment of Kraft lignin and PG as shown in **Figure 43**. The decrease in the solid char residues can be explained by that the formed solids were further depolymerized into oligomers and eventually monomers through reactions like hydrogenolysis, ring hydrogenation, and deoxygenation. The formation of these different oligomers and monomers eventually leads to an increase in the total bio-oil yield as the reaction progresses. For the co-hydrotreatment of Kraft lignin and PG, a maximum bio-oil yield of 56.3% was achieved after 6 h, however, it dropped significantly to 27.5% at 8 h. These results suggest that prolonging the hydrotreatment duration negatively impacted the yield of bio-oils as the monomer units generated might undergo polymerization again and form heavy oligomers and light gases. For the Kraft lignin hydrotreatment, a similar trend of increasing bio-oil yields can also be observed with a maximum bio-oil yield of 27% achieved at 6 h, which slightly dropped to 24%. The decreased bio-oil yields with only a slight increase in the char products after 6 h can be reasoned by the possibility that oxygenated monomers undergo oligomerization forming heavy liquid soluble compounds that are non-detectable by the GC. This is evident by the fact that the decrease in bio-oil yield later in the process is more prominent in the case of co-processing in which oxygenated monomers are present already at the start of the process and remain in high concentrations throughout the process (**Figure 42** a) to d)). These available monomers were likely to oligomerize with prolonged reaction times. Besides, the solid residues formed can also undergo further reactions like liquefaction forming heavy oligomers which lead to poorer bio-oil yield. There are similarities for both cases where Kraft lignin underwent hydrotreatment as a sole reactant and also with PG, such as high production of insoluble solid char products at the early heating stage of the hydrotreatment and

that the char production decreased over time. Another interesting observation that can be obtained by comparing both hydrotreatments with and without PG, is that there was a significant reduction in insoluble solid char formation before 6 h in the case when adding PG. The beneficial effect of adding PG in the co-hydrotreatment was most apparent from 0 h to 6 h which might be reasoned that PG plays a crucial role in stabilizing the hydrotreatment intermediates and suppressing the char formation reaction resulting in a low char yield of 3.7%. This can be further demonstrated by the 4-fold higher char yield of 14.7% at 6 h in the case of only Kraft lignin hydrotreatment (absence of PG). Notably, PG is not as effective during the heating period (before 0 h) in preventing solid formation. This could be connected to the fact that the catalyst is not as effective at enabling hydrogenation reactions at lower temperatures. It was also seen from the non-catalytic experiments that adding PG caused increased solid formation without the catalyst (**Figure 39 a**), Exp 5 and 6).

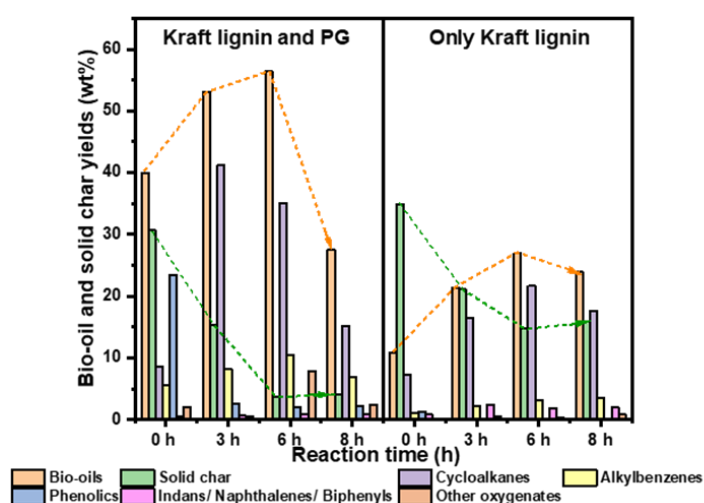


Figure 43. Co-hydrotreatment of Kraft lignin (KL) and PG (mass ratio of KL:PG is 1:1) at 400 °C, total H₂ pressure of 75 bar, 0.75 g of NiMoS catalyst, 2.25 g of Kraft lignin, 75 mL of hexadecane solvent. The bio-oil yields are calculated based on the initial intake of reactants.

These findings further led us to investigate the role of PG in the depolymerization routes of Kraft lignin hydrotreatment. The FTIR spectra of the starting material, i.e. Kraft lignin, and also the lignin-derived char from both Kraft lignin hydrotreatment and co-hydrotreatment with PG for different hydrotreatment times are shown in **Figure 44 a-b**). A broad band at 3327 cm⁻¹, attributed to the hydroxyl groups in phenolic form, and the band at 2937 cm⁻¹ corresponding to the C-H stretching in aromatic methoxy groups can be observed for Kraft lignin starting materials¹⁴⁹. Moreover, the usual C-H deformation in lignin and the carbonyl stretching conjugated with the aromatic ring skeleton at 1454 cm⁻¹ and 1593 cm⁻¹, respectively can be observed in the FTIR spectra¹⁵⁰. The aromatic skeletal vibration of guaiacyl and syringyl units that are present in the lignin aromatic structure can also be identified in the wavenumber range of 1000 cm⁻¹ to 1600 cm⁻¹¹⁵⁰. As the reaction progresses, the absorption peaks of Kraft lignin diminished rapidly from 0 h to 8 h hydrotreatment, indicating the deconstruction of the complex lignin macromolecule structure. The insoluble char residue for the hydrotreatment shows a similar pattern for all runs and also peaks with weak intensity at 1421 cm⁻¹ and 1593 cm⁻¹ were observed indicating its aromaticity. A broad peak around 1124 cm⁻¹, representing the C-H plane deformation of the syringyl unit was also observed for the char residue from all hydrotreatment runs. Interestingly, the structure of the Kraft lignin begins to

deconstruct as early as during the heating period of the reaction (0 h), and adding PG to the reaction did not affect the lignin deconstruction pathway. It was also worth highlighting that this obtained result is in contrast to results in a study by Joffres et al.¹⁵¹. In their study, the FTIR spectra of the initial wheat straw lignin showed a similar pattern as the lignin residue at time zero (reaching 350 °C after 14 minutes)¹⁵¹. It should be noted that our heating period was significantly longer (40 minutes) and also that we used a higher temperature (400 °C). In our study during the heating period of the reactor, the disintegration of the solid Kraft lignin is certainly driven by the increasing temperature regardless of the presence of PG and produces the lignin-derived insoluble char product which further breaks down into smaller lignin fragments for further depolymerization. The high yield of insoluble char at 0 h (after 40 minutes of heating) for both cases (with and without PG) can be reasoned by the lower activity of the catalyst for hydrogenation reactions at the low reaction temperatures. PG rather acted as a protecting agent that stabilizes the reactive depolymerized lignin derivatives preventing and limiting repolymerization, but primarily when the catalytic hydrotreatment reactions have reached their full extent. This is further demonstrated in the ¹³C-NMR measurement, as shown in **Figure 44** c) and d), where several functional groups present in Kraft lignin were not observed in the solid residues even after the heating period (40 minutes). Liquid product analysis confirmed the presence of demethoxylated and deoxygenated products like alkylphenols and aromatics. It can be confirmed also from the ¹³C-NMR spectra that the resultant solid residue primarily consists of both aliphatic and aromatic carbon moieties with only small amounts of methoxy groups and C-O-containing groups.

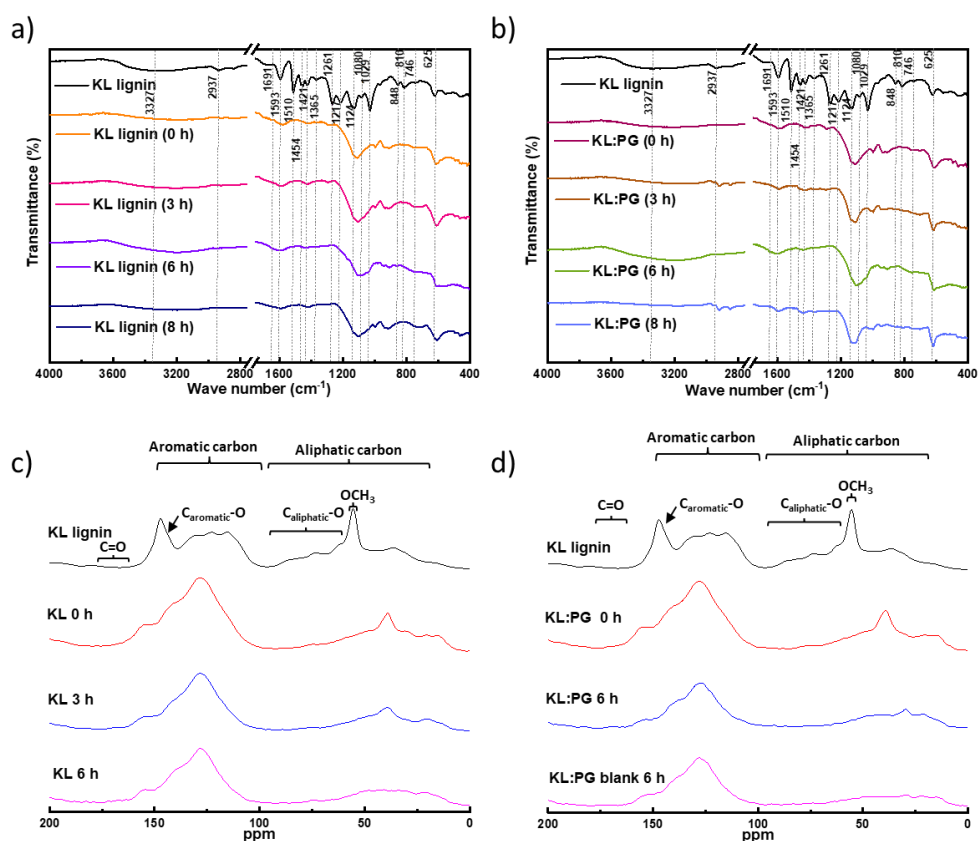


Figure 44. FTIR spectra (a, b) and ¹³C-NMR spectra (c, d) of starting material Kraft lignin and the lignin-derived solid char products from different hydrotreatment times for a) and c) Kraft lignin hydrotreatment and b) and d) Kraft lignin and PG co-hydrotreatment.

It has been reported in various studies that lignin condensation reactions and lignin intermediate repolymerization are the main reason for the formation of undesired condensed solid products which have been referred to as solid char in this study^{94,147,152–155}. These reactions usually involve the formation of quinone methide intermediates which resulted in the generation of the recalcitrant condensed interunit C-C linkages on the ortho- and para-positions that limit further conversion of lignin oligomers to monomers. Moreover, Liu et al. conducted a real-time experimental observation for pyrolysis of model lignin compounds like Guaiacylglycerol- β -guaiacyl ether and guaiacol with/without HSZM-5 and found that the repolymerization of small lignin oligomers can act as a competitive pathway for the formation of heavy oligomers which thereafter are forming lignin-derived char residues¹⁵⁶. In addition, Nakamura et al. studied the condensation reactions of lignin model compounds like guaiacol, methylguaiacol, and methylveratrole under pyrolysis conditions (250 °C, under air atmosphere, and 2 h) and identified the major lignin condensation pathways like vinyl condensation, quinone methide, and radical coupling mechanism¹⁵⁴. Okuda et al. studied the depolymerization of lignin in a mixture of water and phenol at 400 °C for the production of phenolics¹⁵⁵. It was also discussed in their study that the cross-linking reactions between the depolymerized lignin fragments and residual lignin can further form heavier molecular weight fragments leading to the formation of char residues¹⁵⁵. They revealed the addition of phenol as a capping agent in lignin depolymerization was able to capture the reactive species and active sites in larger fragments and suppress the formation of heavier fragments¹⁵⁵. In this study, when PG was supplemented in the Kraft lignin hydrotreatment, the ‘capping’ effect of PG was demonstrated by the progressively decreasing yield of solid char residues in the early extent of the hydrotreatment, and primarily after a sufficiently high reaction temperature was reached to enable catalytic hydrotreatment. The cross-linking reactions were also suppressed by the entrapment of active lignin fragments and also the stabilization of reactive radical species by PG. As the reaction progresses, and with sufficient rates of catalyzed hydrogenolysis and hydrodeoxygenation reactions, the lower molecular compounds like cycloalkanes, alkylbenzenes, and phenolics increase which eventually contributed to an increased bio-oil yield.

4.4.5 Reaction network for pyrolysis oil-assisted Kraft lignin hydrotreatment

Findings in this study have prompted us to discuss further ways to avoid and limit the repolymerization and condensation reactions during the degradation and depolymerization of lignin in the context of hydroconversion. For example, Kim et al. summarized various efforts to avoid the undesired reactions that occurred during the fractionation and depolymerization of lignin, that in turn affected the yield of low molecular weight products⁹⁴. In one of our previous studies, it was shown that the undesired repolymerization and recondensation reactions can be avoided by injecting a lignin slurry in a pre-heated reactor containing solvent and catalyst, to facilitate swift lignin depolymerization¹⁵⁷. This slight alteration of the experimental protocol benefited the deconstruction of lignin by avoiding the undesired repolymerization at the early onset of the reaction during the heating phase of the batch reactor¹⁵⁷. Also in a recent study in which lignin-derived oil was co-fed during the hydrotreatment of a pine pyrolysis oil, it was shown that the co-fed lignin-derived oil inhibited the formation of coke and produced a more stabilized mixture of pyrolysis oil and lignin oil¹⁵⁸.

In this work, a complex feedstock like pyrolysis oil containing molecules with various functional groups, as protecting agents in the early phase of the hydrotreatment, efficiently blocking and limiting the pathway of recondensation and repolymerization, was found to facilitate the depolymerization and liquefaction of lignin. Another point that can be highlighted here was that the compounds present in the additional feed (PO and

oxygenated monomers) used in this study for KL lignin hydrotreatment can also be obtained from the depolymerization of lignin which then prevented the use of a separation process to recover and regenerate the co-feed. **Figure 45** illustrates the proposed multiple pathways of the catalytic reductive liquefaction of Kraft lignin in hexadecane solvent in the presence of a hydrothermally synthesized NiMoS unsupported catalyst. It is facilitated by the presence of oxygenated monomers funneling the lignin radical fragments to hydroconversion reactions producing deoxygenated monomers instead of condensation and repolymerization reactions forming solid char and lignin dimers. Kraft lignin undergoes primarily depolymerization by means of hydrogenolysis and the thermal cracking of the condensed C-C bonds, and the C-O-C ether linkages, forming the primary depolymerized lignin oligomers during the elevation of the hydrotreatment temperature. During this heating period, catalytic hydrogenolysis/hydrotreatment reactions are weaker which favors condensation/repolymerization reactions of the reactive lignin oligomeric intermediates forming condensed insoluble solid residues that led to unwanted solid char production. Moreover, the stabilizing effect of PG and pyrolysis oil to reduce solid formation is most beneficial when catalytic hydrogenolysis and other hydrotreatment reactions increase to their full effect. With the presence of an active unsupported NiMoS catalyst, the stabilized lignin oligomers were able to access the catalytic active sites and further undergo secondary depolymerization, yielding monomers such as cyclic compounds, aromatics, and phenolics and lignin dimers like fused-ring compounds via hydrogenation and deoxygenation.

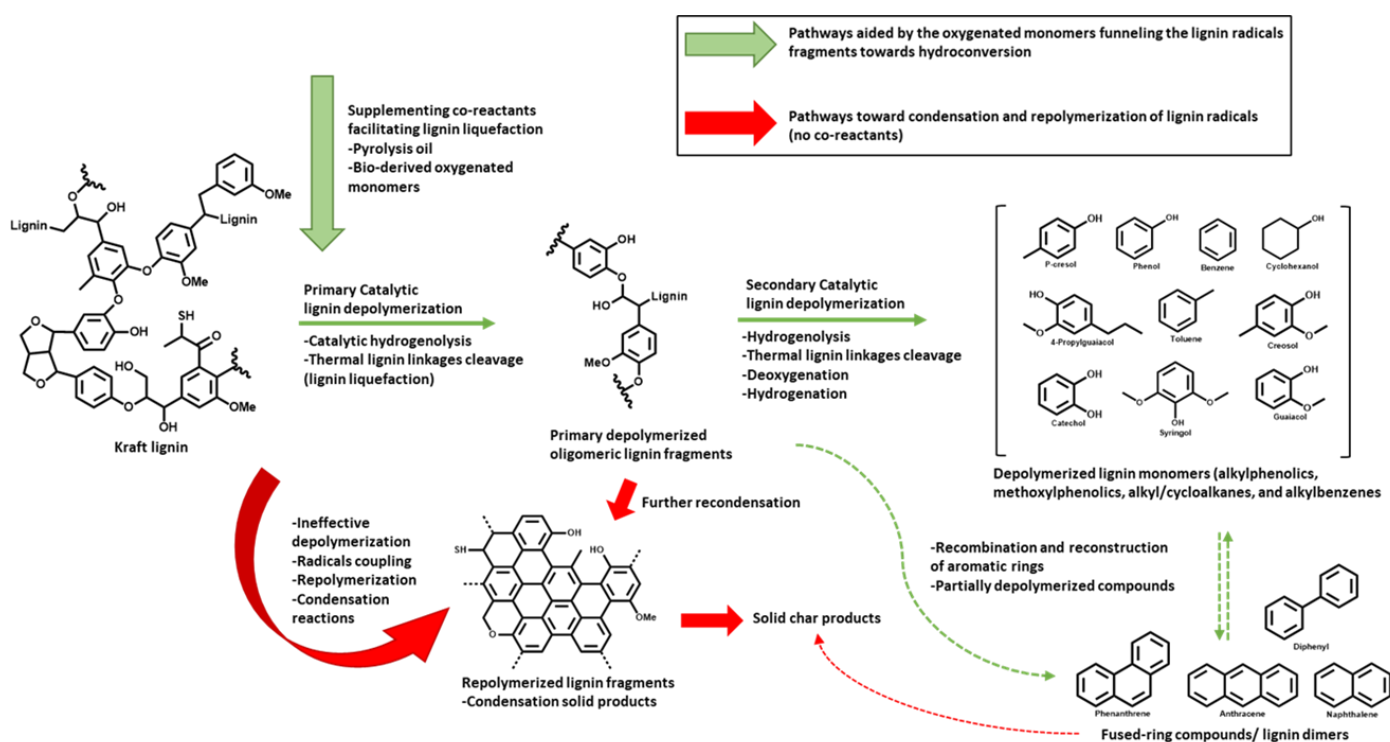


Figure 45. Proposed multiple routes involving the supplement of oxygenated monomers and pyrolysis oil in catalytic lignin depolymerization and liquefaction to solid char, lignin dimers, and deoxygenated monomers in hexadecane solvent in the presence of a hydrothermally synthesized NiMoS unsupported catalyst.

4.5 Pilot slurry hydrocracking and fixed-bed hydrotreating of fast pyrolysis bio-oils (FPBO)

Fast pyrolysis bio-oils, a highly viscous bio-liquid resulting from the fast pyrolysis of lignocellulosic biomass residues, is a potential renewable feedstock that can be further refined for the production of bio-based fuels and chemical intermediates. However, FPBO has detrimental properties such as a high oxygen content, acidity, high water content, and instability during storage. Moreover, the high coking tendencies of the FPBO during hydrotreating can also cause plugging issues. Slurry-based hydroprocessing emerges as a potential technology since such a process is inherently resistant to plugging problems, and the catalyst can be continually withdrawn from, and replaced or recycled to the reactor. The slurry dispersed catalyst used in the process also allowed direct contact of the catalytic material with heavy residue for better hydroconversion¹⁵⁹. In a recent study by Dimitriadis et al., the authors presented a whole processing chain that covered the fast pyrolysis of agricultural residue (straw) producing FPBO, followed by stabilization of the resulting FPBO in an SHC pilot plant¹⁶⁰. The stabilized FPBO then underwent hydrotreatment in a continuous fixed bed reactor, producing bio-derived intermediates, that are fully miscible with fossil feedstocks. Nevertheless, catalyst deactivation and plugging problems were still an issue while processing challenging feedstocks like FPBO.

Previously, several studies have been carried out using the pilot slurry hydrocracking (SHC) plant in RISE ETC, Piteå for the co-hydroprocessing of renewable feeds such as pyrolysis oil and also Kraft lignin residues with fossil residues. For example, a one-stage co-processing of FPBO (0 or 20 wt%) with fossil vacuum residue (at 50 wt%) and vacuum gas oil (VGO) was carried out in the SHC plant using an in-situ generated oil-soluble molybdenum precursor as catalyst¹⁷. The results showed the potential of integrating bio-molecules into the continuous processing of fossil feeds resulting in a low coke yield (~ 1 wt%) and also a highly deoxygenated product. Moreover, in the subsequent study, Bergvall et al. investigated the co-processing of FPBO and VGO at a 20:80 wt% ratio under a continuous mode of operation¹⁶¹. Almost complete deoxygenation (~ 94%) was achieved under the operating conditions of 410-435 °C and 1-2 h residence time. The biogenic carbon was found to be 53-56 wt% under operating conditions. One of the challenges while co-processing renewable feeds and fossil feeds was also to accurately determine the infusion of biogenic carbon to the end product.

Besides FPBO, challenging solid bio-feedstocks like Kraft lignin have also been upgraded in the slurry hydrocracker using VGO as a carrier solvent, producing stabilized bio-crude that can be further processed in existing refining infrastructures¹⁵⁷. One of the main findings in the study was that feeding the cold lignin slurry into a reactor system that has reached the desired reaction temperature can significantly avoid the undesired repolymerization and recondensation reactions of depolymerized lignin intermediates at low temperature (~ 250 °C)¹⁵⁷.

In this study, a two-stage hydrotreatment of FPBO was proposed; the first step involves a slurry hydrocracking of the FPBO over the unsupported NiMoS (from studies III and IV). Then the stabilized FPBO further underwent hydrotreating in a fixed-bed hydrotreater over a supported NiMo sulfide under a continuous mode of operation to remove the remained oxygen content of the stabilized FPBO.

4.5.1 Properties of FPBO

The FPBO used in this study was a liquid product purchased commercially. Its physical and chemical properties are presented in **Table 15**.

Table 15. Chemical properties of as received and dry FPBO in this study.

Property	Method	As received	Dry
Carbon	ASTM D591	46.1 wt%	58.6 wt%
Hydrogen	ASTM D591	6.8 wt%	5.6 wt%
Nitrogen	ASTM D591	0.0 wt%	-
Sulfur	ENISO20884	28.4 wt%	-
Oxygen (calculated)	ASTM D591	47.1 wt%	35.8 wt%
Water	ASTM E203	21.2 wt%	0.0 wt%
Density	EN ISO 12185	1.2 kg/dm ³	-
Solids content	ASTM D7579	0.0 wt%	-
Ash content	EN ISO 6245	0.0 wt%	-
Kinematic viscosity (40 °C)	ASTM D445	28.1 cSt	-
Aliphatic OH functionality	³¹ P-NMR	4.0 mmol/g	-
Phenolic OH functionality	³¹ P-NMR	2.3 mmol/g	-
Carboxylic acid COOH functionality	³¹ P-NMR	0.8 mmol/g	-
Carbonyls	ASTM E3146-18a	4.2 mmol/g	5.3 mmol/g
Total acid number	ASTM D664	1.2 mmol/g	1.5 mmol/g

4.5.2 Liquid products properties

Table 16 presents the chemical properties of the raw FPBO, the slurry product from SHC, and the upgraded liquid product from the fixed bed. As can be observed from **Table 16**, there was a reduction in oxygen content in the slurry upgraded product from 36 wt% (the raw dried FPBO) to 15 wt%, showing the deoxygenation capability of the unsupported NiMoS. The oxygen content of the raw dried FPBO was removed in the form of water and carbon oxides.

Based on ³¹P-NMR analysis (**Table 16**), most of the oxygen present in the oil product obtained after the slurry hydrocracking process was in the form of phenolics. The phenolics concentration was higher in the slurry stabilized product (2.9 mmol/g) compared to the as-received FPBO (2.3 mmol/g). This can be attributed to that the phenolics have a relatively high resistance towards hydrotreatment and hence are enriched in the lower volume of the slurry product and also formed by the demethylation of the methoxy groups during the slurry process. It should also be noted that OH products such as aliphatic hydroxyl groups (0.8 mmol/g) and carboxylic acids (0.5 mmol/g) were lowered in the stabilized slurry product. It can be seen that the carboxylic acid content in the stabilized slurry product was reduced to 0.001 mmol/g after the fixed-bed hydrotreating. Both the aliphatic OH and phenolic OH functionality in the hydrotreated liquid product was significantly lowered as compared to the stabilized slurry feed resulting in a total OH content of 0.005 mmol/g in the final product.

The carbonyl contents in the FPBO are one of the reasons for the instability of the pyrolysis oil as the carbonyls tend to undergo oligomerization and condensation reactions with phenolics forming larger polymeric compounds^{162,163}. According to the ³¹P-NMR analysis, the carbonyl content of the raw FPBO was found to be 4.2 mmol/g and with the slurry hydrocracking process, it was reduced to nearly half and was negligible in the final product after the fixed bed upgrading. Besides, the increase in stability of the FPBO after the slurry process is also evident from its viscosity change after an accelerated aging test for 24 h at 80 °C of the untreated FPBO and slurry products (the heavy fractions). For the untreated FPBO, the viscosity increased from 36.4 to 46.1 cSt while the slurry product showed nearly identical results before and after the aging test (12.2 and 12.0 cSt, respectively). Furthermore, the slurry product showed a residue of 1.4 wt% after heating to 500 °C in an inert atmosphere in a thermogravimetric analyzer (TGA) which is significantly lower than that from the raw FPBO, in which a high amount of residue (20 wt%) was obtained due to coke formation¹⁶⁴.

On the other hand, a high ¹H-NMR signal of alkanes (96 mol%) and aromatics (4 mol%) associated hydrogen were detected for the final hydrotreated product. It was also noticed that after the fixed bed hydrotreating of the slurry product, the content of alkenes, alcohols/ethers, carboxylic acids, and aldehydes was not detected for the upgraded liquid product. This is mainly attributed to the saturation of the alkenes and also the deoxygenation of oxygen-containing compounds. A relatively high proportion of alkanes is also suggested by the high H/C atomic ratio of 1.88 (blue scatter in **Figure 46**).

Table 16. The chemical properties of the FPBO, the stabilized slurry feed, and the hydrotreated fixed-bed liquid products. *As used in the fixed-bed hydrotreatment, **Sample 11 from the fixed-bed hydrotreatment.

Elemental Composition	Unit	FPBO (as received)	FPBO (dry)	Slurry-product*	FB-product**
C	wt%	46.1	58.6	72.5	85.4
H	wt%	6.8	5.6	9.4	13.4
N	wt%	0	-	0.06	< 0.05
S	wt%	0	-	< 0.1	< 0.1
O	wt%	47.1	35.8	15.0	0.5
Water Content	wt%	21.2	0.0	0.0	0.0
¹H-NMR					
Alkanes	mol%	42.3	-	77.8	96.0
Alkene	mol%	10.1	-	4.5	0.0
Alcohol/Ether	mol%	33.0	-	7.8	0.0
Aromatics	mol%	13.4	-	9.9	4.0
COOH/Aldehydes	mol%	1.30	-	0.01	0.0
³¹P-NMR					
Aliphatic OH	mmol/g	4.0	5.1	0.8	0
Phenol OH	mmol/g	2.3	3.0	2.9	0.004
COOH	mmol/g	0.8	1.0	0.5	0.001
Total OH	mmol/g	7.1	9.1	4.2	0.005
Carbonyls	mmol/g	4.2	5.3	2.4	Not detected
Total Acid Number	mmol/g	1.2	1.5	0.7	Not detected
Aromatic content by HPLC-RI					
Mono aromatics	wt%	Not measured		4	29
Di aromatics	wt%			3	2.5
Tri and higher aromatics	wt%			0.4	0.0
Total aromatics	wt%			7.4	31.5

The chemical properties of the hydrotreated fixed-bed products are presented in **Table 17**. When the hydrotreatment temperature was reduced to 340 °C, some differences were observed in the product properties. The oxygen concentration increased slightly to 0.7 wt% for sample 12. This is also evident from the $^1\text{H-NMR}$ data that show levels of alcohols/ethers and the $^{31}\text{P-NMR}$ data that show increased levels of phenols. Some signals from alkenes can also be observed in the $^1\text{H-NMR}$ results, which is not the case at the process temperature of 380 °C. The lower temperature also seems to reduce the proportion of aromatics in the product as can be confirmed by the aromatics analysis using HPLC-RI.

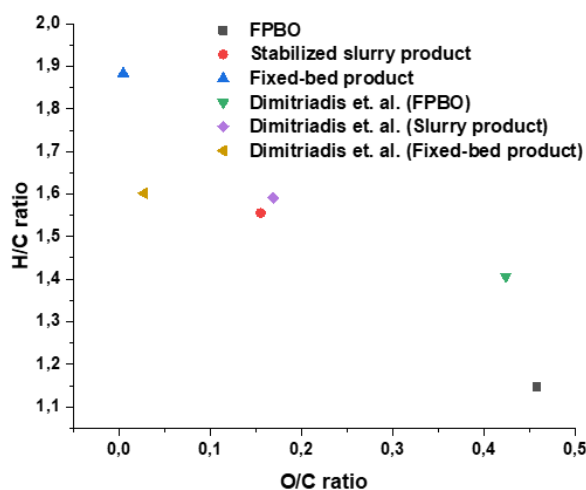


Figure 46. Van Krevelan diagram comparing atomic ratios of O/C and H/C for the FPBO (dry basis) and the upgraded products and also the results from Dimitriadis et al.¹⁶⁰.

Table 17. The chemical properties of the hydrotreated fractions 4 (after 16 h time-on-stream (T.O.S)), 11 (after 50 h T.O.S), 12 (after 56 h T.O.S), and 13 (after 61 h T.O.S) from the fixed-bed hydrotreatment.

Elemental Composition	Unit	Fraction 4	Fraction 11	Fraction 12	Fraction 13
Description		liquid product collected after hydrotreatment at 380 °C, once all LGO is exchanged for stabilized slurry feed	liquid product collected after hydrotreatment at 380 °C, before the temperature starts to decrease	the liquid collected after hydrotreatment at 340 °C	the liquid collected after hydrotreatment at 380 °C after increase from 340 °C
Fixed-bed temperature	(°C)	380	380	340	380
C	wt%	84.9	85.4	85.6	86.1
H	wt%	13.4	13.4	13.7	13.3
N	wt%	0.0	0.0	0.0	0.0
S	wt%	0.0	0.0	0.0	0.0
O	wt%	0.4	0.5	0.7	0.5
¹H-NMR					
Alkanes	mol%	96.4	96.0	97.4	95.8
Alkene	mol%	0.0	0.0	0.1	0.0
Alcohol/Ether	mol%	0.0	0.0	0.1	0.0
Aromatics	mol%	3.6	4.0	2.5	4.2
COOH/Aldehydes /Phenol	mol%	0.0	0.0	0.0	0.0
³¹P-NMR					
Aliphatic OH	mmol/g	Not detected			
Phenol OH	mmol/g	0.0	0.004	0.1	0.0
COOH	mmol/g	0.0	0.001	0.0	0.0
Total OH	mmol/g	0.0	0.005	0.1	0.0
Carbonyls	mmol/g	Not detected			
Total Acid Number	mmol/g	Not detected			
Aromatic content by HPLC-RI					
Mono aromatics	wt%	29	29	19	27
Di aromatics	wt%	1	2	2	4
Tri and higher aromatics	wt%	Not detected			
Total aromatics	wt%	30	31	21	31

The GC × GC-MS FID analysis was performed to further understand the composition of the slurry product and also the hydrotreated products. As can be seen in **Figure 47 a**), a variety of oxygenated compounds (furans, ketones, aldehydes, carboxylic acids, and phenolics) and also paraffinic-derived compounds, deoxygenated aromatics, cycloalkane compounds, dimers, and polyaromatics were present in the stabilized slurry product. This is further evident in the ¹³C NMR spectra of the stabilized slurry products in **Figure 49** and correlated to the results obtained from the ³¹P NMR where the signals representing different OH groups were detected (**Table 16**). In contrast, the upgraded FB product consisted of mainly paraffinic-derived compounds and aromatics (**Figure 47 b**). Similarly, the ¹³C NMR results also show that for the upgraded product, only paraffinic of varying lengths and aromatics are present in the liquid sample (**Figure 49**).

The upgraded FB product was distilled into the two boiling point fractions, < 177 °C and 177 – 343 °C. The two distillation fractions both showed notable contents of cycloalkanes according to the 2D GC × GC-MS FID (49% and 37% at the lower and higher boiling point range, respectively in **Figure 48** c) and d)). Besides, the proportion of aromatics was high, for the distillate fraction with a boiling point of 177 – 343 °C, giving 9.4% aromatics and 17.4% naphthalene compounds (a total of 26.8% aromatic compounds). This is also evident from the ¹³C NMR analysis showing signals in the region representing aromatics. The predominance of cyclic compounds (aromatic and aliphatic) in hydrotreated pyrolysis oils has also been observed by others^{89,165}. It should be noted, when starting the slurry process, hexadecane was first used as a starting solvent in the main reactor to disperse the unsupported catalyst, hence the hexadecane was recovered from the slurry product at the end of the process. As a result, peaks corresponding to hexadecane (impurities retained in the column of the GC-MS) were not integrated and do not make up part of the “paraffinic compounds” in **Figure 47**.

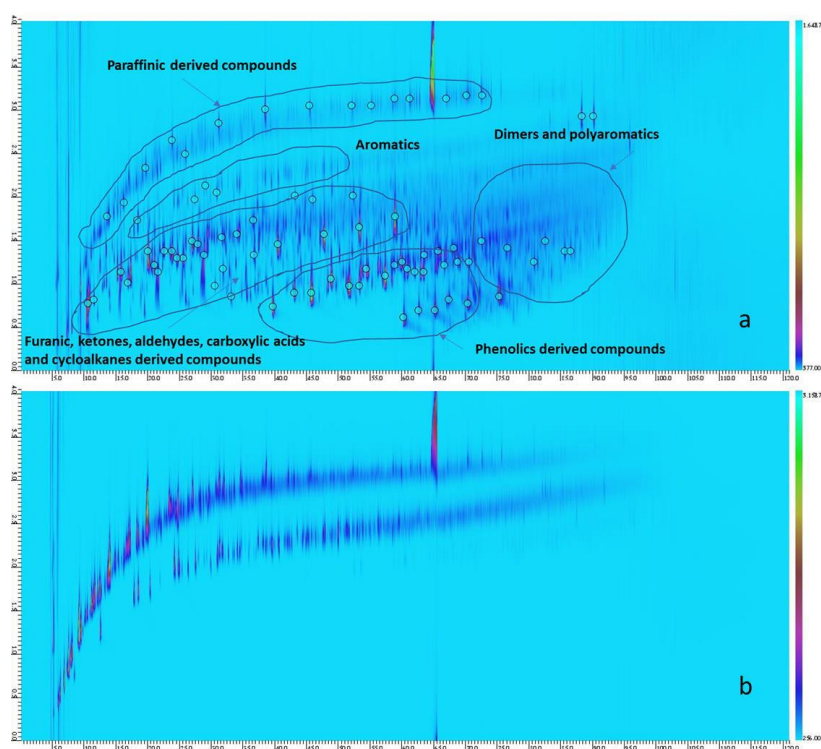


Figure 47. Two-dimensional GC × GC-MS FID spectra of the stabilized slurry products (a) and the hydrotreated fixed-bed product, sample 11 (b).

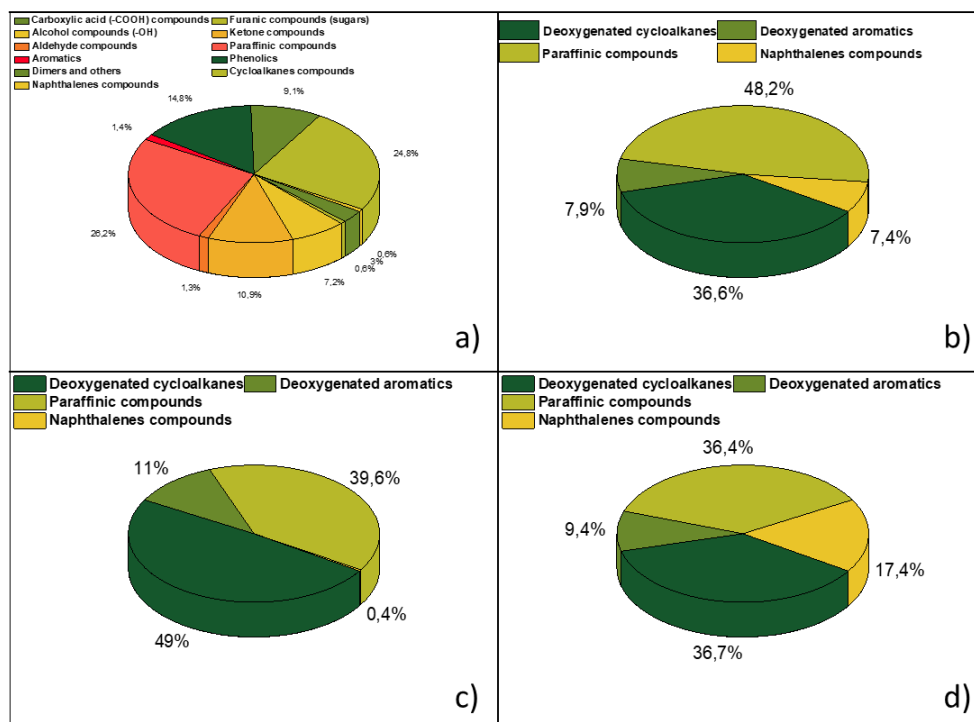


Figure 48. The distribution of compound classes as FID area-% according to GC × GC-MS FID a) slurry-product, b) fixed bed (FB) upgraded product, c) Distillation fraction < 177 °C of FB-product, d) Distillation fraction 177 – 343 °C of FB-product.

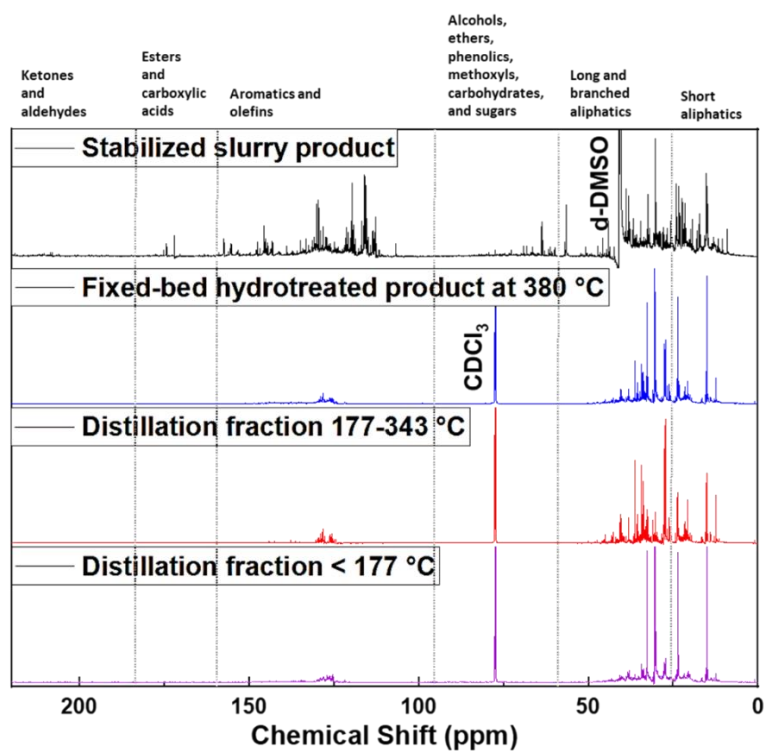


Figure 49. ^{13}C NMR spectra of the stabilized slurry products, fixed bed hydrotreated product at 380 °C, and the distillation fractions.

4.5.3 Process material flow

Figure 50 a) and b) show the normalized product distributions by mass and carbon bases, respectively for the slurry hydrocracking and fixed-bed hydrotreating processes, and their combined balances. The mass balance closure was 99.6% for the SHC process and 96.8% for the FB process and the corresponding carbon balance closures were 89.3% and 85.3%, respectively. The values presented here are normalized to 100% and the mass balances reported are based on the total mass of the liquid and gaseous products (excluding H₂) with closure made with total mass of the feed. The calculation of the carbon balances was performed using the non-normalized mass yields and the non-normalized elemental compositions.

In the SHC process, there is a significant loss of both mass and carbon to water and gaseous products. Among the gaseous products based on mass, quite similar quantities of carbon oxides (7.1 wt% for slurry process, grey bar in the pie chart, **Figure 50** a)) and gaseous hydrocarbons (6.5 wt% for slurry process, orange bar in the pie chart, **Figure 50** a)) were produced. However, CO₂ constituted a three times greater mass yield than CO and was the dominating gaseous species (5.4 wt%), followed by CH₄ (2.8 wt%). The higher removal of oxygen in the form of CO₂ is preferred, as CO₂ involves the removal of twice as many oxygen atoms per carbon atom as compared to CO, which in turn contributes to an increased carbon recovery to the liquid products at a similar deoxygenation level.

For the overall process, the yield of oil produced was 28.7 wt% (**Figure 50** a)) and the recovery of carbon was 67 wt% (**Figure 50** b)). The total H₂ consumption was 33.7 g/kg feed (raw FPBO) in the slurry process and 20.3 g/kg feed in the FB process, which results in a total H₂ consumption for the overall process of 41.5 g/kg processed FPBO (or 52.7 g/kg if expressed per kg dry FPBO).

It should be highlighted that the mass balance for the slurry process was calculated toward the end of the experiment when the heavy product did not contain any of the hexadecane starting oil. Hence, the mass- and carbon balances reported are not affected by the hexadecane recovery to the heavy product during the earlier parts of the experiment. For the FB upgrading process, the effect of the presence of hexadecane in the slurry product used in the FB process was negligible on the carbon balance as the carbon recovery was high for both the hexadecane and the non-hexadecane parts of the slurry feed. For the mass balance, the presence of the remained hexadecane led to a slight overestimation of the yield of oil product (the hexadecane presumably might contribute toward a higher yield of oil production than the remainder of the feed). One of the main hurdles that can be observed from both mass and carbon balances was the production of a large amount of water during the hydroprocessing of FPBO, especially in this study, where there is no heavy fossil residue that acts as a second co-feed. The future implementation of the concept might have to consider recycling and reusing the water stream as a source for hydrogen production.

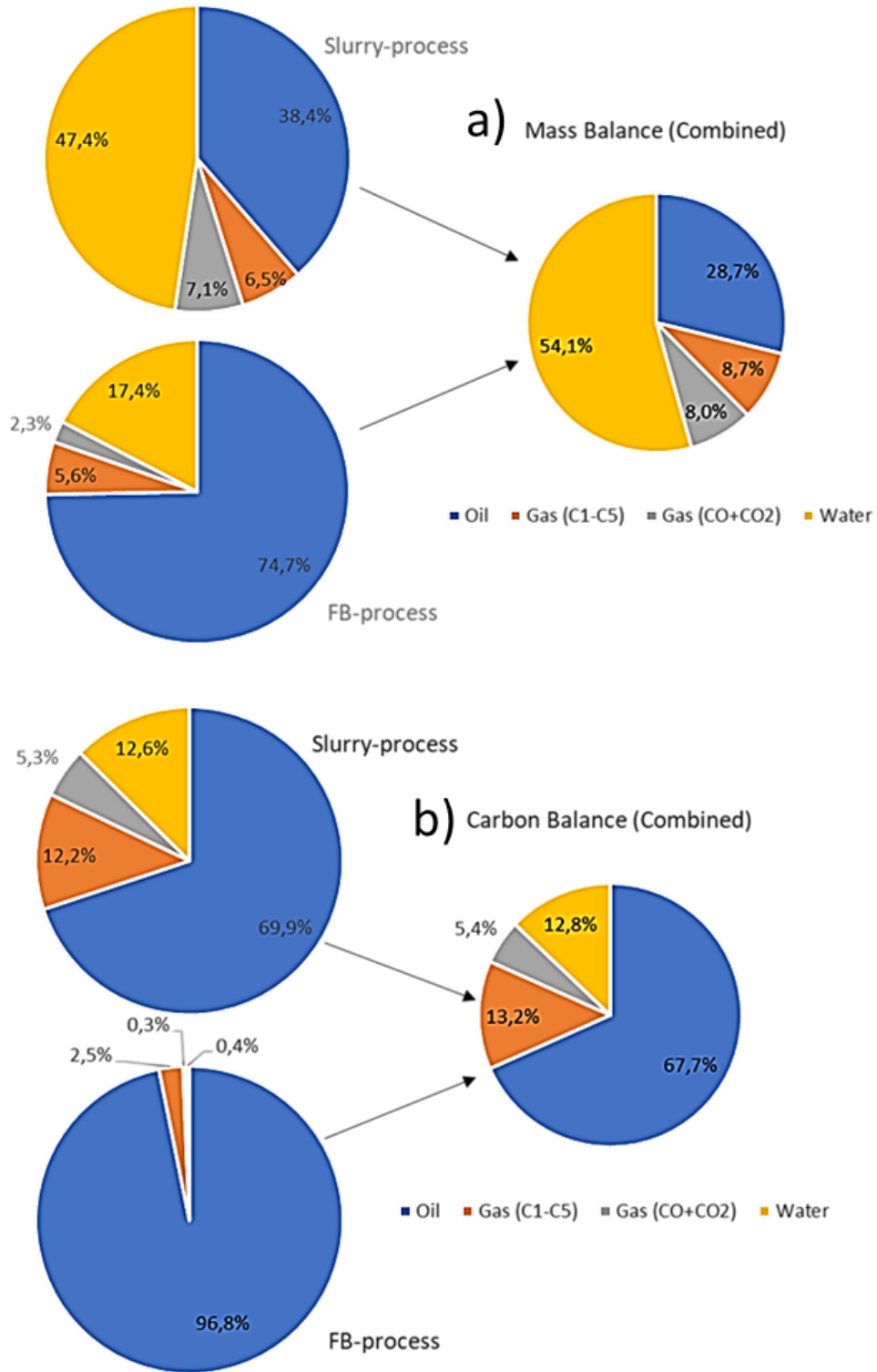


Figure 50. a) Normalized product distributions by a) mass basis and b) carbon basis from the SHC and fixed bed processes and their combination.

5 Conclusions

Forms of transportation, including road, maritime, air, rail, and intermodal require extensive decarbonization measures to reduce their carbon footprints. There is no silver bullet when it comes to combating the global climate crisis, and a shift toward the use of renewable fuels and electrification is inevitable. Hydrotreatment, which involves hydrodeoxygenation, lies at the center of the hydroprocessing of renewable feedstocks employing sulfided catalysts. Challenging feedstocks such as Kraft lignin and pyrolysis oil derived from waste residues require extensive pretreatments, purification, and upgrading methods like hydrotreatment before their products can be applied in fuel and chemical production. In this regard, slurry catalytic hydrotreatment of model feeds, Kraft lignin, and pyrolysis oil were investigated using metal sulfide catalysts in supported and unsupported forms. The catalyst preparation, characterization, and relevant reaction routes covering single and co-processing modes were explored and developed in this doctoral thesis through experiments.

It was found in the first study (**Paper I**) that the impregnation of Ni, Fe, Cu, and Zn into Mo catalysts lowered the rate of demethoxylation, which gave a decrease in the initial PG conversion in the order $\text{Mo} > \text{ZnMo} > \text{CuMo} > \text{FeMo} > \text{NiMo}$. The sulfided NiMo-supported catalyst gave a final yield of 94% for deoxygenated cycloalkanes. In contrast, final deoxygenated cycloalkane yields of 58.1%, 67.2%, and 44.4% were obtained for FeMo-, ZnMo-, and CuMo- supported catalysts, respectively. The deoxygenated cycloalkane yields for the non-promoted Mo-sulfide catalyst were 70%. The results show that Ni promoted the Mo catalyst while impregnating metals, such as Fe, Zn, and Cu, inhibited the formation of deoxygenated cycloalkanes. Interestingly, the selectivity for deoxygenated aromatics increased at higher PG conversion following the order: $\text{ZnMo} > \text{FeMo} > \text{Mo} > \text{NiMo} > \text{CuMo}$, with 16% and 19% aromatics for ZnMo and FeMo catalysts, respectively. Both Zn and Fe had an adverse effect on the HDO activity of PG but changed the selectivity towards aromatics, such as propylbenzene, at full PG conversion. Moreover, a pseudo-first-order kinetic modeling analysis was done for PG HDO, and the model clarified the deoxygenation routes and reaction network. The inclusion of side reactions also improved the model and explained the experimental results, with more than a 90% coefficient of determination for all catalysts. The direct deoxygenation of PG was the major pathway for the removal of oxygen-containing groups with 4-propylphenol being the major intermediate. Hence, the model shows that the proposed reaction routes can be adapted for all the studied catalysts. The influence of promoters on the Mo catalysts is also indicated in the modeling for HDO of PG. For instance, NiMo catalysts show high hydrogenation rates of aromatic rings yielding cycloalkanes. In contrast, Fe- and Mo- promoted catalysts inhibited the hydrogenation of the aromatic ring and facilitated the formation of aromatics.

A simple hydrothermal synthesis method for the preparation of an unsupported MoS_2 catalyst was explored in the second study (**Paper II**). An annealing pretreatment of as-synthesized MoS_2 unsupported catalysts was found to be important to enhance the HDO activity of PG. The unsupported catalysts that had been synthesized for 12 h coupled with pH adjustment and annealing treatment gave the highest degree of deoxygenation of all the catalysts. Creating an acidic environment during catalyst synthesis was found to be important in assisting the micelles growing of MoS_2 catalyst, forming smaller particles that could influence HDO activity. A comparison was made between the HDO of PG and Kraft lignin hydrotreatment using our in-house synthesized MoS_2 and sample of bulk MoS_2 used as catalysts. The results showed that the annealed MoS_2 unsupported catalysts gave high deoxygenation

of Kraft lignin. These results also indicated that highly active-deoxygenation and hydrogenation catalysts could suppress the formation of char and result in a higher yield of bio-oil.

In the subsequent study (**Paper III**), we studied the combination of NiMo sulfides with USY zeolites for Kraft lignin hydrotreatment. The study aimed to gain better insight into the role of the USY zeolite as catalyst support and also the active sulfide metallic component NiMoS in the processing of a complex feedstock like Kraft lignin. The interaction of the catalyst components and also Kraft lignin was explored by understanding the reactions involved such as reductive depolymerization by means of hydrogenolysis, hydrodeoxygenation, and also repolymerization of reactive intermediates to insoluble char residues. The obtained results showed that the non-catalytic depolymerization of Kraft lignin resulted in a high yield of char residues (47 wt%). On the other hand, with the presence of Y30 as a catalyst, the char residues were reduced by 20% owing to its surface acidity that stabilized the reactive lignin intermediates and thus improved the overall bio-oil yield. With the use of NiMo impregnated Y30 catalyst, a yield of 30.5 wt% deoxygenated cycloalkanes and alkylbenzenes with 24 wt% char residues was obtained after 5 h hydrotreatment at 400 °C. In the case of a physical mixture of unsupported NiMoS and Y30, the deoxygenated cycloalkanes and alkylbenzenes selectivity reduced by 30%, and the solid residues also further reduced to 16.7 wt% indicating the improved accessibility of the NiMoS active sites for the lignin fragments. Another main finding was that the liquid product yield could be correlated with the acidities and pore size of the impregnated catalysts, indicating the possibility to tune the properties of the catalysts for a better hydrotreatment performance.

In **Paper IV**, we further explored pyrolysis oil-assisted Kraft lignin reductive liquefaction in a paraffin solvent over the unsupported NiMoS catalyst (used in the previous study). It was shown that the co-processing of Kraft lignin and pine fast pyrolysis oil (PO) resulted in an outstanding char reduction and improved total bio-oil yield. When using an optimum amount of PO as a co-reactant (KL:PO of 1:1) a complete suppression of char was found and we propose that the reason for this is the inhibition of the repolymerization routes of reactive lignin intermediates by the various monomers supplied by the co-fed pyrolysis oil.

To gain further understanding, we examined and demonstrated the potential of co-hydroprocessing Kraft lignin with various oxygenate monomers, as representative for different model compounds for pyrolysis oil, using the same unsupported catalyst. The hydrotreatment was investigated along with reaction parameters including reaction time, temperature, and catalyst loading to assess the effect on insoluble solid char residue yields (%) and the global bio-oil yields (%). Among all the tested model oxygenates as co-reactants, 4-propylguaiacol (PG), which contains hydroxyl, methoxy, and propyl functional groups, was found to have a substantial positive effect in terms of suppressing the production of insoluble recondensed solid products, evidently from the decrease in solid char yield from 14.7% (only Kraft lignin) to an extremely low solid yield of 3.4% at the same reaction conditions (400 °C, total 75 bar hydrogen pressure, and 6 h). Moreover, Kraft lignin starts to deconstruct during the heating period and yielded the highest insoluble char yield when the desired temperature was reached. The added 4-propylguaiacol (PG) in the Kraft lignin hydrotreatment did not affect the deconstruction pathway but rather acted as a stabilization agent stabilizing reactive intermediates. It was also important to highlight the stabilizing effect depends on sufficient rates of catalytic hydrotreatment reactions for it to be effective to reduce solid formation. In the case of a non-catalytic reaction, the addition of PG increased the solid formation.

A ranking considering the char-reducing potential of the individual oxygenated compounds (co-reactant) was provided giving the best performance in limiting solid char formation by the following sequence: PG (hydroxyl, -OH, methoxy, -OCH₃, and propyl, -C₃H₇) > guaiacol (hydroxyl, -OH, methoxy, -OCH₃) > hydroxylacetone (carbonyl, -R₂C=O) > phenol (hydroxyl, -OH) > benzaldehyde (formyl, -R-CH=O) > acetic acid (carboxyl, -COOH) > anisole (methoxy, -OCH₃). The strategy of co-feeding bio-derived monomers and pyrolysis oil in the Kraft lignin hydrotreatment provided insight into co-processing bio-feedstocks and the role of a second co-feed to facilitate efficient lignin depolymerization to increase the desired bio-liquid yield and limit lignin condensation.

In the following study (**Paper V**), we demonstrate the use of the unsupported NiMoS catalyst in the processing of raw FPBO for the production of renewable liquid hydrocarbon. The first step was the slurry process which was found to improve the properties of raw FPBO in terms of reduced oxygen content, stability, and coking tendencies. Downstream upgrading in the fixed bed process under continuous operation mode gave highly deoxygenated (0.5 wt% oxygen) hydrocarbons, equally divided between gasoline and diesel boiling point ranges. The final oil products were distilled into gasoline and diesel boiling point ranges and both were shown to have cycloalkanes as the compound group with the highest concentration, followed by paraffins and aromatics.

The overall process which included both the slurry and fixed bed upgrading resulted in a 29 wt% yield of liquid hydrocarbon product from the FPBO. While for carbon balances, a carbon recovery of 67 wt% as liquid hydrocarbon was achieved. The carbon loss was mainly attributed to the production of gaseous hydrocarbons (13.4 wt%), gaseous carbon oxides (5.5 wt%), and light organic compounds in the water phase. (13 wt%), from mainly the slurry process. The H₂ consumption for both process steps was 52.7 g per kg of processed dry FPBO or 140 g per kg of produced liquid hydrocarbons. FPBO without any fossil residue co-feed was successfully processed first in a slurry hydrocracker and then further upgraded in a continuous downstream fixed bed hydrotreater for 58 h time-on-stream without any notable catalyst deactivation and pressure build-up. Future work will be dedicated to further understanding the feasibility of this process concept and what stabilization degree FPBO requires for further processing. The side products such as a large amount of water produced and also carbon oxides require investigation for further valorization.

A comprehensive review (**Paper VI**) was written and included in this thesis on the topic of the application of metal sulfide catalysts in the valorization of various renewable feedstocks such as triglycerides, monomeric and dimeric phenolic compounds as bio-oil model substrates, pyrolysis oil, and lignin. Several aspects such as sulfide deactivation, reaction kinetics, and mechanism were included. The challenges and potential future research areas covering the efficient upgrading of renewable feed to liquid fuel were discussed. The summary also highlighted the importance of metal sulfides in the hydroprocessing of renewable feedstocks and also the need for further research to facilitate the better integration of potential renewable sources into existing refinery infrastructures.

6 Future outlook

There are different challenges involved while scaling up the hydroprocessing of renewable feedstocks such as triglycerides, FPBO, and lignin-derived oils. One of the common challenges is the deactivation of the catalyst caused by the presence of inorganic impurities in renewable feedstocks. These impurities can poison the catalytic sites, decrease the catalyst lifetime during the time-on-stream, and eventually hamper the processing stability. Future work should focus on understanding the role of these impurities in the activity of the hydrotreating catalyst and also develop purification and pretreatment methods for treating the potential renewable feedstocks prior to upgrading steps. For instance, the investigation of different guard bed adsorbents for different renewable feeds is of interest to effectively remove the impurities via physisorption. The removal of nitrogen content in the bio-feedstocks is also another area that requires more attention. For example, hydrothermal liquefaction (HTL) bio-crudes derived from sewage sludge and also algae oil contains high nitrogen and sulfur-bound polyaromatics that require a pretreatment step to improve the feedstock properties before integrating into refineries. The same issue is also faced while using pyrolysis oil derived from post-consumer plastic waste. Depending on the plastic type, a variety of impurities, such as chlorine, nitrogen, oxygen, metals, silica, asphalt, and acids are also present, and require proper purification methods before the plastic-derived oil can be further utilized for the production of plastics, chemicals, or even fuels.

The one-pot hydrotreatment of Kraft lignin experiments conducted throughout this work shows relevant results in terms of bio-oil yield, product selectivity, and also the reduction of char residues with the use of supported and unsupported metal sulfides. It is apparent that future work will be to further improve the process by modifying and improving the processing mode or experimental protocol to achieve a better bio-oil yield. These processing modes could be a continuous or semi-continuous mode with a constant hydrogen flow that can enable better depolymerization of bio-polymer and also hinders the undesired repolymerization and recondensation of reactive intermediates. Besides, the further implementation of different potential renewable feedstocks into the pilot slurry hydrocracker is important to demonstrate the possibility of the conversion of heavy and ‘difficult to convert’ bio-feeds on a larger scale with the ultimate goal of integrating the concept into existing refinery infrastructure.

It was also shown in one of the studies in this work where the co-processing of pyrolysis oil and lignin slurry in a non-polar hydrocarbon solvent presented a positive synergistic effect during the hydroprocessing. The future work will be to continue this effort in realizing the co-processing strategy at full scale and develop further understanding within this area. The long-term ambition is to process a higher level of renewable feed during co-processing and eventually phase out the use of fossil-derived feeds for the production of either renewable transportation fuel as the end product or bio-intermediates that can be used for further application.

7 Acknowledgments

The Swedish Energy Agency (grant number 2017-010890), Formas (grant number: FR-2021/0005), and Preem AB are gratefully acknowledged for the research funding. I would like to acknowledge the following people who have supported, encouraged, and guided me in different ways during this exciting journey of Ph.D. studies:

- ❖ Supervisors: **Professor Louise Olsson** and **Professor Derek Creaser**, for believing in me and allowing me to explore and conduct my research at KART. I thank you for all your endless efforts, patience, guidance, and supervision in helping me to accomplish this work.
- ❖ Co-supervisor: **Dr. Olov Öhrman** from Preem AB, I am grateful to have you as my co-supervisor and for your contribution throughout these years by giving insightful comments and useful feedback during the discussion in all our project meetings.
- ❖ **Dr. Muhammad Abdus Salam** for all the help and guidance in the lab and also all the interesting discussions during our work since I started my work at KART. I truly enjoyed working with you throughout these years.
- ❖ **Dr. Prakhar Arora** for all your guidance and advice, not only at work but in life. A great teacher, and a role model!
- ❖ Collaborators from RISE ETC: **Dr. Linda Sandström** and **Mr. Niklas Bergvall** for all the interesting discussions during the project meeting. Special thanks to Niklas for getting me involved in the one-week continuous SHC pyrolysis oil run. **Dr. Christian Bernlind** and **Dr. Alexandra Bernlind** for the NMR measurements and the fixed bed hydrotreatment experiments.
- ❖ **Dr. Phuoc Hoang Ho, Dr. Sreetama Ghosh, Dr. Joby Sebastian, Dr. Poonam Sharma, Dr. Abdenour Achour,** and **Dr. Quoc Khanh Tran** for all the useful advice, help in the lab, important discussion, and continuous support in this journey. Special thanks to Phuoc for proofreading the thesis.
- ❖ **Ms. Anna Hjorth, Mr. Linus Kron,** and **Dr. Anders Ahlbom** for your support and encouragement during the teaching of transport phenomena. Your dedication to teaching has positively influenced me to reflect on myself after each teaching session and strive to raise my bar. Special thanks to Anders for all the support and discussions we had and also the kind words during these years.
- ❖ **Professor Claes Niklasson, Professor Anders Rasmuson, Professor Ronnie Andersson, Associate Professor Diana Bernin, Senior Lecturer Dr. Gunnar Eriksson,** and **Professor Per-Anders Carlsson** for getting me onboard into the teaching assistance tasks in Advanced Chemical Engineering and Process Analytical Technology and Transport phenomena.
- ❖ **Ms. Malin Larsson** and **Ms. Johanna Spång** for all the outstanding administrative support.
- ❖ **Mr. Michael Andersson-Sarning** for all the help with the operation and maintenance of the reactor and analytical instruments.
- ❖ **Ms. Rawipa Intakul** and **Mr. Iván Gil Jiménez** are acknowledged for your contributions during your master thesis projects. I have learned a lot being a co-supervisor of your work.
- ❖ **Ms. Jieling Shao** for being the best officemate/friend/colleague and thank you for making office 2208B the happiest office in KART. Thank you for all the support and wonderful discussions during these years.
- ❖ The staff at the Chalmers Material Analysis Laboratory (CMAL) for all the assistance in operating the analytical instruments.
- ❖ All former and present colleagues at KCK, SIKT, and KART, thanks for making Chalmers a wonderful place to work.

At last, I would like to dedicate this work to my family for always giving me the complete freedom to pursue what I enjoy.

You Wayne

June 2023, Göteborg

8 References

- (1) (Institution), E. E. A. Total Greenhouse Gas Emission Trends and Projections in Europe. 2020. <https://www.eea.europa.eu/data-and-maps/indicators/greenhouse-gas-emission-trends-6/assessment-3>.
- (2) EEA. Greenhouse Gas Emissions from Transport in Europe — European Environment Agency. *European Environmental Agency (EEA)*. 2018, pp 1–7. <https://www.eea.europa.eu/data-and-maps/indicators/transport-emissions-of-greenhouse-gases/transport-emissions-of-greenhouse-gases-11>.
- (3) *Trends and Projections in Europe 2022*. <https://doi.org/10.2800/16646>.
- (4) Nogueira, L. A. H.; Souza, G. M.; Cortez, L. A. B.; de Brito Cruz, C. H. Biofuels for Transport. In *Future Energy: Improved, Sustainable and Clean Options for Our Planet*; Elsevier, 2020; pp 173–197. <https://doi.org/10.1016/B978-0-08-102886-5.00009-8>.
- (5) Pier, M. Zeitschrift FrSr Angewandte Chernie. **1931**, No. 50, 953–958.
- (6) Donath, E. E.; Hoering, M. Early Coal Hydrogenation Catalysis. *Fuel Processing Technology* **1977**, *1* (1), 3–20. [https://doi.org/10.1016/0378-3820\(77\)90012-1](https://doi.org/10.1016/0378-3820(77)90012-1).
- (7) van Veen, J. A. R. What’s New? On the Development of Sulphidic HT Catalysts before the Molecular Aspects. *Catal Today* **2017**, *292*, 2–25. <https://doi.org/10.1016/j.cattod.2016.09.027>.
- (8) Christophe Geantet; Payen, E. *2. 4 Activation and Genesis of the Active Phase by Sulfidation*; 2013.
- (9) Jin, S.; Xiao, Z.; Li, C.; Chen, X.; Wang, L.; Xing, J.; Li, W.; Liang, C. Catalytic Hydrodeoxygenation of Anisole as Lignin Model Compound over Supported Nickel Catalysts. *Catal Today* **2014**, *234*, 125–132. <https://doi.org/10.1016/j.cattod.2014.02.014>.
- (10) Kohli, K.; Prajapati, R.; Maity, S. K.; Sharma, B. K. Effect of Silica, Activated Carbon, and Alumina Supports on NiMo Catalysts for Residue Upgrading. *Energies (Basel)* **2020**, *13* (18), 1–16. <https://doi.org/10.3390/en13184967>.
- (11) Mukundan, S.; Atanda, L.; Beltramini, J. Thermocatalytic Cleavage of C-C and C-O Bonds in Model Compounds and Kraft Lignin by NiMoS₂/C Nanocatalysts. *Sustain Energy Fuels* **2019**, *3* (5), 1317–1328. <https://doi.org/10.1039/c8se00576a>.
- (12) Mukundan, S.; Chowdari, R. K.; Beltramini, J. External Solvent-Free Catalytic Hydrodeoxygenation of Softwood Lignin to Aromatics over Carbon–ZrO₂ Supported Ni/MoS₂ Catalysts. *Adv Sustain Syst* **2020**, *2000243*, 1–12. <https://doi.org/10.1002/adsu.202000243>.
- (13) Wang, L.; Xiao, F. S. Nanoporous Catalysts for Biomass Conversion. *Green Chemistry* **2015**, *17* (1), 24–39. <https://doi.org/10.1039/c4gc01622j>.
- (14) Eijsbouts, S.; Mayo, S. W.; Fujita, K. Unsupported Transition Metal Sulfide Catalysts: From Fundamentals to Industrial Application. *Appl Catal A Gen* **2007**, *322* (SUPPL.), 58–66.

- (15) Plantenga, F. L.; Cerfontain, R.; Eijsbouts, S.; Houtert, F. Van; Anderson, G. H.; Miseo, S.; Soled, S.; Riley, K.; Fujita, K.; Inoue, Y.; Nobel, A.; Box, P. O.; Amersfoort, A. E. " NEBULA ": A Hydroprocessing Catalyst with Breakthrough Activity. **2003**, 846–849.
- (16) Bellussi, G.; Rispoli, G.; Landoni, A.; Millini, R.; Molinari, D.; Montanari, E.; Moscotti, D.; Pollesel, P. Hydroconversion of Heavy Residues in Slurry Reactors: Developments and Perspectives. *J Catal* **2013**, *308*, 189–200. <https://doi.org/10.1016/j.jcat.2013.07.002>.
- (17) Bergvall, N.; Sandström, L.; Weiland, F.; Öhrman, O. G. W. Corefining of Fast Pyrolysis Bio-Oil with Vacuum Residue and Vacuum Gas Oil in a Continuous Slurry Hydrocracking Process. *Energy and Fuels* **2020**, *34* (7), 8452–8465. <https://doi.org/10.1021/acs.energyfuels.0c01322>.
- (18) Mattsson, C.; Andersson, S. I.; Belkheiri, T.; Åmand, L. E.; Olausson, L.; Vamling, L.; Theliander, H. Using 2D NMR to Characterize the Structure of the Low and High Molecular Weight Fractions of Bio-Oil Obtained from LignoBoost™ Kraft Lignin Depolymerized in Subcritical Water. *Biomass Bioenergy* **2016**, *95*, 364–377. <https://doi.org/10.1016/j.biombioe.2016.09.004>.
- (19) Resende, F. L. P.; Fraley, S. A.; Berger, M. J.; Savage, P. E. Noncatalytic Gasification of Lignin in Supercritical Water. *Energy and Fuels* **2008**, *22* (2), 1328–1334. <https://doi.org/10.1021/ef700574k>.
- (20) Demirbaş, A. Effect of Lignin Content on Aqueous Liquefaction Products of Biomass. *Energy Convers Manag* **2000**, *41* (15), 1601–1607. [https://doi.org/10.1016/S0196-8904\(00\)00013-3](https://doi.org/10.1016/S0196-8904(00)00013-3).
- (21) Doherty, W. O. S.; Mousavioun, P.; Fellows, C. M. Value-Adding to Cellulosic Ethanol: Lignin Polymers. *Ind Crops Prod* **2011**, *33* (2), 259–276. <https://doi.org/10.1016/j.indcrop.2010.10.022>.
- (22) Samec, J.; Di Francesco, D.; Dahlstrand, C.; Löfstedt, J.; Orebom, A.; Verendel, J.; Carrick, christopher; Håkansson, Å.; Eriksson, S.; Rådberg, H.; Wallmo, H.; Wimby, M.; Huber, F.; Federsel, C.; Backmark, mattias. De-bottlenecking a Pulp Mill by Producing Biofuels from Black Liquor in 3 Steps. *ChemSusChem* **2021**, 1–13. <https://doi.org/10.1002/cssc.202100496>.
- (23) Chakar, F. S.; Ragauskas, A. J. Review of Current and Future Softwood Kraft Lignin Process Chemistry. *Ind Crops Prod* **2004**, *20* (2), 131–141. <https://doi.org/10.1016/j.indcrop.2004.04.016>.
- (24) Lundberg, V. *Chemical and Biochemical Biorefineries in Kraft Pulp Mills – Process Integration and Economics for Three Concepts*; 2014.
- (25) Patel, M.; Kumar, A. Production of Renewable Diesel through the Hydroprocessing of Lignocellulosic Biomass-Derived Bio-Oil: A Review. *Renewable and Sustainable Energy Reviews* **2016**, *58*, 1293–1307. <https://doi.org/10.1016/j.rser.2015.12.146>.
- (26) Mäki-Arvela, P.; Murzin, D. Hydrodeoxygenation of Lignin-Derived Phenols: From Fundamental Studies towards Industrial Applications. *Catalysts* **2017**, *7* (265), 265.
- (27) Furimsky, E. Catalytic Hydrodeoxygenation. **2000**, *199*, 147–190.

- (28) Prasomsri, T.; Shetty, M.; Murugappan, K.; Román-Leshkov, Y. Insights into the Catalytic Activity and Surface Modification of MoO₃ during the Hydrodeoxygenation of Lignin-Derived Model Compounds into Aromatic Hydrocarbons under Low Hydrogen Pressures. *Energy Environ Sci* **2014**, *7* (8), 2660–2669. <https://doi.org/10.1039/c4ee00890a>.
- (29) García-Mendoza, C.; Santolalla-Vargas, C. E.; Woolfolk, L. G.; del Ángel, P.; de los Reyes, J. A. Effect of TiO₂ in Supported NiWS Catalysts for the Hydrodeoxygenation of Guaiacol. *Catal Today* **2021**, *377* (June), 145–156.
- (30) Hong, Y. K.; Lee, D. W.; Eom, H. J.; Lee, K. Y. The Catalytic Activity of Sulfided Ni/W/TiO₂ (Anatase) for the Hydrodeoxygenation of Guaiacol. *J Mol Catal A Chem* **2014**, *392*, 241–246. <https://doi.org/10.1016/j.molcata.2014.05.025>.
- (31) Tavizón-Pozos, J. A.; Suárez-Toriello, V. A.; Del Ángel, P.; De Los Reyes, J. A. Hydrodeoxygenation of Phenol over Sulfided CoMo Catalysts Supported on a Mixed Al₂O₃-TiO₂ Oxide. *International Journal of Chemical Reactor Engineering* **2016**, *14* (6), 1211–1223. <https://doi.org/10.1515/ijcre-2016-0038>.
- (32) Ferrari, M.; Bosmans, S.; Maggi, R.; Delmon, B.; Grange, P. CoMo/Carbon Hydrodeoxygenation Catalysts: Influence of the Hydrogen Sulfide Partial Pressure and of the Sulfidation Temperature. *Catal Today* **2001**, *65* (2–4), 257–264. [https://doi.org/10.1016/S0920-5861\(00\)00559-9](https://doi.org/10.1016/S0920-5861(00)00559-9).
- (33) Ruiz, P. E.; Frederick, B. G.; Sisto, W. J. De; Austin, R. N.; Radovic, L. R.; Leiva, K.; García, R.; Escalona, N.; Wheeler, M. C. Guaiacol Hydrodeoxygenation on MoS₂ Catalysts: Influence of Activated Carbon Supports. **2012**, *27*, 44–48. <https://doi.org/10.1016/j.catcom.2012.06.021>.
- (34) Mukundan, S.; Konarova, M.; Atanda, L.; Ma, Q.; Beltramini, J. Guaiacol Hydrodeoxygenation Reaction Catalyzed by Highly Dispersed, Single Layered MoS₂/C. *Catal Sci Technol* **2015**, *5* (9), 4422–4432. <https://doi.org/10.1039/c5cy00607d>.
- (35) Templis, C. C.; Revelas, C. J.; Papastylianou, A. A.; Papayannakos, N. G. Phenol Hydrodeoxygenation over a Reduced and Sulfided NiMo/γ-Al₂O₃ Catalyst. *Ind Eng Chem Res* **2019**, *58* (16), 6278–6287. <https://doi.org/10.1021/acs.iecr.8b06465>.
- (36) Badawi, M.; Paul, J. F.; Payen, E.; Romero, Y.; Richard, F.; Brunet, S.; Popov, A.; Kondratieva, E.; Gilson, J. P.; Mariey, L.; Travert, A.; Maugé, F. Hydrodésoxygénation de Composés Phénoliques En Présence de Catalyseurs Sulfurés (Co)Mo/Al₂O₃: Une Étude Expérimentale et Théorique. *Oil and Gas Science and Technology* **2013**, *68* (5), 829–840. <https://doi.org/10.2516/ogst/2012041>.
- (37) Romero, Y.; Richard, F.; Brunet, S. Hydrodeoxygenation of 2-Ethylphenol as a Model Compound of Bio-Crude over Sulfided Mo-Based Catalysts: Promoting Effect and Reaction Mechanism. *Appl Catal B* **2010**, *98* (3–4), 213–223. <https://doi.org/10.1016/j.apcatb.2010.05.031>.
- (38) Romero, Y.; Richard, F.; Brunet, S. Hydrodeoxygenation of 2-Ethylphenol as a Model Compound of Bio-Crude over Sulfided Mo-Based Catalysts: Promoting Effect and Reaction Mechanism. *Appl Catal B* **2010**, *98* (3–4), 213–223. <https://doi.org/10.1016/j.apcatb.2010.05.031>.

- (39) Yang, Y.; Gilbert, A.; Xu, C. (Charles). Hydrodeoxygenation of Bio-Crude in Supercritical Hexane with Sulfided CoMo and CoMoP Catalysts Supported on MgO: A Model Compound Study Using Phenol. *Appl Catal A Gen* **2009**, *360* (2), 242–249. <https://doi.org/10.1016/j.apcata.2009.03.027>.
- (40) Leiva, K.; Martinez, N.; Sepulveda, C.; García, R.; Jiménez, C. A.; Laurenti, D.; Vrinat, M.; Geantet, C.; Fierro, J. L. G.; Ghampson, I. T.; Escalona, N. Hydrodeoxygenation of 2-Methoxyphenol over Different Re Active Phases Supported on SiO₂ Catalysts. *Appl Catal A Gen* **2015**, *490*, 71–79. <https://doi.org/10.1016/j.apcata.2014.10.054>.
- (41) Leiva, K.; Sepúlveda, C.; García, R.; Fierro, J. L. G.; Escalona, N. Effect of Water on the Conversions of 2-Methoxyphenol and Phenol as Bio-Oil Model Compounds over ReS₂/SiO₂ Catalyst. *Catal Commun* **2014**, *53*, 33–37. <https://doi.org/10.1016/j.catcom.2014.04.023>.
- (42) Sepúlveda, C.; García, R.; Reyes, P.; Ghampson, I. T.; Fierro, J. L. G.; Laurenti, D.; Vrinat, M.; Escalona, N. Hydrodeoxygenation of Guaiacol over ReS₂/Activated Carbon Catalysts. Support and Re Loading Effect. *Appl Catal A Gen* **2014**, *475*, 427–437. <https://doi.org/10.1016/j.apcata.2014.01.057>.
- (43) Ruiz, P. E.; Leiva, K.; Garcia, R.; Reyes, P.; Fierro, J. L. G.; Escalona, N. Relevance of Sulfiding Pretreatment on the Performance of Re/ZrO₂ and Re/ZrO₂-Sulfated Catalysts for the Hydrodeoxygenation of Guayacol. *Appl Catal A Gen* **2010**, *384* (1–2), 78–83. <https://doi.org/10.1016/j.apcata.2010.06.009>.
- (44) Sepúlveda, C.; Escalona, N.; García, R.; Laurenti, D.; Vrinat, M. Hydrodeoxygenation and Hydrodesulfurization Co-Processing over ReS₂ Supported Catalysts. *Catal Today* **2012**, *195* (1), 101–105. <https://doi.org/10.1016/j.cattod.2012.05.047>.
- (45) Infantes-Molina, A.; Pawelec, B.; Fierro, J. L. G.; Loricera, C. V.; Jiménez-López, A.; Rodríguez-Castellón, E. Effect of Ir and Pt Addition on the HDO Performance of RuS₂/SBA-15 Sulfide Catalysts. *Top Catal* **2015**, *58* (4–6), 247–257. <https://doi.org/10.1007/s11244-015-0366-0>.
- (46) Jongerius, A. L.; Jastrzebski, R.; Bruijninx, P. C. A.; Weckhuysen, B. M. CoMo Sulfide-Catalyzed Hydrodeoxygenation of Lignin Model Compounds: An Extended Reaction Network for the Conversion of Monomeric and Dimeric Substrates. *J Catal* **2012**, *285* (1), 315–323. <https://doi.org/10.1016/j.jcat.2011.10.006>.
- (47) Şenol, O. I.; Ryymin, E. M.; Viljava, T. R.; Krause, A. O. I. Effect of Hydrogen Sulphide on the Hydrodeoxygenation of Aromatic and Aliphatic Oxygenates on Sulphided Catalysts. *J Mol Catal A Chem* **2007**, *277* (1–2), 107–112. <https://doi.org/10.1016/j.molcata.2007.07.033>.
- (48) Gutierrez, A.; Turpeinen, E. M.; Viljava, T. R.; Krause, O. Hydrodeoxygenation of Model Compounds on Sulfided CoMo/γ-Al₂O₃ and NiMo/γ-Al₂O₃ Catalysts; Role of Sulfur-Containing Groups in Reaction Networks. *Catal Today* **2017**, *285*, 125–134. <https://doi.org/10.1016/j.cattod.2017.02.003>.
- (49) Ryymin, E. M.; Honkela, M. L.; Viljava, T. R.; Krause, A. O. I. Competitive Reactions and Mechanisms in the Simultaneous HDO of Phenol and Methyl Heptanoate over Sulphided NiMo/γ-Al₂O₃. *Appl Catal A Gen* **2010**, *389* (1–2), 114–121. <https://doi.org/10.1016/j.apcata.2010.09.010>.

- (50) Massoth, F. E.; Politzer, P.; Concha, M. C.; Murray, J. S.; Jakowski, J.; Simons, J. Catalytic Hydrodeoxygenation of Methyl-Substituted Phenols: Correlations of Kinetic Parameters with Molecular Properties. *Journal of Physical Chemistry B* **2006**, *110* (29), 14283–14291. <https://doi.org/10.1021/jp057332g>.
- (51) Cheah, Y. W.; Salam, M. A.; Arora, P.; Öhrman, O.; Creaser, D.; Olsson, L. Role of Transition Metals on MoS₂-Based Supported Catalysts for Hydrodeoxygenation (HDO) of Propylguaiacol. *Sustain Energy Fuels* **2021**, *5* (7), 2097–2113. <https://doi.org/10.1039/d1se00184a>.
- (52) Wang, W.; Zhang, K.; Li, L.; Wu, K.; Liu, P.; Yang, Y. Synthesis of Highly Active Co-Mo-S Unsupported Catalysts by a One-Step Hydrothermal Method for p-Cresol Hydrodeoxygenation. *Ind Eng Chem Res* **2014**, *53*, 19001–19009.
- (53) Online, V. A.; Wang, W.; Li, L.; Wu, K.; Zhu, G.; Tan, S.; Li, W.; Yang, Y. RSC Advances MoS₂ Nanosheets and Their Hydrodeoxygenation. **2015**, 61799–61807. <https://doi.org/10.1039/c5ra09690a>.
- (54) Wu, K.; Wang, W.; Guo, H.; Yang, Y.; Huang, Y.; Li, W.; Li, C. Engineering Co Nanoparticles Supported on Defect MoS₂-x for Mild Deoxygenation of Lignin-Derived Phenols to Arenes. *ACS Energy Lett* **2020**, *5* (4), 1330–1336. <https://doi.org/10.1021/acseenergylett.0c00411>.
- (55) Wang, W.; Tan, S.; Wu, K.; Zhu, G.; Liu, Y.; Tan, L.; Huang, Y.; Yang, Y. Hydrodeoxygenation of P-Cresol as a Model Compound for Bio-Oil on MoS₂: Effects of Water and Benzothiophene on the Activity and Structure of Catalyst. *Fuel* **2018**, *214*, 480–488.
- (56) Wu, K.; Liu, Y.; Wang, W.; Huang, Y.; Li, W.; Shi, Q.; Yang, Y. Preparation of Hydrophobic MoS₂, NiS₂-MoS₂ and CoS₂-MoS₂ for Catalytic Hydrodeoxygenation of Lignin-Derived Phenols. *Molecular Catalysis* **2019**, *477* (110537).
- (57) Wang, W.; Li, L.; Tan, S.; Wu, K.; Zhu, G.; Liu, Y.; Xu, Y.; Yang, Y. Preparation of NiS₂/MoS₂ Catalysts by Two-Step Hydrothermal Method and Their Enhanced Activity for Hydrodeoxygenation of p-Cresol. *Fuel* **2016**, *179*, 1–9. <https://doi.org/10.1016/j.fuel.2016.03.068>.
- (58) Tran, C. C.; Stankovikj, F.; Garcia-Perez, M.; Kaliaguine, S. Unsupported Transition Metal-Catalyzed Hydrodeoxygenation of Guaiacol. *Catal Commun* **2017**, *101* (July), 71–76. <https://doi.org/10.1016/j.catcom.2017.07.029>.
- (59) Cao, J.; Zhang, Y.; Wang, L.; Zhang, C.; Zhou, C. Unsupported MoS₂-Based Catalysts for Bio-Oil Hydrodeoxygenation: Recent Advances and Future Perspectives. *Front Chem* **2022**, *10* (June), 1–7. <https://doi.org/10.3389/fchem.2022.928806>.
- (60) Song, W.; Zhou, S.; Hu, S.; Lai, W.; Lian, Y.; Wang, J.; Yang, W.; Wang, M.; Wang, P.; Jiang, X. Surface Engineering of CoMoS Nanosulfide for Hydrodeoxygenation of Lignin-Derived Phenols to Arenes. *ACS Catal* **2019**, *9* (1), 259–268. <https://doi.org/10.1021/acscatal.8b03402>.

- (61) Wang, W.; Li, L.; Wu, K.; Zhu, G.; Tan, S.; Liu, Y.; Yang, Y. Highly Selective Catalytic Conversion of Phenols to Aromatic Hydrocarbons on CoS₂/MoS₂ Synthesized Using a Two Step Hydrothermal Method. *RSC Adv* **2016**, *6* (37), 31265–31271. <https://doi.org/10.1039/c5ra27066a>.
- (62) Yoosuk, B.; Tumnantong, D.; Prasassarakich, P. Unsupported MoS₂ and CoMoS₂ Catalysts for Hydrodeoxygenation of Phenol. *Chem Eng Sci* **2012**, *79*, 1–7. <https://doi.org/10.1016/j.ces.2012.05.020>.
- (63) Yoosuk, B.; Tumnantong, D.; Prasassarakich, P. Amorphous Unsupported Ni-Mo Sulfide Prepared by One Step Hydrothermal Method for Phenol Hydrodeoxygenation. *Fuel* **2012**, *91*, 246–252.
- (64) Yang, Y. Q.; Tye, C. T.; Smith, K. J. Influence of MoS₂ Catalyst Morphology on the Hydrodeoxygenation of Phenols. *Catal Commun* **2008**, *9* (6), 1364–1368. <https://doi.org/10.1016/j.catcom.2007.11.035>.
- (65) Wang, W.; Zhang, K.; Qiao, Z.; Li, L.; Liu, P.; Yang, Y. Hydrodeoxygenation of P-Cresol on Unsupported Ni-W-Mo-S Catalysts Prepared by One Step Hydrothermal Method. *Catal Commun* **2014**, *56*, 17–22. <https://doi.org/10.1016/j.catcom.2014.06.024>.
- (66) Wang, C.; Wang, D.; Wu, Z.; Wang, Z.; Tang, C.; Zhou, P. Effect of W Addition on the Hydrodeoxygenation of 4-Methylphenol over Unsupported NiMo Sulfide Catalysts. *Appl Catal A Gen* **2014**, *476*, 61–67. <https://doi.org/10.1016/j.apcata.2014.02.010>.
- (67) Wang, C.; Wu, Z.; Tang, C.; Li, L.; Wang, D. The Effect of Nickel Content on the Hydrodeoxygenation of 4-Methylphenol over Unsupported NiMoW Sulfide Catalysts. *Catal Commun* **2013**, *32* (3), 76–80. <https://doi.org/10.1016/j.catcom.2012.11.031>.
- (68) Whiffen, V. M. L.; Smith, K. J. Hydrodeoxygenation of 4-Methylphenol over Unsupported MoP, MoS₂, and MoO_x Catalysts. *Energy and Fuels* **2010**, *24* (9), 4728–4737. <https://doi.org/10.1021/ef901270h>.
- (69) Wang, W.; Li, L.; Zhang, K.; Qiao, Z.; Liu, P.; Yang, Y. Hydrodeoxygenation of P-Cresol on MoS₂: The Effect of Adding Hexadecyl Trimethyl Ammonium Bromide during the Catalyst Synthesis. *Reaction Kinetics, Mechanisms and Catalysis* **2014**, *113* (2), 417–429. <https://doi.org/10.1007/s11144-014-0763-6>.
- (70) Wang, W.; Li, L.; Wu, K.; Zhang, K.; Jie, J.; Yang, Y. Preparation of Ni-Mo-S Catalysts by Hydrothermal Method and Their Hydrodeoxygenation Properties. *Appl Catal A Gen* **2015**, *495*, 8–16. <https://doi.org/10.1016/j.apcata.2015.01.041>.
- (71) Guo, X.; Wang, W.; Wu, K.; Huang, Y.; Shi, Q.; Yang, Y. Biomass and Bioenergy Preparation of Fe Promoted MoS₂ Catalysts for the Hydrodeoxygenation of p - Cresol as a Model Compound of Lignin-Derived Bio-Oil. *Biomass Bioenergy* **2019**, *125* (February), 34–40. <https://doi.org/10.1016/j.biombioe.2019.04.014>.
- (72) Vutolkina, A. V.; Baigildin, I. G.; Glotov, A. P.; Pimerzin, A. A.; Akopyan, A. V.; Maximov, A. L.; Karakhanov, E. A. Hydrodeoxygenation of Guaiacol via in Situ H₂ Generated through a Water Gas Shift Reaction over Dispersed NiMoS Catalysts from Oil-Soluble Precursors: Tuning the Selectivity towards Cyclohexene. *Appl Catal B* **2022**, *312* (February), 121403. <https://doi.org/10.1016/j.apcatb.2022.121403>.

- (73) Cheah, Y. W.; Salam, M. A.; Sebastian, J.; Ghosh, S.; Öhrman, O.; Creaser, D.; Olsson, L. Thermal Annealing Effects on Hydrothermally Synthesized Unsupported MoS₂ for Enhanced Deoxygenation of Propylguaiacol and Kraft Lignin. *Sustain Energy Fuels* **2021**, *5*, 5270.
- (74) Joffres, B.; Nguyen, M. T.; Laurenti, D.; Lorentz, C.; Souchon, V.; Charon, N.; Daudin, A.; Quignard, A.; Geantet, C. Lignin Hydroconversion on MoS₂-Based Supported Catalyst: Comprehensive Analysis of Products and Reaction Scheme. *Appl Catal B* **2016**, *184*, 153–162. <https://doi.org/10.1016/j.apcatb.2015.11.005>.
- (75) Zingler, M.; Martin, H.; Gabrielsen, J.; Lasse, R.; Arendt, P.; Degn, A. A Perspective on Catalytic Hydropyrolysis of Biomass Abbreviations : **2021**, *143* (April 2020).
- (76) Grilc, M.; Likozar, B.; Levec, J. Hydrodeoxygenation and Hydrocracking of Solvolysed Lignocellulosic Biomass by Oxide, Reduced and Sulphide Form of NiMo, Ni, Mo and Pd Catalysts. *Appl Catal B* **2014**, *150–151*, 275–287. <https://doi.org/10.1016/j.apcatb.2013.12.030>.
- (77) Grilc, M.; Veryasov, G.; Likozar, B.; Jesih, A.; Levec, J. Hydrodeoxygenation of Solvolysed Lignocellulosic Biomass by Unsupported MoS₂, MoO₂, Mo₂C and WS₂ Catalysts. *Appl Catal B* **2015**, *163*, 467–477. <https://doi.org/10.1016/j.apcatb.2014.08.032>.
- (78) Ji, N.; Diao, X.; Li, X.; Jia, Z.; Zhao, Y.; Lu, X.; Song, C.; Liu, Q.; Li, C. Toward Alkylphenols Production: Lignin Depolymerization Coupling with Methoxy Removal over Supported MoS₂Catalyst. *Ind Eng Chem Res* **2020**, *59* (39), 17287–17299. <https://doi.org/10.1021/acs.iecr.0c01255>.
- (79) Kumar, C. R.; Anand, N.; Kloekhorst, A.; Cannilla, C.; Bonura, G.; Frusteri, F.; Barta, K.; Heeres, H. J. Solvent Free Depolymerization of Kraft Lignin to Alkyl-Phenolics Using Supported NiMo and CoMo Catalysts. *Green Chemistry* **2015**, *17* (4921).
- (80) Narani, A.; Chowdari, R. K.; Cannilla, C.; Bonura, G.; Frusteri, F.; Heeres, H. J.; Barta, K. Efficient Catalytic Hydrotreatment of Kraft Lignin to Alkylphenolics Using Supported NiW and NiMo Catalysts in Supercritical Methanol. *Green Chemistry* **2015**, *17* (5046). <https://doi.org/DOI: 10.1039/c5gc01643f>.
- (81) Pu, J.; Nguyen, T. S.; Leclerc, E.; Lorentz, C.; Laurenti, D.; Pitault, I.; Tayakout-Fayolle, M.; Geantet, C. Lignin Catalytic Hydroconversion in a Semi-Continuous Reactor: An Experimental Study. *Appl Catal B* **2019**, *256* (May), 117769. <https://doi.org/10.1016/j.apcatb.2019.117769>.
- (82) Pu, J.; Laurenti, D.; Geantet, C.; Tayakout-Fayolle, M.; Pitault, I. Kinetic Modeling of Lignin Catalytic Hydroconversion in a Semi-Batch Reactor. *Chemical Engineering Journal* **2020**, *386* (June 2019), 122067. <https://doi.org/10.1016/j.cej.2019.122067>.
- (83) Shumeiko, B.; Auersvald, M.; Straka, P.; Šimáček, P.; Vrtiška, D.; Kubička, D. Efficient One-Stage Bio-Oil Upgrading over Sulfided Catalysts. *ACS Sustain Chem Eng* **2020**, *8*, 15149–15167.
- (84) Sirous-Rezaei, P.; Creaser, D.; Olsson, L. Reductive Liquefaction of Lignin to Monocyclic Hydrocarbons: ReS₂/Al₂O₃ as Efficient Char Inhibitor and Hydrodeoxygenation Catalyst. *Appl Catal B* **2021**, *297* (March), 120449. <https://doi.org/10.1016/j.apcatb.2021.120449>.

- (85) Achour, A.; Bernin, D.; Creaser, D.; Olsson, L. Evaluation of Kraft and Hydrolysis Lignin Hydroconversion Over Unsupported Nimos Catalyst. *Chemical Engineering Journal* **2022**, 453 (P2), 139829. <https://doi.org/10.2139/ssrn.4090192>.
- (86) Abdus Salam, M.; Wayne Cheah, Y.; Hoang Ho, P.; Bernin, D.; Achour, A.; Nejadmoghadam, E.; Öhrman, O.; Arora, P.; Olsson, L.; Creaser, D. Elucidating the Role of NiMoS-USY during the Hydrotreatment of Kraft Lignin. *Chemical Engineering Journal* **2022**, 442 (January). <https://doi.org/10.1016/j.cej.2022.136216>.
- (87) Divya R. Parapati, Vamshi K. Guda, Venkata K. Penmetsa, Philip H. Steele, S. K. T. Single Stage Hydroprocessing of Pyrolysis Oil in a Continuous Packed-Bed Reactor. *Environ Prog Sustain Energy* **2014**, 33 (3), 676–680. <https://doi.org/10.1002/ep>.
- (88) Elliott, D. C.; Hart, T. R.; Neuenschwander, G. G.; Rotness, L. J.; Olarte, M. V.; Zacher, A. H.; Solantausta, Y. Catalytic Hydroprocessing of Fast Pyrolysis Bio-Oil from Pine Sawdust. In *Energy and Fuels*; 2012; Vol. 26, pp 3891–3896. <https://doi.org/10.1021/ef3004587>.
- (89) Elliot, D. C.; Heeres, H. J.; Eikon. *Catalytic Hydroprocessing of Bio-Oils of Different Types*.
- (90) Janosik, T.; Nilsson, A. N.; Hällgren, A. C.; Hedberg, M.; Bernlind, C.; Rådberg, H.; Ahlsén, L.; Arora, P.; Öhrman, O. G. W. Derivatizing of Fast Pyrolysis Bio-Oil and Coprocessing in Fixed Bed Hydrotreater. *Energy and Fuels* **2022**, 36 (15), 8274–8287. <https://doi.org/10.1021/acs.energyfuels.2c01608>.
- (91) Zhang, Y.; Monnier, J.; Ikura, M. Bio-Oil Upgrading Using Dispersed Unsupported MoS₂ Catalyst. *Fuel Processing Technology* **2020**, 206 (March), 106403. <https://doi.org/10.1016/j.fuproc.2020.106403>.
- (92) Priharto, N.; Ronsse, F.; Prins, W.; Hita, I.; Deuss, P. J.; Heeres, H. J. Hydrotreatment of Pyrolysis Liquids Derived from Second-Generation Bioethanol Production Residues over NiMo and CoMo Catalysts. *Biomass Bioenergy* **2019**, 126 (November 2018), 84–93. <https://doi.org/10.1016/j.biombioe.2019.05.005>.
- (93) Izhar, S.; Uehara, S.; Yoshida, N.; Yamamoto, Y.; Morioka, T.; Nagai, M. Hydrodenitrogenation of Fast Pyrolysis Bio-Oil Derived from Sewage Sludge on NiMo/Al₂O₃ Sulfide Catalyst. *Fuel Processing Technology* **2012**, 101, 10–15. <https://doi.org/10.1016/j.fuproc.2012.03.012>.
- (94) Kim, K. H.; Kim, C. S. Recent Efforts to Prevent Undesirable Reactions from Fractionation to Depolymerization of Lignin: Toward Maximizing the Value from Lignin. *Front Energy Res* **2018**, 6 (SEP), 1–7. <https://doi.org/10.3389/fenrg.2018.00092>.
- (95) Gong, Z.; Shuai, L. Lignin Condensation, an Unsolved Mystery. *Trends Chem* **2023**, 1–4. <https://doi.org/10.1016/j.trechm.2022.12.005>.
- (96) Lan, W.; Luterbacher, J. S. Preventing Lignin Condensation to Facilitate Aromatic Monomer Production. *Chimia (Aarau)* **2019**, 73 (7–8), 591–598. <https://doi.org/10.2533/chimia.2019.591>.
- (97) Questell-Santiago, Y. M.; Galkin, M. V.; Barta, K.; Luterbacher, J. S. Stabilization Strategies in Biomass Depolymerization Using Chemical Functionalization. *Nat Rev Chem* **2020**, 4 (6), 311–330. <https://doi.org/10.1038/s41570-020-0187-y>.

- (98) Toledano, A.; Serrano, L.; Labidi, J. Improving Base Catalyzed Lignin Depolymerization by Avoiding Lignin Repolymerization. *Fuel* **2014**, *116*, 617–624. <https://doi.org/10.1016/j.fuel.2013.08.071>.
- (99) Hernández-Ramos, F.; Fernández-Rodríguez, J.; Alriols, M. G.; Labidi, J.; Erdocia, X. Study of a Renewable Capping Agent Addition in Lignin Base Catalyzed Depolymerization Process. *Fuel* **2020**, *280* (June), 118524. <https://doi.org/10.1016/j.fuel.2020.118524>.
- (100) Belkheiri, T.; Andersson, S. I.; Mattsson, C.; Olausson, L.; Theliander, H.; Vamling, L. Hydrothermal Liquefaction of Kraft Lignin in Subcritical Water: Influence of Phenol as Capping Agent. *Energy and Fuels* **2018**, *32* (5), 5923–5932. <https://doi.org/10.1021/acs.energyfuels.8b00068>.
- (101) Brandi, F.; Antonietti, M.; Al-Naji, M. Controlled Lignosulfonate Depolymerization: Via Solvothermal Fragmentation Coupled with Catalytic Hydrogenolysis/Hydrogenation in a Continuous Flow Reactor. *Green Chemistry* **2021**, *23* (24), 9894–9905. <https://doi.org/10.1039/d1gc01714d>.
- (102) Huang, X.; Korányi, T. I.; Boot, M. D.; Hensen, E. J. M. Catalytic Depolymerization of Lignin in Supercritical Ethanol. *ChemSusChem* **2014**, *7* (8), 2276–2288. <https://doi.org/10.1002/cssc.201402094>.
- (103) Huang, X.; Korányi, T. I.; Boot, M. D.; Hensen, E. J. M. Ethanol as Capping Agent and Formaldehyde Scavenger for Efficient Depolymerization of Lignin to Aromatics. *Green Chemistry* **2015**, *17* (11), 4941–4950. <https://doi.org/10.1039/c5gc01120e>.
- (104) Ahmad, Z.; Mahmood, N.; Yuan, Z.; Paleologou, M.; Xu, C. C. Effects of Process Parameters on Hydrolytic Treatment of Black Liquor for the Production of Low-Molecular-Weight Depolymerized Kraft Lignin. *Molecules* **2018**, *23* (10). <https://doi.org/10.3390/molecules23102464>.
- (105) Gong, Z.; Yang, G.; Huang, L.; Chen, L.; Luo, X.; Shuai, L. Phenol-Assisted Depolymerisation of Condensed Lignins to Mono-/Poly-Phenols and Bisphenols. *Chemical Engineering Journal* **2022**, No. November, 140628. <https://doi.org/10.1016/j.cej.2022.140628>.
- (106) Shuai, L.; Masoud Talebi, A.; Ydna M., Q.-S.; Florent, H.; Yanding, L.; Hoon, Ki.; Richard, M.; Clint, C.; John, R.; Jeremy S., L. Formaldehyde Stabilization Facilitates Lignin Monomer Production during Biomass Depolymerization. *Science (1979)* **2016**, *354* (6310), 329–334.
- (107) Roberts, V. M.; Stein, V.; Reiner, T.; Lemonidou, A.; Li, X.; Lercher, J. A. Towards Quantitative Catalytic Lignin Depolymerization. *Chemistry - A European Journal* **2011**, *17* (21), 5939–5948. <https://doi.org/10.1002/chem.201002438>.
- (108) Mathieu, Y.; Vidal, J. D.; Arribas Martínez, L.; Abad Fernández, N.; Iborra, S.; Corma, A. Molecular Oxygen Lignin Depolymerization: An Insight into the Stability of Phenolic Monomers. *ChemSusChem* **2020**, *13* (17), 4743–4758. <https://doi.org/10.1002/cssc.202001295>.
- (109) Ahlbom, A.; Maschietti, M.; Nielsen, R.; Lyckeskog, H.; Hasani, M.; Theliander, H. Using Isopropanol as a Capping Agent in the Hydrothermal Liquefaction of Kraft Lignin in Near-Critical Water. *Energies (Basel)* **2021**, *14* (4). <https://doi.org/10.3390/en14040932>.

- (110) Parto, S. G.; Christensen, J. M.; Pedersen, L. S.; Tjosås, F.; Jensen, A. D. Solvothermal Conversion of Lignosulfonate Assisted by Ni Catalyst: Investigation of the Role of Ethanol and Ethylene Glycol as Solvents. *Catalysts* **2018**, *8* (11). <https://doi.org/10.3390/catal8110502>.
- (111) Qi, S.; Wang, G.; Sun, H.; Wang, L.; Liu, Q.; Ma, G.; Parvez, A. M.; Si, C. Using Lignin Monomer As a Novel Capping Agent for Efficient Acid-Catalyzed Depolymerization of High Molecular Weight Lignin to Improve Its Antioxidant Activity. *ACS Sustain Chem Eng* **2020**, *8* (24), 9104–9114. <https://doi.org/10.1021/acssuschemeng.0c02366>.
- (112) Jacobs, B.; Nieuwenhove, I. Van; Lauwaert, J.; Saegher, T. De; Gracia, J. Valorizing Kraft Lignin by a Catalytic Reductive Depolymerization in Ethanol / Water with Formic Acid as a Supplementary H₂ Donor. *Waste Biomass Valorization* **2022**, No. 0123456789. <https://doi.org/10.1007/s12649-022-01958-9>.
- (113) Ahlbom, A.; Maschietti, M.; Nielsen, R.; Lyckeskog, H.; Hasani, M.; Theliander, H. On the Hydrothermal Depolymerisation of Kraft Lignin Using Glycerol as a Capping Agent. *Holzforschung* **2023**. <https://doi.org/10.3390/en14040932>.
- (114) Arora, P.; Ojagh, H.; Woo, J.; Lind Grennfelt, E.; Olsson, L.; Creaser, D. Investigating the Effect of Fe as a Poison for Catalytic HDO over Sulfided NiMo Alumina Catalysts. *Appl Catal B* **2018**, *227*, 240–251. <https://doi.org/10.1016/J.APCATB.2018.01.027>.
- (115) Wang, W.; Li, L.; Wu, K.; Zhu, G.; Tan, S.; Li, W.; Yang, Y. Hydrothermal Synthesis of Bimodal Mesoporous MoS₂ Nanosheets and Their Hydrodeoxygenation Properties. *RSC Adv* **2015**, *5* (76), 61799–61807. <https://doi.org/10.1039/c5ra09690a>.
- (116) Salam, M. A.; Arora, P.; Ojagh, H.; Cheah, Y. W.; Olsson, L.; Creaser, D. NiMoS on Alumina-USY Zeolites for Hydrotreating Lignin Dimers: Effect of Support Acidity and Cleavage of C-C Bonds. *Sustain Energy Fuels* **2019**, *4* (1), 149–163. <https://doi.org/10.1039/c9se00507b>.
- (117) Ferdous, D.; Dalai, A. K.; Adjaye, J.; Kotlyar, L. Surface Morphology of NiMo/Al₂O₃ Catalysts Incorporated with Boron and Phosphorus: Experimental and Simulation. *Appl Catal A Gen* **2005**, *294* (1), 80–91. <https://doi.org/10.1016/j.apcata.2005.07.025>.
- (118) Lindfors, C.; Mäki-Arvela, P.; Paturi, P.; Aho, A.; Eränen, K.; Hemming, J.; Peurla, M.; Kubička, D.; Simakova, I. L.; Murzin, D. Y. Hydrodeoxygenation of Isoeugenol over Ni- And Co-Supported Catalysts. *ACS Sustain Chem Eng* **2019**, *7* (17), 14545–14560. <https://doi.org/10.1021/acssuschemeng.9b02108>.
- (119) Tieuli, S.; Mäki-Arvela, P.; Peurla, M.; Eränen, K.; Wärnå, J.; Cruciani, G.; Menegazzo, F.; Murzin, D. Y.; Signoretto, M. Hydrodeoxygenation of Isoeugenol over Ni-SBA-15: Kinetics and Modelling. *Appl Catal A Gen* **2019**, *580* (February), 1–10. <https://doi.org/10.1016/j.apcata.2019.04.028>.
- (120) Byskov, L. S.; Nørskov, J. K.; Clausen, B. S.; Topsøe, H. DFT Calculations of Unpromoted and Promoted MoS₂-Based Hydrodesulfurization Catalysts. *J Catal* **1999**, *187* (1), 109–122. <https://doi.org/10.1006/jcat.1999.2598>.

- (121) Fahim, M. A.; Alsahhaf, T. A.; Elkilani, A. Refinery Feedstocks and Products. *Fundamentals of Petroleum Refining* **2010**, 11–31. <https://doi.org/10.1016/b978-0-444-52785-1.00002-4>.
- (122) Thring, R. W.; Katikaneni, S. P. R.; Bakhshi, N. N. Production of Gasoline Range Hydrocarbons from Alcell Lignin Using HZSM-5 Catalyst. *Fuel processing technology* **2000**, 62 (1), 17–30. [https://doi.org/10.1016/S0378-3820\(99\)00061-2](https://doi.org/10.1016/S0378-3820(99)00061-2).
- (123) Lian, J.; Ma, J.; Duan, X.; Kim, T.; Li, H.; Zheng, W. One-Step Ionothermal Synthesis of γ -Al₂O₃ Mesoporous Nanoflakes at Low Temperature. *Chemical Communications* **2010**, 46 (15), 2650–2652. <https://doi.org/10.1039/b921787h>.
- (124) Akhtar, M. S.; Riaz, S.; Mehmood, R. F.; Ahmad, K. S.; Alghamdi, Y.; Malik, M. A.; Naseem, S. Surfactant and Template Free Synthesis of Porous ZnS Nanoparticles. *Mater Chem Phys* **2017**, 189, 28–34. <https://doi.org/10.1016/j.matchemphys.2016.12.027>.
- (125) Han, W.; Nie, H.; Long, X.; Li, M.; Yang, Q.; Li, D. Effects of the Support Brønsted Acidity on the Hydrodesulfurization and Hydrodenitrogenation Activity of Sulfided NiMo/Al₂O₃ Catalysts. *Catal Today* **2017**, 292, 58–66. <https://doi.org/10.1016/j.cattod.2016.11.049>.
- (126) Biesinger, M. C. Advanced Analysis of Copper X-Ray Photoelectron Spectra. *Surface and Interface Analysis* **2017**, 49 (13), 1325–1334. <https://doi.org/10.1002/sia.6239>.
- (127) Vuori, A.; Bredenberg, J. B. son. Hydrogenolysis and Hydrocracking of the Carbon-Oxygen Bond: 5. Hydrogenolysis of 4-Propylguaiaicol by Sulfided CoO-MoO₃(γ -Al₂O₃). *Holzforschung* **1984**, 38 (5), 253–262. <https://doi.org/10.1515/hfsg.1984.38.5.253>.
- (128) Vuori, A.; Helenius, A.; Bredenberg, J. B. S. Influence of Sulphur Level on Hydrodeoxygenation. *Appl Catal* **1989**, 52 (1), 41–56. [https://doi.org/10.1016/S0166-9834\(00\)83371-0](https://doi.org/10.1016/S0166-9834(00)83371-0).
- (129) Song, S.; Zhang, J.; Yan, N. Support Effects in the De-Methoxylation of Lignin Monomer 4-Propylguaiaicol over Molybdenum-Based Catalysts. *Fuel Processing Technology* **2020**, 199 (November 2019), 106224. <https://doi.org/10.1016/j.fuproc.2019.106224>.
- (130) He, Y.; Bie, Y.; Lehtonen, J.; Liu, R.; Cai, J. Hydrodeoxygenation of Guaiacol as a Model Compound of Lignin-Derived Pyrolysis Bio-Oil over Zirconia-Supported Rh Catalyst: Process Optimization and Reaction Kinetics. *Fuel* **2019**, 239 (August 2018), 1015–1027. <https://doi.org/10.1016/j.fuel.2018.11.103>.
- (131) Bomont, L.; Alda-Onggar, M.; Fedorov, V.; Aho, A.; Peltonen, J.; Eränen, K.; Peurla, M.; Kumar, N.; Wärnä, J.; Russo, V.; Mäki-Arvela, P.; Grénman, H.; Lindblad, M.; Murzin, D. Y. Production of Cycloalkanes in Hydrodeoxygenation of Isoleugenol Over Pt- and Ir-Modified Bifunctional Catalysts. *Eur J Inorg Chem* **2018**. <https://doi.org/10.1002/ejic.201800391>.
- (132) Santos, J. L.; Alda-Onggar, M.; Fedorov, V.; Peurla, M.; Eränen, K.; Mäki-Arvela, P.; Centeno, M.; Murzin, D. Y. Hydrodeoxygenation of Vanillin over Carbon Supported Metal Catalysts. *Appl Catal A Gen* **2018**, 561 (March), 137–149. <https://doi.org/10.1016/j.apcata.2018.05.010>.

- (133) Zhang, C.; Li, P.; Liu, X.; Liu, T.; Jiang, Z.; Li, C. Applied Catalysis A , General Morphology-Performance Relation of (Co) MoS₂ Catalysts in the Hydrodesulfurization of FCC Gasoline. *Appl Catal A Gen* **2018**, *556* (January), 20–28. <https://doi.org/10.1016/j.apcata.2018.02.026>.
- (134) Kruk, M.; Jaroniec, M. Gas Adsorption Characterization of Ordered Organic - Inorganic Nanocomposite Materials. **2001**, 3169–3183. <https://doi.org/10.1021/cm0101069>.
- (135) Lin, H.; Chen, X.; Li, H.; Yang, M.; Qi, Y. Hydrothermal Synthesis and Characterization of MoS₂ Nanorods. *Mater Lett* **2010**, *64* (15), 1748–1750. <https://doi.org/10.1016/j.matlet.2010.04.032>.
- (136) Jagminas, A.; Niaura, G.; Žalneravičius, R.; Trusovas, R.; Račiukaitis, G.; Jasulaitiene, V. Laser Light Induced Transformation of Molybdenum Disulphide-Based Nanoplatelet Arrays. *Sci Rep* **2016**, *6* (November), 2–10. <https://doi.org/10.1038/srep37514>.
- (137) Bremmer, G. M.; van Haandel, L.; Hensen, E. J. M.; Frenken, J. W. M.; Kooyman, P. J. The Effect of Oxidation and Resulfidation on (Ni/Co)MoS₂ Hydrodesulfurisation Catalysts. *Appl Catal B* **2019**, *243* (2019), 145–150. <https://doi.org/10.1016/j.apcatb.2018.10.014>.
- (138) Benoist, L.; Gonbeau, D.; Pfister-Guillouzo, G.; Schmidt, E.; Meunier, G.; Levasseur, A. XPS Analysis of Oxido-Reduction Mechanisms during Lithium Intercalation in Amorphous Molybdenum Oxysulfide Thin Films. *Solid State Ion* **1995**, *76* (1–2), 81–89. [https://doi.org/10.1016/0167-2738\(94\)00226-I](https://doi.org/10.1016/0167-2738(94)00226-I).
- (139) Solymosi, F.; Cserényi, J.; Szöke, A.; Bánsági, T.; Oszkó, A. Aromatization of Methane over Supported and Unsupported Mo-Based Catalysts. *J Catal* **1997**. <https://doi.org/10.1006/jcat.1997.1478>.
- (140) Salam, M. A.; Cheah, Y. W.; Ho, P. H.; Olsson, L.; Creaser, D. Hydrotreatment of Lignin Dimers over NiMoS-USY: Effect of Silica/Alumina Ratio. *Sustain Energy Fuels* **2021**, *5* (13), 3445–3457. <https://doi.org/10.1039/d1se00412c>.
- (141) Salam, M. A.; Arora, P.; Ojagh, H.; Cheah, Y. W.; Olsson, L.; Creaser, D. NiMoS on Alumina-USY Zeolites for Hydrotreating Lignin Dimers: Effect of Support Acidity and Cleavage of C-C Bonds. *Sustain Energy Fuels* **2019**, *4* (1). <https://doi.org/10.1039/c9se00507b>.
- (142) Ho, P. H.; Woo, J.; Ilmasani, R. F.; Salam, M. A.; Creaser, D.; Olsson, L. The Effect of Si/Al Ratio on the Oxidation and Sulfur Resistance of Beta Zeolite-Supported Pt and Pd as Diesel Oxidation Catalysts. *ACS Engineering Au* **2022**, *2* (1), 27–45. <https://doi.org/10.1021/acseengineeringau.1c00016>.
- (143) Guan, W.; Tsang, C. W.; Lin, C. S. K.; Len, C.; Hu, H.; Liang, C. A Review on High Catalytic Efficiency of Solid Acid Catalysts for Lignin Valorization. *Bioresour Technol*. Elsevier Ltd February 1, 2020. <https://doi.org/10.1016/j.biortech.2019.122432>.
- (144) Horáček, J.; Homola, F.; Kubičková, I.; Kubička, D. Lignin to Liquids over Sulfided Catalysts. *Catal Today* **2012**, *179* (1), 191–198. <https://doi.org/10.1016/j.cattod.2011.06.031>.
- (145) Li, N.; Wei, L.; bibi, R.; Chen, L.; Liu, J.; Zhang, L.; Zheng, Y.; Zhou, J. Catalytic Hydrogenation of Alkali Lignin into Bio-Oil Using Flower-like Hierarchical MoS₂-Based Composite Catalysts. *Fuel* **2016**, *185*, 532–540. <https://doi.org/10.1016/j.fuel.2016.08.001>.

- (146) Pinheiro Pires, A. P.; Arauzo, J.; Fonts, I.; Domine, M. E.; Fernández Arroyo, A.; Garcia-Perez, M. E.; Montoya, J.; Chejne, F.; Pfromm, P.; Garcia-Perez, M. Challenges and Opportunities for Bio-Oil Refining: A Review. *Energy and Fuels* **2019**, *33* (6), 4683–4720. <https://doi.org/10.1021/acs.energyfuels.9b00039>.
- (147) Hosoya, T.; Kawamoto, H.; Saka, S. Secondary Reactions of Lignin-Derived Primary Tar Components. *J Anal Appl Pyrolysis* **2008**, *83* (1), 78–87. <https://doi.org/10.1016/j.jaap.2008.06.003>.
- (148) Bourbiaux, D.; Pu, J.; Rataboul, F.; Djakovitch, L.; Geantet, C.; Laurenti, D. Reductive or Oxidative Catalytic Lignin Depolymerization: An Overview of Recent Advances. *Catal Today* **2021**, *373* (February 2020), 24–37. <https://doi.org/10.1016/j.cattod.2021.03.027>.
- (149) Gilarranz, M. A.; Rodríguez, F.; Oliet, M.; García, J.; Alonso, V. Phenolic OH Group Estimation by FTIR and UV Spectroscopy. Application to Organosolv Lignins. *Journal of Wood Chemistry and Technology* **2001**, *21* (4), 387–395. <https://doi.org/10.1081/WCT-100108333>.
- (150) Kubo, S.; Kadla, J. F. Hydrogen Bonding in Lignin: A Fourier Transform Infrared Model Compound Study. *Biomacromolecules* **2005**, *6* (5), 2815–2821. <https://doi.org/10.1021/bm050288q>.
- (151) Joffres, B.; Lorentz, C.; Vidalie, M.; Laurenti, D.; Quoineaud, A. A.; Charon, N.; Daudin, A.; Quignard, A.; Geantet, C. Catalytic Hydroconversion of a Wheat Straw Soda Lignin: Characterization of the Products and the Lignin Residue. *Appl Catal B* **2014**, *145*, 167–176. <https://doi.org/10.1016/j.apcatb.2013.01.039>.
- (152) Xu, W.; Miller, S. J.; Agrawal, P. K.; Jones, C. W. Depolymerization and Hydrodeoxygenation of Switchgrass Lignin with Formic Acid. *ChemSusChem* **2012**, *5* (4), 667–675. <https://doi.org/10.1002/cssc.201100695>.
- (153) Jongerius, A. L.; Bruijninx, P. C. A.; Weckhuysen, B. M. Liquid-Phase Reforming and Hydrodeoxygenation as a Two-Step Route to Aromatics from Lignin. *Green Chemistry* **2013**, *15* (11), 3049–3056. <https://doi.org/10.1039/c3gc41150h>.
- (154) Nakamura, T.; Kawamoto, H.; Saka, S. Condensation Reactions of Some Lignin Related Compounds at Relatively Low Pyrolysis Temperature. *Journal of Wood Chemistry and Technology* **2007**, *27* (2), 121–133. <https://doi.org/10.1080/02773810701515143>.
- (155) Okuda, K.; Umetsu, M.; Takami, S.; Adschiri, T. Disassembly of Lignin and Chemical Recovery — Rapid Depolymerization of Lignin without Char Formation in Water – Phenol Mixtures. **2004**, *85*, 803–813. <https://doi.org/10.1016/j.fuproc.2003.11.027>.
- (156) Liu, C.; Chen, X.; Liu, X.; Cui, C.; Zhou, Z.; Jia, L.; Qi, F. Evidence of a Phenolic Pool as a Key Intermediate for Zeolite-Catalyzed Lignin Pyrolysis. *Angewandte Chemie - International Edition* **2021**, *60* (5), 2643–2647. <https://doi.org/10.1002/anie.202011937>.
- (157) Bergvall, N.; Sandström, L.; Cheah, Y. W.; Öhrman, O. G. W. Slurry Hydroconversion of Solid Kraft Lignin to Liquid Products Using Molybdenum- and Iron-Based Catalysts. *Energy and Fuels* **2022**, *36* (17), 10226–10242. <https://doi.org/10.1021/acs.energyfuels.2c01664>.

- (158) Lv, D. C.; Jiang, K.; Li, K.; Liu, Y. Q.; Wang, D.; Ye, Y. Y. Effective Suppression of Coke Formation with Lignin-Derived Oil during the Upgrading of Pyrolysis Oils. *Biomass Bioenergy* **2022**, *159* (May 2021), 106425. <https://doi.org/10.1016/j.biombioe.2022.106425>.
- (159) Zhang, S.; Liu, D.; Deng, W.; Que, G. A Review of Slurry-Phase Hydrocracking Heavy Oil Technology. *Energy and Fuels*. November 2007, pp 3057–3062. <https://doi.org/10.1021/ef700253f>.
- (160) Dimitriadis, A.; Bergvall, N.; Johansson, A. C.; Sandström, L.; Bezergianni, S.; Tourlakidis, N.; Meca, L.; Kukula, P.; Raymakers, L. Biomass Conversion via Ablative Fast Pyrolysis and Hydroprocessing towards Refinery Integration: Industrially Relevant Scale Validation. *Fuel* **2023**, *332*. <https://doi.org/10.1016/j.fuel.2022.126153>.
- (161) Bergvall, N.; Molinder, R.; Johansson, A. C.; Sandström, L. Continuous Slurry Hydrocracking of Biobased Fast Pyrolysis Oil. *Energy and Fuels* **2021**, *35* (3), 2303–2312. <https://doi.org/10.1021/acs.energyfuels.0c03866>.
- (162) Diebold, J. P. *A Review of the Chemical and Physical Mechanisms of the Storage Stability of Fast Pyrolysis Bio-Oils*; 2000. <http://www.doe.gov/bridge>.
- (163) Oasmaa, A.; Korhonen, J.; Kuoppala, E. An Approach for Stability Measurement of Wood-Based Fast Pyrolysis Bio-Oils. In *Energy and Fuels*; 2011; Vol. 25, pp 3307–3313. <https://doi.org/10.1021/ef2006673>.
- (164) Broumand, M.; Khan, M. S.; Yun, S.; Hong, Z.; Thomson, M. J. The Effect of Thermo-Catalytic Reforming of a Pyrolysis Bio-Oil on Its Performance in a Micro-Gas Turbine Burner. *Applications in Energy and Combustion Science* **2021**, *5*. <https://doi.org/10.1016/j.jaecs.2020.100017>.
- (165) Yin, W.; Wang, Z.; Yang, H.; Venderbosch, R. H.; Heeres, H. J. Catalytic Hydrotreatment of Biomass-Derived Fast Pyrolysis Liquids Using Ni and Cu-Based PRICAT Catalysts. *Energy and Fuels* **2022**, *36* (23), 14281–14291. <https://doi.org/10.1021/acs.energyfuels.2c02485>.